BUREAU OF MINES

APPLIED PHYSICS RESEARCH LABORATORY

COLLEGE PARK, MARYLAND

UNITED STATES DEPARTMENT OF THE INTERIOR

Contract No.: 2939
ARPA Order No.: 172-61
Project Code No.: 8100

Contractor: APRL, USBM
Amount of Contract: $55,000.
Project Leader: H. R. Nicholls
Union 4-3100, Ext. 79

Report No. E 48.1.1

SHEAR AND LONGITUDINAL WAVES FROM
H E DETONATIONS IN TUFF-- Comparison of
Tuff and Granite Data

Final Report-August 1963

U. S. Bureau of Mines
Applied Physics Research Laboratory

Research Sponsored by Advanced Research Project Agency

Prepared for:

Defense Atomic Support Agency
Washington 25, D. C.

DDC Availability Notice- Qualified requestors may obtain copies of
this report from Defense Documentation
Center

CONTENTS

ii.

<center>CONTENTS (Con' t)</center>

<center>FIGURES</center>

CONTENTS (Con' t)

CONTENTS (Con' t)

iv.

<div align="center">CONTENTS (Con' t)</div>

CONTENTS (Con' t)

TABLES

CONTENTS (Con' t)

SHEAR AND LONGITUDINAL WAVES FROM HE

DETONATIONS IN TUFF--Comparison of Tuff and Granite Data

by

Harry R. Nicholls[1] and Verne E. Hooker[1]

INTRODUCTION

The investigations described in this report were performed by APRL as part of the VELA UNIFORM Point Source Research Program under Contract No. 2939, ARPA Order No. 172-61, Project Code No. 8100. The scope of the work as proposed to and authorized by the Defense Atomic Support Agency were:

1. To conduct an experimental research program to investigate the generation of shear and longitudinal waves. Tests to be conducted in two media under varying geologic conditions and using high explosives as a source.

2. To conduct an experimental research program to investigate the effects of characteristic impedance matching in two media using several types of high explosives.

Results obtained from field tests conducted in a granite-gneiss medium as part of the program were reported previously (Nicholls and Hooker, 1962). This report presents the results from a series of field tests conducted in tuff near Camp Verde, Arizona. This report also compares the similarities and differences between data obtained in tuff and granite-gneiss.

---

[1] Research Geophysicist.

Both authors are with the Applied Physics Research Laboratory, Bureau of Mines, U. S. Department of the Interior, College Park, Md.

2.

ACKNOWLEDGMENTS

INSTRUMENTATION

Strain gages and accelerometers were used. The strain gages consisted of resistance-wire strain gage elements, mounted on short lengths of 2-1/8 inch diameter tuff core (Obert and Duvall, 1949). The tuff was obtained from the Nevada Test Site to expedite the program. Commercially available piezo-electric accelerometers were cemented to the cores with an epoxy cement. Figure 1 shows a core with strain gage attached at upper end and accelerometer mounted and sealed with neoprene cement. Surface instrumentation was accomplished with accelerometers mounted to solid steel gage mounts. Battery operated pre-amplifiers were used in conjunction with the accelerometers to provide electrical impeaance matching and to minimize signal reduction from line losses.

The output signals from the gages were carried by 500 feet long shielded cables to a recording trailer. These signals were fed into a 14-channel pre-amplifier system inside the trailer. These amplifiers provided the necessary electrical impedance match between gage and recorder and provided amplification or attenuation as needed to deliver proper input voltages to the recorder. The recorder was a 14-channel FM magnetic record-reproduce system. Readout of the data was accomplished by playback from the tape recorder system into a direct-writing oscillograph. The output of a timing oscillator was played into the oscillograph during playback to provide reference timing lines on each paper record. A chronograph contactor or target was inserted into each charge when a zero time was desired. The target and appropriate circuitry produced a

Fig. 1 - Typical Strain Gage and Accelerometer Construction.

4.

steep-fronted pulse at the instant of charge detonation. The overall frequency response of the system was considered to be flat (+ 12%) from 10-10,000 cycles per second.

Amplitude analysis was accomplished by calibrating the system, exclusive of gages, with a known input signal prior to each shot. The known calibration signal, the recorded earth motion pulse, pre-amplifier gain, and gage sensitivity were then used to calculate the amplitude. Playback records were made for analysis after each shot during the field program to determine proper pre-amplifier gain settings for subsequent shots. Additional playbacks were made for final analysis at the laboratory. All acceleration data from the deep shots were integrated electronically to yield particle velocity for comparison with strain data. The frequency response of the integration system was flat (+ 20%) from 40-10,000 cycles per second.

The instrumentation for rate of detonation measurement of each explosive consisted of two chronograph contactors, a go-circuit, a stop-circuit, and a microsecond interval counter. As the detonation of the explosive proceeded up the explosive column, the first chronograph contactor started the counter. As the detonation wave arrived at the second contactor, at a known distance from the first, the counter stopped. Interval times and distances were recorded for rate of detonation calculations.

TEST SITE

All tests were conducted in a water-lain volcanic tuff deposit near Camp Verde, Arizona. The specific location was the NE 1/4, SW 1/4, SE 1/4, Section 19, T13N, R6E of the Gila and Salt River Base and Meridian. The general area known as the Cottonwood Basin was located approximately ten miles southeast of Camp Verde between State Highway 9 and the Verde River. The location constituted part of the Coconino National Forest and was under the direct supervision of the Beaver Creek Forest Ranger Station.

Lithologically, the Hackberry Mountain tuff is of recent origin, possibly deposited as recently as 1,000 years ago. Many facies changes are evident in the several hundred feet of section exposed in outcrops, arroyos, and road cuts. The deposit includes loosely-cemented tuff, tuff-breccia,

and agglomerate. Large boulders of tuff are prevalent higher up in the geologic section. Thin layers of sandstone are obvious lower in the section. The area tested appeared to be a uniform non-welded tuff with soil cover ranging from none to about five feet. The tuff is generally grey or buff in color and becomes brown or pink when wet. Two 50 feet deep NX core holes were drilled to inspect the tuff in the area of interest. Visual inspection of the recovered core indicated a rather uniform tuff section with no breccia or agglomerate encountered. The tuff, however, was not uniform based upon laboratory mechanical property tests and upon subsequent in situ velocity determinations. The longitudinal and shear velocities of the core samples were determined in the laboratory by the resonant frequency method. The elastic constants were calculated from the velocities and the density of the tuff. As shown in table 1, the tuff samples could be divided into two distinct types based on velocity and density measurements. The shear and longitudinal velocities were also measured in situ. These values, considered reliable within $\pm 3\%$, are given in table 1 with the calculated elastic constants.

SHEAR WAVE GENERATION

Test Purpose

A considerable amount of data concerning the generation and propagation of shear waves has been obtained and reported from the tests in granite-gneiss (Nicholls and Hooker, 1962). Conclusions previously stated from the analysis of the granite-gneiss data were that the medium was probably a prime mechanism of shear wave generation and that no shear wave enhancement due to shot hole geometry was discernible. The granite-gneiss, due to the gneissic banding, may have contributed significantly to shear wave generation and overshadowed such possible sources as cratering or the radial cracking in the vicinity of the shot hole.

It was believed that the tuff would be a more homogeneous, isotropic medium than the granite-gneiss. Thus, identification of shot hole conditions and/or other source conditions which contributed significantly to shear wave generation might be accomplished. In addition, coverage was to be expanded so that data were recorded around the circumference of a large diameter circle from detonations at the center. Coverage would be around a full $360°$ rather than about $170°$ as in previous work.

TABLE 1.- Mechanical properties

Property	H M tuff [1]		NTS tuff [1]		Grout [1]	In situ [2]
	Group 1	Group 2	Group 1	Group 2		
No. of samples	4	2	9	10	3	
Density, lb/ft^2	97.3 ± .7	120 ± 5	98.7 ± .4	100.7±2.8	78.3±1.8	106
Long. vel., ft/sec	4000 ± 470	8600 ± 520	6690 ± 980	7280±630	6060±560	5560
Shear vel., ft/sec	2790 ± 270	5630 ± 520	4530 ± 610	4910±422	3730±370	3230
Poisson's ratio	.031	.168	.092	.101	.128	.245
Young's modulus, psi x 10^6	.336	1.92	.954	1.27	.618	.595
Modulus of rigidity, psi x 10^6	.164	.822	.437	.577	.274	.239

1/ Resonant frequency method.

2/ Measured at the surface of the tuff.

Experimental Procedure

Preliminary surface testing in the tuff was designed to determine the following: whether shear waves could be generated by detonating small explosive charges, and if so, optimum charge size for shear wave generation; propagation laws for elastic waves traveling near the surface of the tuff; shear and longitudinal propagation velocities in the medium; verification of techniques and methods previously used.

To effect the study, a series of shallow vertical holes 1-1/2 inches in diameter and 8 inches deep were drilled in the tuff. Soil cover at these locations was removed. A plan view of the test holes is shown in figure 2. Gage mounts consisted of solid steel blocks attached by press fit to studs which were 6 inches long and 1/2 inch in diameter. The studs were set in a hole as shown in figure 3. Grout was then poured around the stud and inside a cardboard form to a depth on the mount of 1/2 inch. The grout used had been developed for use in tuff by the Concrete Division of the U. S. Army Engineer Waterways Experiment Station, at Jackson, Mississippi. The properties of the grout were as shown in table 1.

Gages were attached by screws to each mount. Electrical isolation was obtained by inserting a small insulating washer between the accelerometer and the mount. Two gages were used at each location, one oriented to measure radial motion, and a second oriented to measure horizontal transverse motion. Small charges of high explosives were detonated, and earth motions were recorded at the gage locations with shot-to-gage distances varying from 50 to 200 feet.

On the basis of the data from the surface linear array, a surface circular array of gage locations was laid out with a radius of 100 feet as shown in figure 4. A charge weight of .075 pounds of a 45% bulk strength semi-gelatin type of explosive was chosen for most of the succeeding shots. Instrumentation limitations permitted the use of six pairs of gages on each shot although there were 8 possible gage locations around the circle. A total of ten shots were detonated with a pair of gages at each location from southwest, clockwise, to east, inclusive. Figure 5 is an enlarged view of the shot point locations. The gages were then moved to locations ranging from east, clockwise, to northwest, inclusive and an additional

8

O Shothole
● Gage position
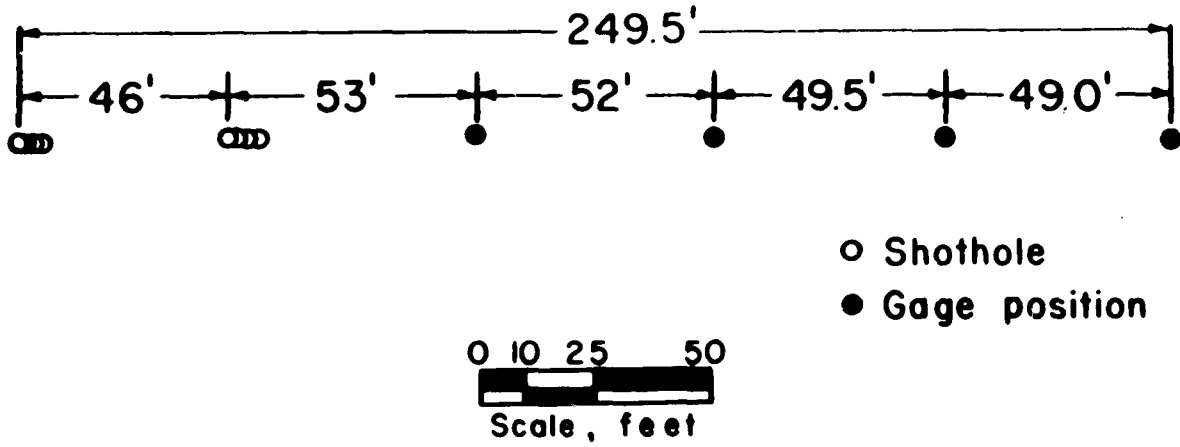
Fig. 2 - Plan View of Test Area- Surface Array.
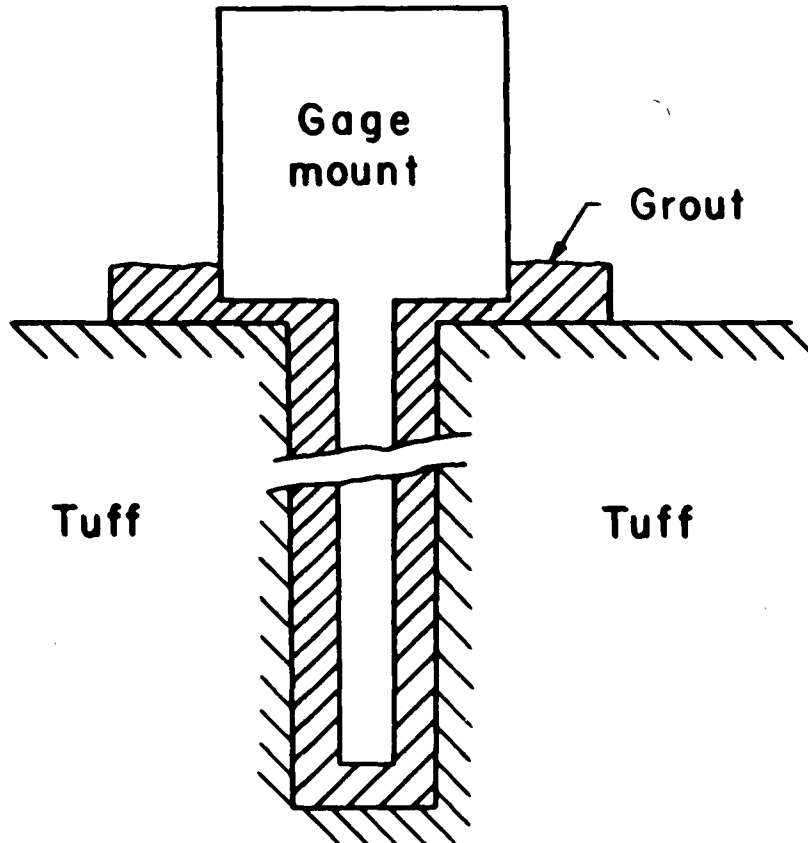
Fig. 3 - Typical Gage Mount Installation- Surface Test.

N

NW

NE

W

E

N

Shot
holes

SW

SE

S

● Gage holes

0 20 50   100

○ Center of array,
see section below

Scale, feet
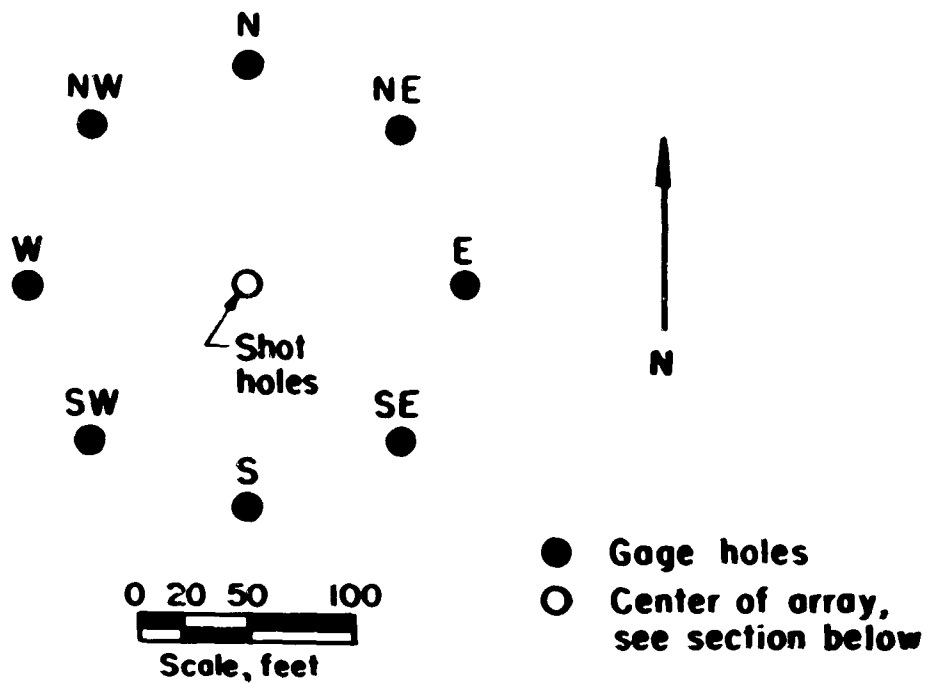
Fig. 4 - Plan View of Test Area- Circular Array.

○
○ }17

○
11
○
10
○
9
○
8

○ ○   ○
16 15 8

○ ○ ○   ○ ○ ○
16 15   19 22 23
○ ○ ○
14 13 11

Enlarged plan of
shotpoint area

○
18

○ ○
24 26

○
29

0 2 5   10

○
20
○
21

Scale, feet

○ }27
○
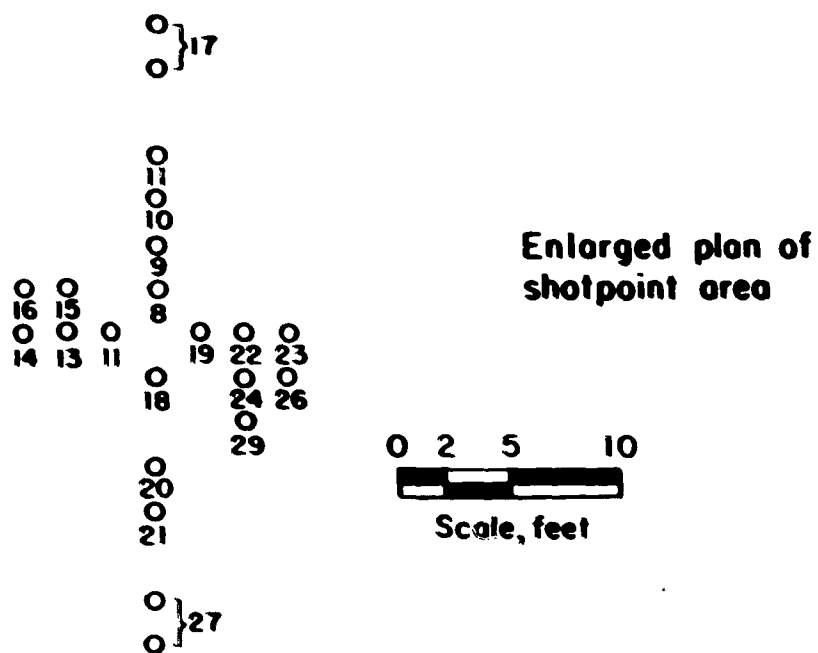
Fig. 5 - Enlarged Plan of Shot Point Area- Circular Array.

ten shots were detonated with depths, etc., corresponding to those of the
first ten shots. Charges in shot holes 8 to 10, 12 to 15, 18 and 20 to 25,
were detonated at various depths to investigate the effect of charge depth
and/or cratering on the amplitudes of the generated shear waves. Charge
depths varied from 0.5 to 3.83 feet. The charges were 1-1/8 inches in
diameter, 1 to 2 inches long and tamped to completely fill the hole. A
seismic type electric blasting cap was used to initiate each charge deto-
nation. A chronograph contactor was inserted into each charge to pro-
vide a zero or detonation time.

Shots 11 and 19 were placed at a depth of 3.83 feet and the shot hole was
then filled to the surface with grout. The grout was permitted to harden
before detonating the explosive in an attempt to simulate a point source
type of charge. Shots 16 and 26 each consisted of a 1-foot long charge of
400 grain/foot detonating fuse. The charge was centered in the hole pro-
viding an annular air space 1/2 inch thick around the charge. The air
space decoupled the charge from the drill hole and reduced the amount
of cracking and crushing in the hole.

Shots 17 and 27 each consisted of two charges joined by detonating fuse.
These shots were based on the principle of pre-splitting (Paine, Holmes
and Clark, 1962). The purpose was to establish and propagate a crack
between the two holes (2 feet apart) and thereby enhance the amplitude
of the shear wave generated. Shot 27 was not useable, however, be-
cause the detonating fuse did not detonate the second charge and ampli-
tudes from the single charge were too small to be recorded.

Data Analysis

A typical set of particle acceleration versus time records from the
surface linear array is shown in figure 6. The arrivals of the longi-
tudinal and shear waves are noted as P and S respectively. The re-
sponse of the radial gages indicates one difficulty encountered through-
out the test series. The first peak (downward for these records) was
generally much smaller in amplitude than the second peak. This is not
typical of most other rock types investigated. It was impossible to
achieve optimum gain settings for both the first and second peaks, so
the amplitude of most first peaks as recorded is small. The first
arrival of the pulse and the subsequent propagation velocity was there-
fore subject to more error than normal. However, because of large

RG / **R = 95 ft** — P

TG / **R = 95 ft** — S

RG / **R = 147 ft** — P

RG / **R = 196.5 ft** — P

TG / **R = 196.5** — S

Time scale, 10 milliseconds
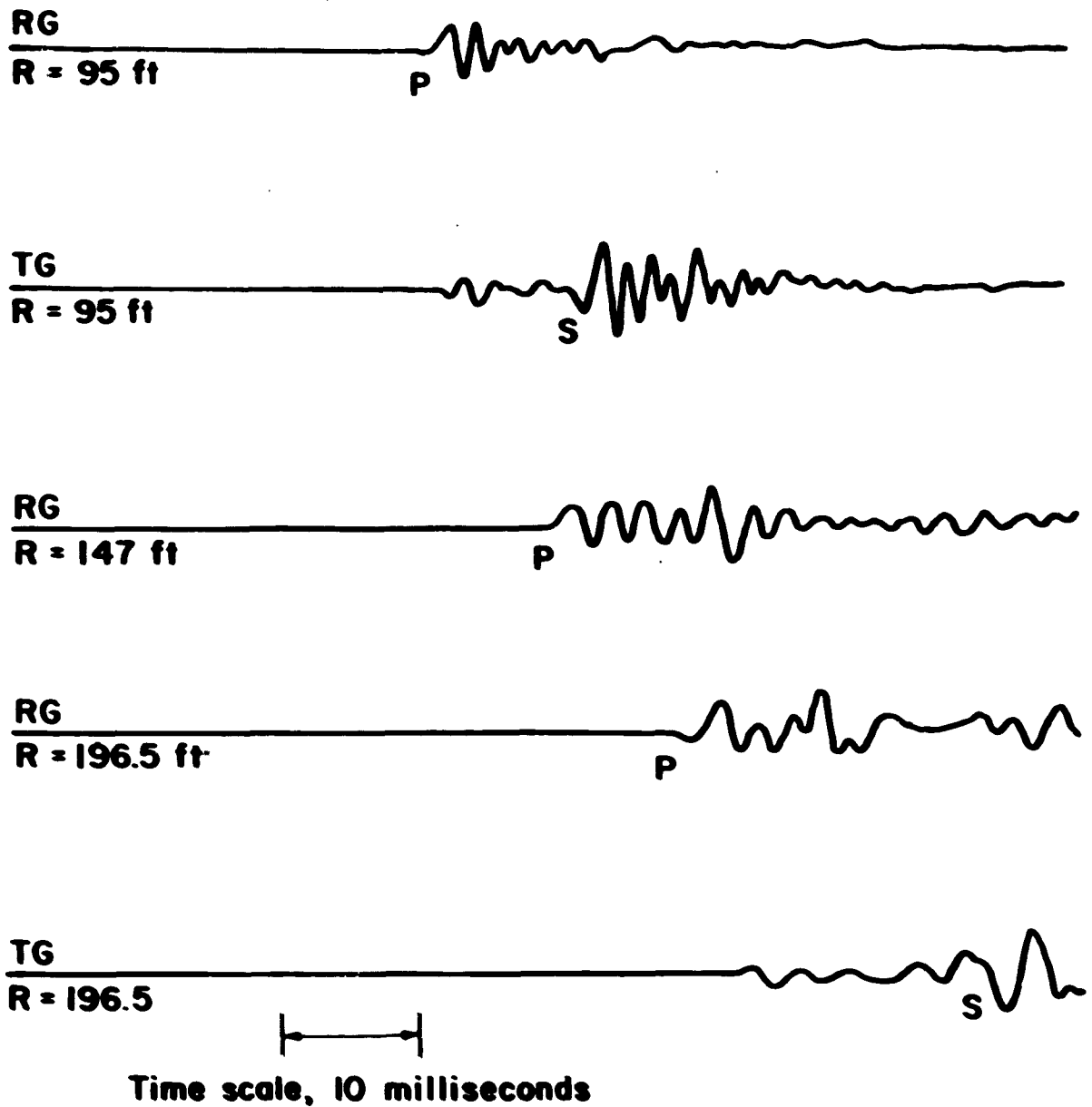
RG = Radial gage
TG = Transverse gage
R = Shot-to-gage distance
P = P wave arrival
S = S wave arrival

Fig. 6 - Typical Particle Motion Recordings.

12.

travel times, the error was not excessive. The limitation of "picking" the first arrival time precisely, precludes the use of this early portion of the pulse for period or pulse width study.

Figure 7 shows an enlargement of radial and transverse recordings and the measurements made. The quality of both tracings shown is considered good. The radial gage tracing is representative of all radial data. About 50% of the transverse data are of this quality and the balance vary from poor to no recognizable shear wave arrival.

Table 2 gives the data from shots 2 through 7 of the surface linear array. Shear wave arrivals were not identifiable at shot-to-gage distances less than 95 feet. No useable information was recorded at 250 feet because of lack of sensitivity in recording.

The calculated longitudinal and shear wave propagation velocities were 5,560 and 3,230 feet/second, respectively.

Figure 8 includes plots of scaled particle acceleration versus scaled distance for data from the first and second peaks. Most of the data is from the radial gages. The second peak data are about a factor of four larger than the first peak data, and have a slightly lower slope. The transverse or shear wave data are shown with solid symbols. The first peak shear wave data are not consˀdered reliable because of the limitations in picking the first portion of the pulse. The second peak shear wave amplitude data agree with the corresponding radial motion amplitudes both in slope and magnitude.

Scaled period data have been plotted versus scaled distance as shown in figure 9. The period data may be interpreted in either of two ways. At a given distance, the period of a pulse generated by a small charge will be substantially smaller than the period from a large charge. For a given charge size, the period of a pulse recorded at a small distance will be substantially less than the period recorded at large distances. Both interpretations are substantially correct. If frequency, the reciprocal of period, is considered, the frequency from small charges is higher than from large charges and frequency decreases with distance traveled as would be expected. The few data points from shear waves indicate that somewhat shorter periods or higher frequencies might be
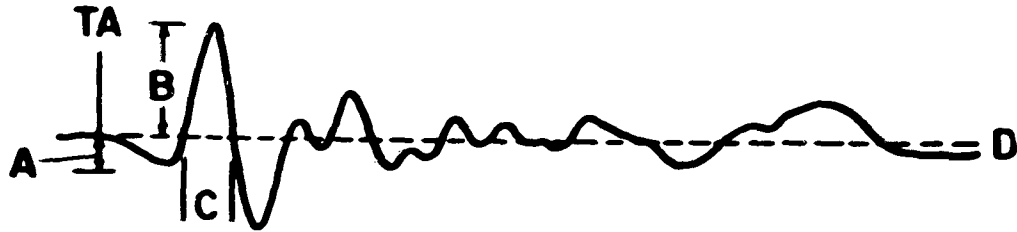
Tracing of record from radial gage
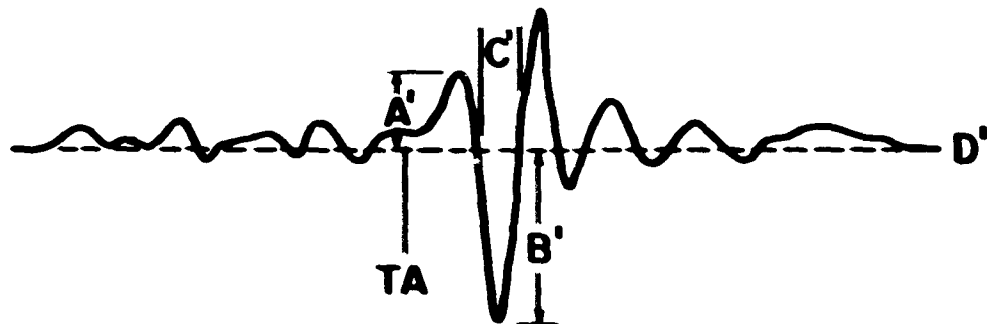
Tracing of record from transverse gage

TA = Arrival of P or S wave
A or A' = 1st peak amplitude
B or B' = 2nd peak amplitude
C or C' = One-half pulse width
D or D' = Record base line

Fig. 7 - Typical Data Measurements- Surface Studies.

14.

TABLE 2. - Surface linear array test data

Shot No., charge weight, charge volume$^{\frac{1}{3}}$	Gage orientation[1]	Distance ft	Scaled distance R/V$^{\frac{1}{3}}$ ft/ft	Acceleration 1st peak A g's
2	R	51	455	.0658
W=.101 lb	R	103	920	.00482
V$^{\frac{1}{3}}$=.112 ft				
3	R	49	345	------
W=.207 lb	R	101	711	.00759
V$^{\frac{1}{3}}$=.142 ft	R	150.5	1060	.00183
4	R	47	290	.204
W=.303 lb	R	99	611	.0158
V$^{\frac{1}{3}}$=.162 ft	R	148.5	917	.00435
	R	197.5	1219	.00181
5	R	99	798	.0247
W=.135 lb	T	151	1218	.00400
V$^{\frac{1}{3}}$=.124 ft	R	200.5	1617	.000900
	T	200.5	1617	.00962
6	R	97	782	------
W=.135 lb	T	97	782	.0249
V$^{\frac{1}{3}}$=.124 ft	R	149	1202	.00190
	R	198.5	1601	.000900
	T	198.5	1601	.00231
7	R	95	963	.00254
W=.068 lb	T	95	963	.0143
V$^{\frac{1}{3}}$=.0986 ft	R	147	1491	.00222
	R	196.5	1993	.000571
	T	196.5	1993	.00299

1/ R = Radial gage; T = Transverse gage, measured values are shear motion.

TABLE 2. - Surface linear array test data

Scaled acceleration 1st peak $AV^{\frac{1}{3}}$, g-ft	Acceleration 2nd peak A, g's	Scaled acceleration 2nd peak $AV^{\frac{1}{3}}$, g-ft	Period T, ms	Scaled period $T/V^{\frac{1}{3}}$, ms/ft	Arrival time P wave ms	Arrival time S wave ms
.00737	.165	.0185	2.65	23.7	----	
.000540	.289	.0324	4.22	37.7	----	
-----	.395	.0561	2.65	18.7	8.76	
.00108	.0493	.00700	4.54	32.0	17.01	
.000260	.0183	.00260	3.91	27.5	28.04	
.0330	.663	.107	2.71	16.7	8.25	
.00256	.111	.0180	3.91	24.1	17.51	
.000705	.0275	.00446	4.28	26.4	27.66	
.000293	.00726	.00118	6.30	38.9	36.04	
.00307	.0494	.00612	2.71	21.8	18.27	
.000496	.0105	.00130	3.15	25.4		52.35
.000112	.00360	.000446	5.67	45.7	36.47	
.000573	.00782	.000970	3.65	29.4		62.56
-----	.0512	.00635	1.89	15.2	18.27	
.00309	.0497	.00616	2.27	18.3		29.30
.000236	.0114	.00141	3.02	24.3	26.52	
.000112	.00234	.000290	5.92	47.7	34.02	
.000286	.00480	.000595	3.59	28.9		59.85
.000250	.0355	.00350	2.58	26.1	17.58	
.00141	.0374	.00369	2.39	24.1		28.85
.000219	.0104	.00103	4.50	46.5	24.95	
.0000563	.00228	.000225	4.54	45.9	35.78	
.000295	.00359	.000354	4.73	47.8		58.46

16.

$$AV^{\frac{1}{3}} = 7.05 \times 10^6 (R/V^{\frac{1}{3}})^{-3.15}$$

$$AV^{\frac{1}{3}} = 4.88 \times 10^6 (R/V^{\frac{1}{3}})^{-3.33}$$

SCALED PARTICLE ACCELERATION-$AV^{\frac{1}{3}}$, g's x ft

▲ 1st peak, radial

○ 2nd peak, radial

▲ 1st peak, transverse

● 2nd peak, transverse

.11
.1
.08
.06
.04
.02
.01
.008
.006
.004
.002
.001
.0008
.0006
.0004
.0002
.0001

100   200   400 600 1000   2000   4000

SCALED DISTANCE-$R/V^{\frac{1}{3}}$, ft/ft
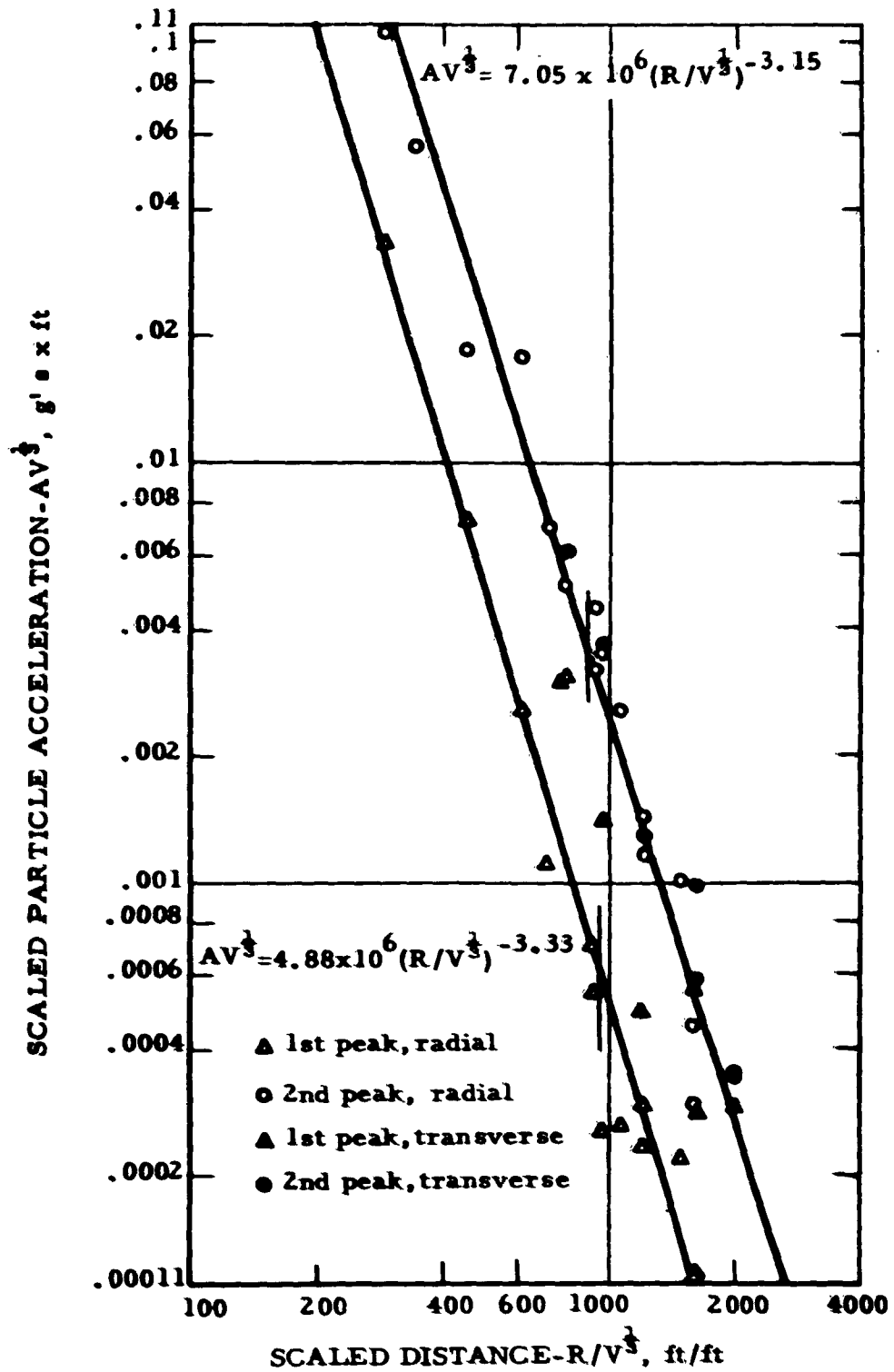
Fig. 8 — Scaled Particle Acceleration versus Scaled Distance-
Surface Linear Array
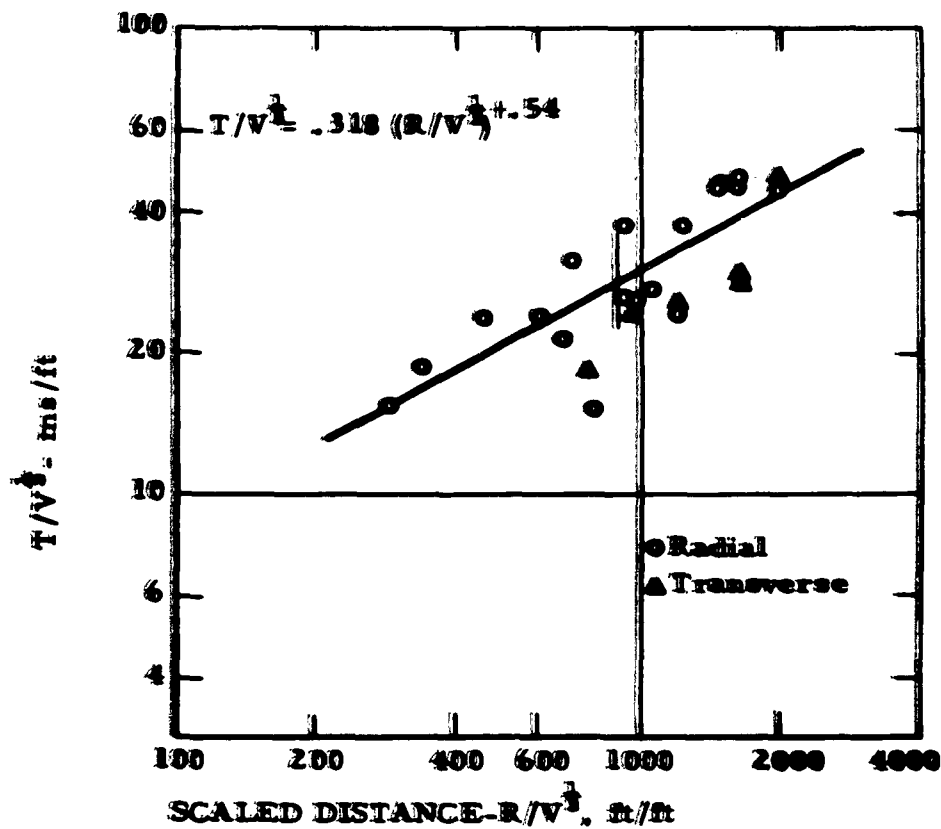
Fig. 9 - Scaled Period vs. Scaled Distance.

18.

expected from shear waves than from longitudinal waves. However, the period data as read from shear and longitudinal waves may not be directly comparable. Furthermore, the small differences noted would not provide sufficient separation for the use of electronic filtering as a routine tool for identification of shear waves.

Data from the surface circular array are given in table 3. The range of scaled distances (672 feet/feet to 1140 feet/feet) does not permit a comparison of accelerations directly. Scaled accelerations vary by more than a factor of five over these scaled distances if the regression slope, -3.15, is considered valid for these data. All values were therefore adjusted or normalized to the values which would have been obtained had all the gages been placed at a scaled distance of 1000 feet/feet. Also, the data from shots 16, 17, and 26, have been adjusted for the difference in charge sizes. The adjusted radial or longitudinal values are given in table 4. The data are rearranged by shot depth, shot hole condition and direction. The data appear to be quite random at first glance. Usual statistical analysis methods are too rigorous considering the number of unfilled blanks in the table. Also, from the surface linear array, scatter by a factor of about 2.5 times would be within one standard deviation of a least square determination. If direction or shot is considered separately, most values in the table would fall within plus or minus one standard deviation from the mean for the set of data. General conclusions can be drawn as follows:

1. Values obtained in north, northeast, or east direction are higher than values obtained in the other directions.

2. Values obtained in the south direction are lower than values obtained in other directions.

3. The most scatter occurs in the north direction and the least in the south direction.

4. The largest amplitudes are generally associated with shots 8, 9, 12, 17, and 18, which are at shallow depths.

5. The values from the decoupled shots 16 and 26 are smaller than coupled shot data as expected.

6. The values from shots 11, 14, and 23, are smaller in general, and are from the deepest shots. However, shot 19 does not fit this pattern.

7. On the basis of statement 4 and 6, a slight trend of decreasing longitudinal amplitude with increasing shot hole depth may be implied.

Shear wave acceleration amplitudes have been tabulated in table 5. The values have been adjusted for a scaled distance of 1000 feet/feet and for a scaled charge size of .102 feet. No values are given for the gage in the northeast direction because of the "ringing" or oscillatory character of data from this location which obscured shear wave arrivals. Shear waves were identified on about 84% of the records where "ringing" did not exist. Shear wave generation, transmission, and identification are generally good. Shear wave amplitudes are usually less than the corresponding longitudinal wave amplitudes. General conclusions can be drawn as follows:

1. Shear wave amplitudes were greater in the east and northwest directions.

2. Shear wave amplitudes were smaller in the north and southeast directions.

3. The most scatter occurs in the west direction and the least in the north direction.

4. Shear wave amplitudes appear to be considerably larger from the charges which were cemented in place.

An analysis technique used in the granite report (Nicholls and Hooker, 1961) was again used in analyzing the data from tuff. A certain amount of randomness existed in the longitudinal wave amplitude from point to point around the circle. Additional variations were noted at the same gage locations from two shots at different positions but at the same depth. These variations are attributed to variations in the rock either at the shothole or over the propagation path, or both. The variations evident in the longitudinal wave amplitudes might also be expected to appear in the recorded amplitudes of the shear waves. In an attempt to remove the variations,

TABLE 3. - Surface circular array data

Shot No., explosive, charge wt., charge volume[3]	Gage location & orientation[1]	Distance R ft	Scaled distance R/V^{1/3} ft/ft	Arrival time P wave t_p ms	Arrival time S wave t_s ms	Period T ms	Scaled period T/V^{1/3} ms/ft	Acceleration A g's	Scaled acceleration AV^{1/3} g'-s-ft
8-SG 45	SW-R	101.4	994	18.14		2.90	28.4	.0627	.00640
W=.075 lb	W-R	100.0	980	18.96		2.90	28.4	.0595	.00607
V^{1/3}=.102 ft	NW-R	98.6	966	19.53		2.77	27.2	.0699	.00713
	NW-T	98.6	966		31.82	2.77	27.2	.0027	.00231
Depth[2] =.5 ft	N-R	98.0	960	19.66		2.77	27.2	.121	.0123
	N-T	98.0	960		32.76	2.39	23.4	.0275	.00280
	NE-R	98.6	966	19.22		3.02	29.6	.110	.0112
	E-R	100.0	980	20.41		3.15	30.9	.0962	.00981
	E-T	100.0	980		32.76	3.78	37.0	.0335	.00342
9-SG 45	SW-R	102.9	1010	18.33		3.27	32.0	.102	.0104
W=.075 lb	SW-T	102.9	1010		33.39	2.52	24.7	.0311	.00317
V^{1/3}=.102 ft	W-R	100.1	981	18.27		3.53	34.6	.0719	.00733
Depth=1.0 ft	NW-R	97.2	953	18.77		2.39	23.4	.0683	.00697
	NW-T	97.2	953		30.37	2.77	27.1	.0460	.00469
	N-R	96.0	941	18.65		2.52	24.7	.191	.0195
	NE-R	97.2	953	18.96		3.28	32.1	.112	.0114
	E-R	100.1	981	19.91		3.40	33.3	.102	.0104
	E-T	100.1	981		32.76	4.03	39.5	.0565	.00576

10- SG 45
W = .075 lb
$V^{\frac{1}{3}} = .102$ ft
Depth = 2.0 ft

Gage								
SW-R	104.3	1020	18.77		3.53	34.6	.0947	.00966
SW-T	104.3	1020		33.39	2.52	24.7	.0273	.00277
W-R	100.2	982	19.03		3.53	34.6	.0576	.00588
NW-R	95.9	940	18.33		2.52	24.7	.0722	.00736
NW-T	95.9	940		30.05	2.77	27.1	.0487	.00497
N-R	94.0	922	18.33		2.52	24.7	.198	.0202
N-T	94.0	922		31.94	2.27	22.2	.0147	.00150
NE-R	95.9	940	18.90		3.40	33.3	.0952	.00971
E-R	100.2	982	20.35		3.53	34.6	.0864	.00881
E-T	100.2	982			4.03	39.5	.0395	.00403

11- SG 45
W = .075 lb
$V^{\frac{1}{3}} = .102$ ft
Depth = 3.83 ft
Charge cemented
in drill hole

Gage								
SW-R	98.6	967			3.53	34.6	.0809	.00825
W-R	98.0	961			3.53	34.6	.0378	.00386
W-T	98.0	961		31.00	2.27	22.2	.0553	.00564
NW-R	98.6	967	18.96		2.52	24.7	.0422	.00430
NW-T	98.6	967		30.62	2.02	19.8	.0568	.00579
N-R	100.0	980	18.71		2.77	27.1	.0859	.00876
N-T	100.0	980		32.76	2.27	22.2	.0210	.00214
NE-R	101.4	994	19.22		3.53	34.6	.0496	.00506
E-R	102.0	1000	20.66		3.02	29.6	.0432	.00441
E-T	102.0	1000		32.19	3.28	32.1	.0541	.00552

12- SG 45
W = .075 lb
$V^{\frac{1}{3}} = .102$ ft
Depth = 1.0 ft

Gage								
SW-R	105.8	1040	18.90		3.40	33.3	.0924	.00942
SW-T	105.8	1040		33.96	2.39	23.4	.0301	.00307
W-R	100.3	983	18.90		3.15	30.9	.0640	.00653
W-T	100.3	983		32.13	2.27	22.2	.0744	.00759
NW-R	94.5	926	18.21		2.39	23.4	.0766	.00781
NW-T	94.5	926		29.67	2.52	24.7	.0426	.00435
N-R	92.0	902	17.77		2.52	24.7	.236	.0241
N-T	92.0	902		31.37	2.77	27.1	.0356	.00363
NE-R	94.5	926	18.71		3.40	33.3	.119	.0121
E-R	100.3	983	20.66		3.40	33.3	.107	.0109
E-T	100.3	983		33.89	3.78	37.0	.0511	.00521

1/ Location is 100 ft at azimuth shown. R = radial gage, T = transverse gage, values are shear motion.
2/ Depth is measured from surface to bottom of charge.

TABLE 3. - Surface circular array data

Shot No., explosive, charge wt., charge volume	Gage location & orientation [1]	Distance R ft	Scaled distance R/V^{1/3} ft/ft	Arrival time P wave t_p ms	Arrival time S wave t_s ms	Period T ms	Scaled period T/V^{1/3} ms/ft	Acceleration A g's	Scaled acceleration AV^{1/3} g's-ft
13 - SG 45	SW-R	97.2	953	17.01		3.28	32.1	.0713	.00727
W=.075 lb	SW-T	97.2	953		29.93	2.65	35.8	.0247	.00252
$V^{1/3}$=.102 ft	W-R	96.0	941	17.64		2.77	27.1	.0724	.00738
Depth = 1.5 ft	W-T	96.0	941			2.27	22.2	.0364	.00371
	NW-R	97.2	953	19.22		2.52	24.7	.0771	.00786
	NW-T	97.2	953		30.81	2.27	22.2	.0557	.00568
	N-R	100.1	981	19.53		2.77	27.1	.0821	.00837
	N-T	100.1	981		32.19	2.39	23.4	.0274	.00279
	NE-R	102.9	1010	20.10		3.28	32.1	.0813	.00829
	E-R	104.0	1020	20.60		3.53	34.6	.0821	.00837
	E-T	104.0	1020		32.76	3.91	38.3	.0374	.00381
14 - SG 45	SW-R	95.9	940	17.14		3.40	33.3	.0429	.00429
W=.075 lb	SW-T	95.9	940		30.24	3.15	30.9	.0346	.00353
$V^{1/3}$=.102 ft	W-R	94.0	922	17.39		2.77	27.1	.0411	.00419
Depth = 3.83 ft	NW-R	95.9	940	18.65		2.52	24.7	.0531	.00542
	NW-T	95.9	940		29.99			.0581	.00593
	N-R	100.2	982	19.09		2.65	26.0	.0463	.00472
	N-T	100.2	982		31.44	3.28	32.1	.0183	.00187
	NE-R	104.3	1020	19.78		3.78	37.1	.0496	.00506
	E-R	106.0	1040	20.85		3.78	37.1	.0638	.00651

15 - SG 45
W = .075 lb
V$^{1/3}$ = .102 ft
Depth = 2.5 ft

Gage								
SW-R	98.7	968	17.51		3.03	29.7	.0637	.00650
SW-T	98.7	968		31.19	3.65	35.8	.0124	.00126
W-R	96.0	941	17.58		2.90	28.4	.0691	.00705
W-T	96.0	941		31.00	2.65	26.0	.0474	.00483
NW-R	95.8	939	18.77		2.39	23.4	.0822	.00838
NW-T	95.8	939		30.05	2.02	19.8	.0608	.00620
N-R	98.1	962	18.77		2.52	24.7	.0902	.00920
N-T	98.1	962		32.44	2.39	23.4	.0229	.00233
NE-R	101.5	995	19.53		3.53	34.6	.0714	.00728
E-R	104.0	1020	20.85		3.53	34.6	.0657	.00670
E-T	104.0	1020		32.76	4.28	41.9	.0295	.00299

16 - 400 grain/ft
detonating fuse
W = .0571 lb
V$^{1/3}$ = .093 ft
Depth = 1.0 ft

Gage								
SW-R	97.3	1050	17.58		3.28	35.3	.0397	.00369
W-R	94.0	1010	17.01		2.77	29.8	.0535	.00498
W-T	94.0	1010		30.43	3.65	39.2	.0187	.00174
NW-R	94.4	1020	18.33		2.52	27.1	.0832	.00774
NW-T	94.4	1020		29.93	2.02	21.7	.0568	.00528
N-R	98.2	1060	18.90		2.52	27.1	.0762	.00709
N-T	98.2	1060		32.13	2.52	27.1	>.0192	.00179
NE-R	103.0	1110	20.22		3.28	35.3	.0560	.00521
E-R	106.0	1140	21.29		3.53	37.9	.0451	.00419
E-T	106.0	1140			4.03	43.3	.0441	.00410

17 - SG 45
2 charges
W = .150 lb
V$^{1/3}$ = .128 ft
Depth = 0.5 ft

Gage								
SW-R	108.8	850	20.16		3.53	27.6	.0895	.0115
W-R	100.7	787	18.90		2.77	21.6	.150	.0192
NW-R	90.6	708	18.02		2.65	20.7	.229	.0293
NW-T	90.6	708		28.16	2.27	17.7	.0738	.00945
N-R	86.0	672	17.14		2.52	19.7	.219	.0280
N-T	86.0	672		29.74	2.02	15.8	.0566	.00724
NE-R	90.6	708	18.14		3.28	25.6	.232	.0297
E-R	100.7	787	20.92		3.02	23.6	.256	.0328
E-T	100.7	787		33.83	3.53	27.6	.0700	.00896

1/ Location is 100 ft at azimuth shown. R = radial gage, T = transverse gage. values are shear motion.

2/ Depth is measured from surface to bottom of charge.

TABLE 3. - Surface circular array data

Shot No., explosive, charge wt., charge volume³	Gage location & orientation 1/	Distance R ft	Scaled distance R/V^⅓ ft/ft	Arrival time P wave t_p ms	Arrival time S wave t_s ms	Period T ms	Scaled period T/V^⅓ ms/ft	Accele-ration A g's	Scaled accele-ration AV^⅓ g's-ft
18- SG 45	E-R	100.0	980	20.03		2.77	27.1	.118	.0120
W=.075 lb	E-T	100.0	980		31.44	3.28	32.1	.0341	.00348
V^⅓=.102 ft	SE-R	98.6	967	19.09		2.77	27.1	.0828	.00845
Depth = 0.5 ft	SE-T	98.6	967		30.93	2.52	24.7	.0257	.00262
	S-R	98.0	961	17.26		2.52	24.7	.0586	.00598
	S-T	98.0	961		30.18	2.39	23.4	.0336	.00343
	SW-R	98.6	967	17.96		3.28	32.1	.0552	.00563
	SW-T	98.6	967		32.26	3.28	32.1	.0420	.00428
	W-R	100.0	980	18.77		2.65	26.0	.0659	.00672
	NW-R	101.4	994	20.10		2.52	24.7	.0760	.00775
	NW-T	101.4	994		32.38	2.14	21.0	.0379	.00387
19- SG 45	E-R	98.0	961	18.90		3.28	32.1	.0822	.00838
W=.075 lb	E-T	98.0	961		30.93	3.78	37.0	.0253	.00258
V^⅓=.102 ft	SE-R	98.6	967	18.40		3.40	33.3	.0556	.00567
Depth = 3.83 ft	SE-T	98.6	967		30.24	2.65	26.0	.0397	.00405
Charge cemented	S-R	100.0	980	17.39		2.77	27.1	.0547	.00558
in drill hole	S-T	100.0	980		30.11	2.65	26.0	.0464	.00473
	SW-R	101.4	994	17.70		3.78	37.0	.0535	.00546
	SW-T	101.4	994		31.37	2.52	24.7	.0437	.00446
	W-R	102.0	1000	18.84		3.15	30.9	.0502	.00512
	NW-R	101.4	994	19.28		2.65	26.0	.0597	.00609
	NW-T	101.4	994		31.44	2.52	24.7	.0515	.00525

20- SG 45
W=.075 lb
$V^{\frac{1}{3}}$=.102 ft
Depth = 2.0 ft

E-R	100.2	982	20.85		3.15	30.9	.0929	.00948
E-T	100.2	982		33.39	4.41	43.2	.0162	.00165
SE-R	95.9	940	19.59		2.77	27.1	.0682	.00696
SE-T	95.9	940		30.43	2.27	22.2	.0153	.00156
S-R	94.0	922	16.76		2.77	27.1	.0566	.00577
S-T	94.0	922		30.24	2.39	23.4	.0336	.00343
SW-R	95.9	940	17.64		3.28	32.1	.0436	.00445
SW-T	95.9	940		31.50	3.78	37.0	.0137	.00140
W-R	100.2	982	19.03		2.90	28.4	.0495	.00505
NW-R	104.3	1020	21.04		2.65	26.0	.0473	.00482

21- SG 45
W=.075 lb
$V^{\frac{1}{3}}$=.102 ft
Depth = 1.0 ft

E-R	100.3	983	20.92		3.53	34.6	.101	.0103
E-T	100.3	983		30.30	4.41	43.2	.0512	.00522
SE-R	94.5	926	19.53		2.90	28.4	.0964	.00983
SE-T	94.5	926		30.49			.00509	.000519
S-R	92.0	902	16.88		2.77	27.1	.0637	.00650
S-T	92.0	902		30.11	2.52	24.7	.0495	.00413
SW-R	94.5	926	17.20		3.15	30.9	.0573	.00584
SW-T	94.5	926		31.44	3.53	34.6	.0256	.00261
W-R	100.3	983	19.09		2.77	27.1	.0645	.00658
W-T	100.3	983			2.39	23.4	.0117	.00119
NW-R	105.8	1040	21.86		2.77	27.1	.0555	.00566

22- SG 45
W=.075 lb
$V^{\frac{1}{3}}$=.102 ft
Depth = 1.5 ft

E-R	96.0	941	19.78		3.15	30.9	.0930	.00949
E-T	96.0	941		32.38	3.78	37.0	.0311	.00317
SE-R	97.2	953	19.66		3.15	30.9	.0712	.00726
SE-T	97.2	953		32.07	2.77	27.1	.0283	.00289
S-R	100.1	981	18.71		2.77	27.1	.0495	.00505
S-T	100.1	981		31.82	4.03	39.5	.0153	.00156

1/ Location is 100 ft at azimuth shown. R = radial gage, T = transverse gage, values are shear motion.
2/ Depth is measured from surface to bottom of charge.

TABLE 3. - Surface circular array data

Shot No., explosive, charge wt., charge volume³	Gage location & orientation[1/]	Distance R ft	Scaled distance R/V^⅓ ft/ft	Arrival time P wave t_p ms	Arrival time S wave t_s ms	Period T ms	Scaled period T/V^⅓ ms/ft	Acceleration A g's	Scaled acceleration AV^⅓ g's-ft
22 - SG 45 W=.075 lb V^⅓=.102 ft Depth = 1.5 ft	SW-R	102.9	1010	19.85		2.90	28.4	.0436	.00445
	SW-T	102.9	1010		34.71	3.02	29.6	.0160	.00163
	W-R	104.0	1020	20.10		3.15	30.9	.0434	.00443
	W-T	104.0	1020			2.52	24.7	.00434	.000443
	NW-R	102.9	1010	20.66		2.77	27.1	.0573	.00584
	NW-T	102.9	1010		33.45	2.39	23.4	.0309	.00315
23 - SG 45 W=.075 lb V^⅓=.102 ft Depth = 3.83 ft	E-R	94.0	922	19.66		3.40	33.3	.0737	.00752
	E-T	94.0	922		30.24	3.65	35.8	.0420	.00428
	SE-R	95.9	940	19.28		3.65	35.8	.0549	.00560
	SE-T	95.9	940		30.81	3.02	29.6	.0405	.00413
	S-R	100.2	982	18.21		3.02	29.6	.0354	.00361
	S-T	100.2	982		31.56	2.65	26.0	.0275	.00281
	SW-R	104.3	1020	19.59		3.15	30.9	.0324	.00330
	SW-T	104.3	1020		33.52	2.39	23.4	.0294	.00300
	W-R	106.0	1040	19.59		4.16	40.8	.0310	.00316
	W-T	106.0	1040			2.77	27.1	.0157	.00160
	NW-R	104.3	1020	20.79		2.52	24.7	.0296	.00302
	NW-T	104.3	1020		33.45	2.14	21.0	.0414	.00422

24- SG 45 W=.075 lb V^(1/3)=.102 ft Depth = 2.5 ft								
E-R	96.0	941	19.59		3.40	33.3	.0994	.0101
E-T	96.0	941		32.07	3.78	37.0	.0545	.00556
SE-R	95.8	939	19.59		3.28	32.1	.0697	.00711
SE-T	95.8	939		31.50	3.28	32.1	.1372	.00379
S-R	98.1	962	18.33		2.77	27.1	.0531	.00542
S-T	98.1	962		31.63	2.77	27.1	.0330	.00337
SW-R	101.5	995	19.09		3.40	33.3	.0410	.00418
W-R	104.0	1020	19.91		3.40	33.3	.0410	.00418
W-T	104.0	1020		34.78	2.65	26.0	.0210	.00214
NW-R	104.3	1020	21.17		2.90	28.4	.0462	.00471
NW-T	104.3	1020		33.39	2.39	23.4	.0358	.00365

25- SG 45 W=.075 lb V^(1/3)=.102 ft Depth = 2.5 ft								
E-R	96.1	942	20.16		3.28	32.1	.123	.0125
E-T	96.1	942		32.19	3.78	37.0	.0467	.00476
SE-R	94.3	925	19.23		3.40	33.3	.0742	.00757
SE-T	94.3	925		30.62	3.02	29.6	.0340	.00347
S-R	96.1	942	17.64		2.77	27.1	.0655	.00668
S-T	96.1	942		30.93	2.52	24.7	.0458	.00467
SW-R	100.2	982	18.71		3.53	34.6	.0436	.00445
SW-T	100.2	982		34.21	2.77	27.1	.0384	.00392
W-R	104.1	1020	20.29		3.15	30.9	.0434	.00434
W-T	104.1	1020		34.95	2.77	27.1	.0194	.00198
NW-R	105.7	1040	21.29		2.90	28.4	.0425	.00434
NW-T	105.7	1040		34.02	2.39	23.4	.0247	.00252

1/ Location is 100 ft at azimuth shown. R = radial gage, T = transverse gage, values are shear motion.
2/ Depth is measured from surface to bottom of charge.

27.

TABLE 3. - Surface circular array data

Shot No., explosive, charge wt., charge volume$^{\frac{1}{3}}$	Gage location & orientation 1/	Distance R ft	Scaled distance R/V$^{\frac{1}{3}}$ ft/ft	Arrival time P wave t_p ms	Arrival time S wave t_s ms	Period T ms	Scaled period T/V$^{\frac{1}{3}}$ ms/ft	Scaled Acceleration A g's	Scaled acceleration A V$^{\frac{1}{3}}$ g's-ft
26 - 400 grain/ft detonating fuse W=.0571 lb V$^{\frac{1}{3}}$=.093 ft Depth = 1.0 ft	E-R	94.0	1010	19.47		3.27	35.2	.0930	.00865
	E-T	94.0	1010		31.69	5.29	56.9	.0390	.00363
	SE-R	94.4	1020	19.66		3.02	32.5	.0697	.00648
	SE-T	94.4	1020		30.24	2.27	24.4	.0202	.00188
	S-R	98.2	1060	18.90		2.77	29.8	.0442	.00411
	S-T	98.2	1060		31.31	3.53	37.9	.0360	.00335
	SW-R	103.0	1110	19.78		3.40	36.6	.0299	.00278
	SW-T	103.0	1110		34.97	3.65	39.2	.0448	.00417
	W-R	106.0	1140	20.29		2.65	28.5	.0248	.00231
	W-T	106.0	1140		35.28	2.52	27.1	.0303	.00282
	NW-R	105.7	1140	21.36		2.52	27.1	.0314	.00292
	NW-T	105.7	1140		34.52	3.91	42.0	.0154	.00143

1/ Location is 100 ft at azimuth shown. R = radial gage, T = transverse gage, values are shear motion.
2/ Depth is measured from surface to bottom of charge.

TABLE 4.- Longitudinal acceleration [1]/ as a function of depth and direction

Shot & depth	Direction N	NE	E	SE	S	SW	W	NW
8- 9.5 ft	.107	.0980	.0909			.0612	.0563	.0625
17 [2]/ 0.5 ft	.0783	.0979	.151			.0675	.0883	.0965
18 - 0.5 ft			.111	.0744	.0516	.0496	.0619	.0745
9 - 1.0 ft	.158	.0960	.0955			.105	.0674	.0587
12- [3]/ 1.0 ft	.171	.0930	.101			.105	.0607	.0601
16 [3]/ - 1.0 ft	.0833	.0711	.0621			.0421	.0504	.0808
21- 1.0 ft			.0957	.0756	.0460	.0451	.0611	.0628
26 [3]/ - 1.0 ft			.0874	.0676	.0484	.0379	.0342	.0432
13- 1.5 ft	.0772	.0838	.0874			.0600	.0596	.0662
22- 1.5 ft			.0767	.0611	.0465	.0449	.0462	.0590
10- 2.0 ft	.153	.0783	.0816			.101	.0543	.0593
20- 2.0 ft			.0877	.0561	.0436	.0359	.0468	.0504
15- 2.5 ft	.0798	.0713	.0700			.0575	.0570	.0687
24- 2.5 ft			.0820	.0571	.0470	.0407	.0437	.0492
25- 2.5 ft			.102	.0580	.0542	.0412	.0462	.0481
14- 3.83 ft	.0437	.0528	.0722			.0346	.0318	.0437
23- 3.83 ft [4]/			.0571	.0452	.0334	.0345	.0351	.0315
11- 3.83 ft [4]/	.0807	.0486	.0432			.0741	.0378	.0333
19- 3.83 ft [4]/			.0725	.0500	.0513	.0525	.0502	.0586

[1]/ Adjusted to $R/V^{\frac{1}{3}} = 1000$ and $V^{\frac{1}{3}} = .102$.

[2]/ Two charges.

[3]/ Detonating fuse-decoupled shot.

[4]/ Charges cemented in shothole.

TABLE 5. - Shear acceleration as a function of depth and direction 1/

Shot & depth	Direction N	NE	E	SE	S	SW	W	NW
8- 0.5 ft	.0243	-- 2/	.0315					.0204
17- 0.5 ft 3/	.0203	----	.0414			----	----	.0312
18- 0.5 ft	----	----	.0322	.0231	.0297	.0379	----	.0373
9- 1.0 ft	.0258	----	.0529			.0320	----	.0395
12- 1.0 ft	>.0211	----	.0486			.0342	.0708	.0323
16- 1.0 ft 4/			.0609				.0177	.0553
21- 1.0 ft			.0485	.0040	.0302	.0201	.0111	----
26- 1.0 ft 4/			.0366	.0196	.0395	.0569	.0417	.0212
13- 1.5 ft 4/	.0259	----	.0400	.0243	.0144	.0213	.0301	.0480
22- 1.5 ft			.0256			.0165	.0462	.0318
10- 2.0 ft	.0114	----	.0374			.0292	----	.0402
20- 2.0 ft			.0154	.0126	.0260	.0113	----	----
15- 2.5 ft	.0203	----	.0313			.0112	.0392	.0500
24- 2.5 ft			.0450	.0305	.0292	----	.0224	.0381
25- 2.5 ft			.0386	.0266	.0379	.0362	.0207	.0279
14- 3.83 ft	.0173	----	----			.0285	----	.0480
23- 3.83 ft			.0325	.0338	.0260	.0314	.0178	.0441
11- 3.83 ft 5/	.0192	----	.0541			----	.0489	.0512
19- 3.83 ft 5/			.0224	.0357	.0437	.0430	----	.0508

1/ Adjusted to $R/V^{1/3}$ = 1000 and $V^{1/3}$ = .102.
2/ -- signifies no identifiable shear motion.
3/ Two charges.
4/ Detonating fuse- decoupled shot.
5/ Charges cemented in shotholes.

the shear amplitudes were expressed as a ratio of the longitudinal amplitudes and are given in table 6. General conclusions can be drawn as follows:

1. Largest values for the ratio of amplitudes were obtained in the south and northwest directions.

2. Smallest ratio values were obtained in the north direction.

3. Largest values of the ratio of amplitude were obtained from shots 11, 14, 19, 23, 24, and 25, which were the deepest shots.

4. A few high values for the ratio were obtained from shots 16 and 26 which were the decoupled shots.

All period data were converted to frequency so that the predominant frequencies obtained from shear and longitudinal waves could be compared. The average frequency of the longitudinal waves was 335 ± 37 cycles per second. The average frequency for the shear waves was 358 ± 69 cycles per second. The average of the ratios of longitudinal frequency to shear frequency was 1.06 ± .17. These data verify that no real differences exist in the frequencies of the two waves as recorded. Filtering techniques under these conditions would have added nothing to identification of the shear waves.

Table 7 gives a summary of the data obtained from the circular array. The velocities and amplitudes are averaged for each direction. The elastic constants are calculated assuming the density of tuff to be 106 pounds per cubic foot. No real correlation between the elastic constants and shear wave amplitude was discernible. The amplitude of the shear wave was strongly affected by direction of propagation. For many individual pairs of records, a correlation exists between the shear and longitudinal wave amplitudes. The shear amplitude is usually larger if the longitudinal amplitude is small and vice versa.

A strong velocity gradient exists in the test area increasing in the south and southwest directions. Additionally, shot point location has a strong effect on propagation velocities. Those shot points east of a north-south

TABLE 6. - A_s/A_p, ratio of shear to longitudinal amplitudes

Shot & depth	Direction N	NE	E	SE	S	SW	W	NW
8- .5 ft	.227	.1/	.347			----	----	.326
17- .5 ft 2/	.260	----	.275			----	----	.324
18- .5 ft			.290	.310		.764	----	.501
9- 1.0 ft	----	----	.554		.575	.305	----	.673
12- 1.0 ft	.109	----	.481			.326	1.17	.538
16- 1.0 ft 3/	>.254	----	.981				.351	.685
21- 1.0 ft			.507	.053	.657	.447	.182	----
26- 1.0 ft 3/			.419	.290	.815	1.50	1.22	.492
13- 1.5 ft	.335		.458			.355	.505	.725
22- 1.5 ft			.333	.317	.310	.367	1.00	.540
10- 2.0 ft	.075	----	.458			.289	----	.678
20- 2.0 ft			.176	.225	.596	.315	----	----
15- 2.5 ft	.255	----	.439			.195	.688	.728
24- 2.5 ft			.549	.534	.621	----	.513	.775
25- 2.5 ft			.378	.460	.699	.879	.448	.580
14- 3.83 ft	.396	----	----	.737	.778	.824	----	1.10
23- 3.83 ft	.238	----	.569			.910	.507	1.40
11- 3.83 ft 4/			1.25			----	1.29	1.54
19- 3.83 ft 4/			.309	.714	.852	.819	----	.867

1/ Signifies no identifiable shear waves.
2/ Two charges.
3/ Detonating fuse-decoupled shot.
4/ Charges cemented in shothole.

TABLE 7.- **Summary- Circular array data**

	N	NE	E	SE	S	SW	W	NW
Longitudinal velocity V_p, ft/sec	5150	5130	4930	4970	5480	5430	5330	5070
Shear velocity V_s, ft/sec	3020		3080	3120	3160	3090	3070	3160
Young's modulus E, $\times 10^6$ psi	.517		.512	.524	.573	.552	.541	.541
Poisson's ratio	.238		.180	.175	.251	.261	.252	.182
Modulus of rigidity μ, $\times 10^6$ psi	.209		.217	.223	.229	.219	.216	.229
Lame's constant λ, $\times 10^6$ psi	.190		.122	.120	.231	.238	.219	.131
Bulk Modulus k, $\times 10^6$ psi	.329		.267	.269	.383	.384	.363	.284
Longitudinal amplitude A_p, g's (average)	.103	.0791	.0856	.0606	.0469	.0574	.0521	.0583
Shear amplitude A_s, g's (average)	.0206	----	.0386	.0233	.0307	.0293	.0333	.0393
Ratio, A_s/A_p	.215	----	.462	.404	.655	.437	.414	.656

34.

line through the center of the area yield velocities up to 400 feet per
second faster, measured in any radial direction, than shot points west
of the center line. Most of these shot points are less than 10 feet apart.
On the basis of the in situ velocity changes noted and the laboratory de-
termined values, the tuff appears to be a very inhomogeneous mass with
many stringers, lenses, boulders, etc. The medium changes drastically
laterally and with depth and these variations are not visually detectable.

Discussion of Results

No unique physical mechanism was determined as the source of generated
shear waves. Charge depth, maximum crater formation, minimum shot
hole fracturing through decoupled shots did not have strong effects on the
amplitude of the shear wave generated. The amplitude of both longitudinal
and shear waves was dependent upon the direction of propagation. The
ratio of shear to longitudinal amplitudes also varied with azimuth.

The period of frequency of both wave types varied slightly with azimuth.
However, no significant differences existed between the predominant fre-
quencies of either wave due to depth, shothole condition, or direction.

The results generally compare with those obtained from similar tests in
granite (Nicholls and Hooker, 1962). Similar results have also been re-
ported from large chemical explosive tests and from nuclear tests.

Conclusions

The primary purpose of this portion of the program was to study the
generation and propagation of shear waves from an explosive source and
to compare these results to theory and to longitudinal waves propagated
in the same media. It was believed that a better understanding of shear
waves might assist in the identification of the type of earth motion which
generated particular seismic waves. That is, some distinction between
man-made and naturally-induced seismic waves might provide a positive
nuclear detection system.

The study of shear waves appeared to offer a simple solution since a
point source theoretically should not generate shear waves. Studies in
two rock types, granite and tuff, indicate that under the test conditions

imposed, shear waves are always present. The presence or absence of shear waves does not appear to be adequate to delineate between explosive and natural seismic sources.

In both rock types, it is assumed that conditions approaching a point source were never met sufficiently to preclude shear wave generation. Additionally, the inhomogeneity and isotropy of both rock types may have contributed greatly to the shear wave generation. Any departure from symmetry at the source or from a uniform media generates shear waves or converts other waves to shear waves. The amount of fracturing and crushing of rock at the source appears to have little bearing on the amplitude of shear waves.

A directional effect was noted in both granite and tuff with shear wave enhancement in preferred directions in both rock types. The directional effect undoubtedly varies from one site to another and probably within a site if the medium is not uniform.

Shear waves are probably generated by all explosive sources because of non-symmetry and enhanced by conversion during propagation.

36.

CHARACTERISTIC IMPEDANCE COUPLING

Test Purpose

The primary purpose of the linear array test series in tuff was to study the effects of characteristic impedance matching in the tuff medium. The characteristic impedance of a rock is defined as the product of rock density and longitudinal propagation velocity. Similarly, for an explosive, characteristic impedance is the product of explosive density and detonation velocity. The ratio of the characteristic impedance of the explosive to the characteristic impedance of the rock is defined as the characteristic impedance ratio. It has been shown that if this ratio is nearly 1.0, the pressure or stress transmitted to the medium is approximately the pressure generated by the explosion and that the energy transferred to the rock is a maximum (Nicholls and Hooker, 1962). If the ratio is much less than 1.0, the stress in the medium is greater than that predicted by acoustic theory but the amount of energy transferred is considerably less. Shock wave theory indicates that pressure enhancement may be greater than the factor of 2.0 predicted by acoustic theory (Courant and Friedricks, 1948; Nicholls and Duvall, 1963).

The test was designed to provide data for a study of the effects of characteristic impedance on explosion-generated strain, acceleration, and particle velocity and strain energy. The tests in granite covered a range of characteristic impedance ratios from .16 to .52. The tests in tuff as planned would provide data over a range of ratios from .40 to 1.90. This range was not accomplished in the tuff however.

Experimental Procedure

The linear array test area was prepared by air drilling 6-inch diameter shotholes and 3-inch diameter gage holes vertically to a depth so that the center of gravity of the explosive charges and the recording gages would be on a common horizontal plane at an average depth of 26 feet. In the process of drilling, air blast caused considerable erosion on the walls of the holes. Subsequently, all gage holes were reamed to 3-1/4 inches in diameter to insure easier and more reliable placement of the gages.

38.

A core of rock with a strain gage and accelerometer attached, as previously described in this report, was cemented into each gage hole. The cores were tuff, obtained from the Nevada Test Site. On the basis of laboratory determined mechanical properties of the tuff core (table 1), the tuff could be divided into two types. The distinction between types was not as great as for the Hackberry Mountain tuff and did not significantly affect the results. The properties of the grout used to cement these gages in were given in table 1. These gage units were placed with sufficient accuracy so that shot-to-gage distances were known within 0.2 feet and were oriented to measure radial strains and particle motions. A plan view of the test area is shown in figure 10. Two parallel sets of drillholes are shown. The B1-B4 series of holes were used for small charges detonated as calibration shots. Holes S1-S8 were shotholes and holes Aϵ1 thru Aϵ12 were gage holes.

The shooting sequence in each of the two arrays was from the outermost hole toward the gage holes so that no broken rock was between the shot and the gages. Strain and particle acceleration were recorded from each shot at six different shot-to-gage distances. No data were obtained from one accelerometer because of a broken lead wire down in the hole which could not be reached for repair.

The explosive charges were single, rigid packed cartridges 5-1/2 inches in diameter and 30 inches in length. Physical properties of the four explosives used are given in table 8. Each charge was primed at the bottom with a No. 6 seismic electric blasting cap and a 50-gram PETN booster. Detonation rates of the explosives were measured by inserting a pair of targets 2 feet apart in the cylindrical charge and recording the time for the detonation wave to travel from one target to the other on a microsecond chronograph counter. Three feet of sand stemming was sufficient to contain three of the explosives and yet permit the hole to blow so that reentry could be made for cavity measurements. However, the first two shots of SG 45 did not blow, and after unsuccessful attempts at cavity reentry, the sand stemming was reduced to 2 feet for the remaining SG 45 shots.
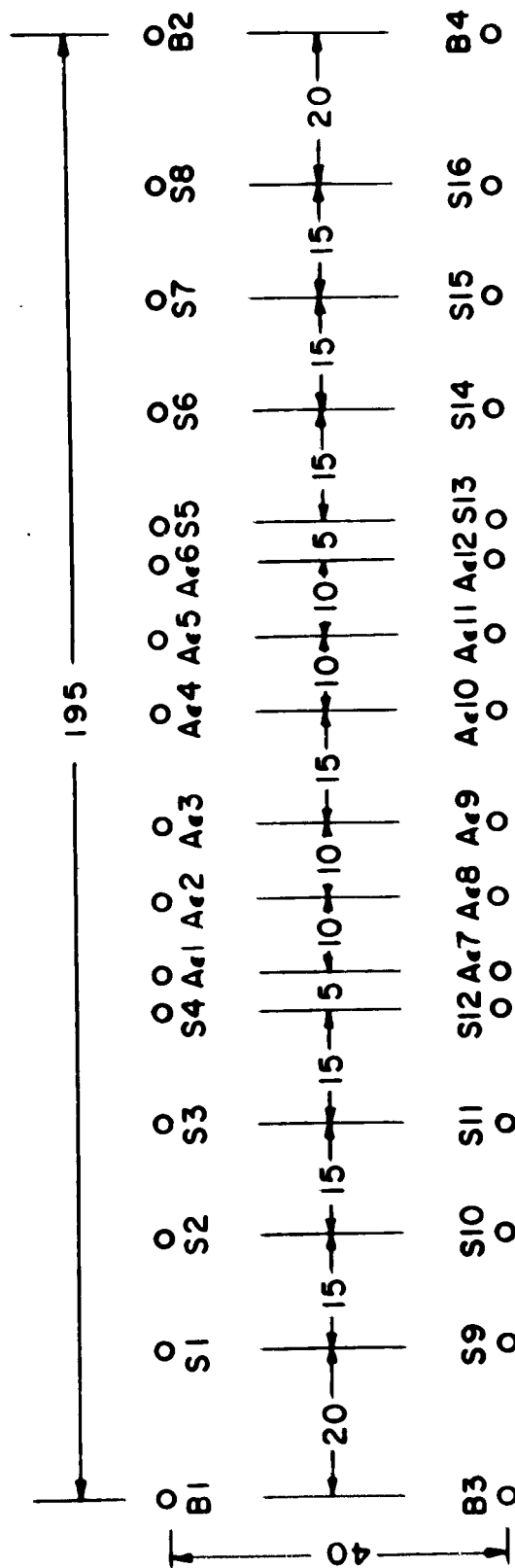
Fig. 10 - Plan View of Linear Array Test Area.

TABLE 8.- Properties of explosives

Explosive	Weight density ρ lb/ft³	Detonation velocity C ft/sec	Characteristic impedance (ρC)_e lb-sec/in³	Impedance ratio $\frac{(\rho C)_e}{(\rho C)_r}$	Detonation pressure P lb/in² x 10⁶	Ballistic mortar parameter NRT ft-lb/ft³ x 10⁶	Total energy $\frac{NRT}{\gamma-1}$ ft-lb/ft³ x 10⁶
AD 10	64.6	7,570	8.8	.76	.20	14.1	70.5
AD 20A	52.7	10,200	9.7	.84	.32	16.2	81.0
AD-P	47.6	10,500	9.0	.78	.32	14.7	73.5
SG 45	70.9	17,540	22.3	1.92	1.11	24.8	124

Data Analysis

A set of typical records obtained in tuff is shown in figure 11. Trace 2 represents the radial particle velocity at gage A5 as electronically integrated from the recorded acceleration. At the shot-to-gage distances of the test series, the pulse shapes of radial strain and radial particle velocity should be identical as is evident in comparing the early parts of traces 1 and 2. In later portions of the traces, agreement is not expected because of reflections from the air-tuff surface. The time and amplitude measurements made on each recorded pulse for detailed study are shown in figure 12.

Strain

The primary purpose of the analysis of the strain pulse data was to determine how radial strain was propagated in tuff and how it was affected by different explosives. Also, the arrival times of the strain pulses were used in the determination of the subsurface propagation velocity. An attempt was made to record a zero or detonation time for the first few shots but extreme shot noise which deteriorated the quality of these records forced abandonment of the procedure. As a result, interval arrival times, using the closest gage to the shot as a reference, were used for propagation velocity measurements. Velocity variations were noted at depth as in the surface studies. However, an additional contributing factor to the variations in the subsurface data may have been that propagation velocity varied with stress level. The average propagation velocity for all 16 shots was 6,080 ± 460 feet per second.

From strain record measurements, peak strain versus scaled distance was plotted on log-log coordinates for each of the 16 shots. Study of these plots revealed that nominal gage sensitivities were not proper and to some extent, gage corrections would be needed. Probable causes of such differences in sensitivity are either in the elastic properties of the cement or the degree of bonding between the gage and rock. To obtain the amplitude corrections, a least-square line was determined for each shot and an analysis of variance made for the total number of shots. The statistical analysis indicated that a common slope could be used for all of the data. A standard gage was selected from each array and ratios of the

1. Strain (μ in/in) recorded at gage ϵ5

34.6

2. Velocity (in/sec) integrated from gage A5

.925

3. Acceleration (g's) recorded at gage 5

4.52
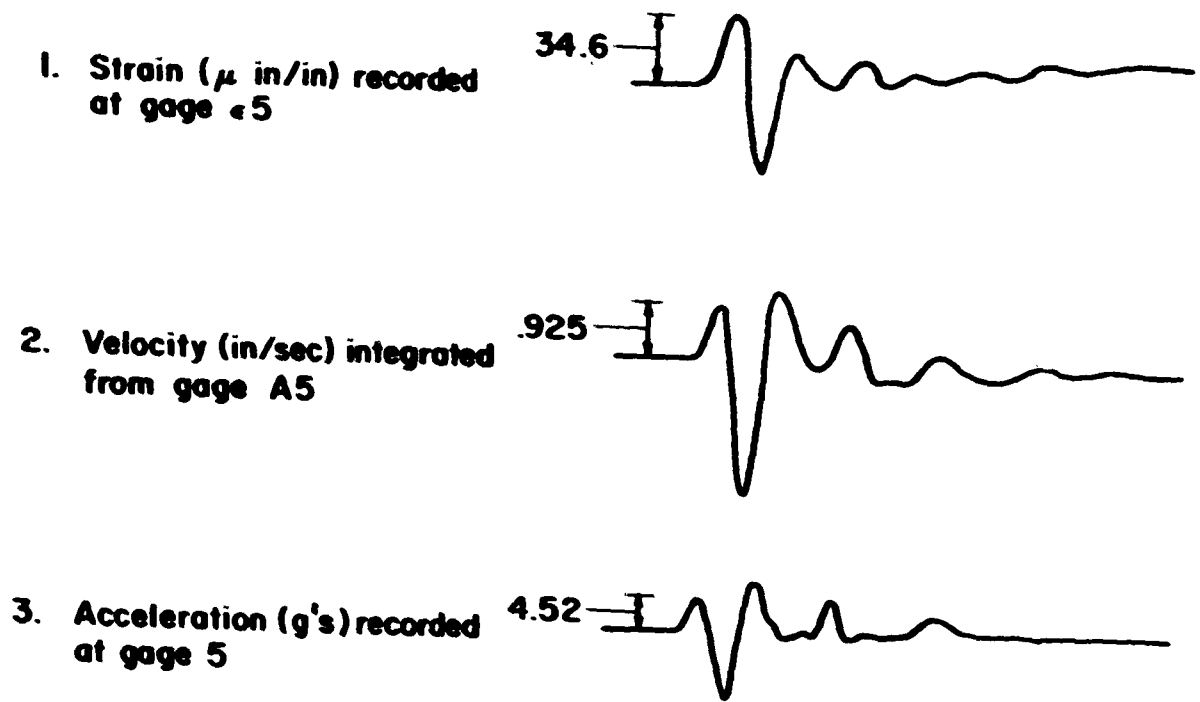
6.250 milliseconds

Shot no. 17-S6
Explosive-26.6 lb ADIO
Distance = 30 ft

Fig. 11 - Typical Pulse Shapes.
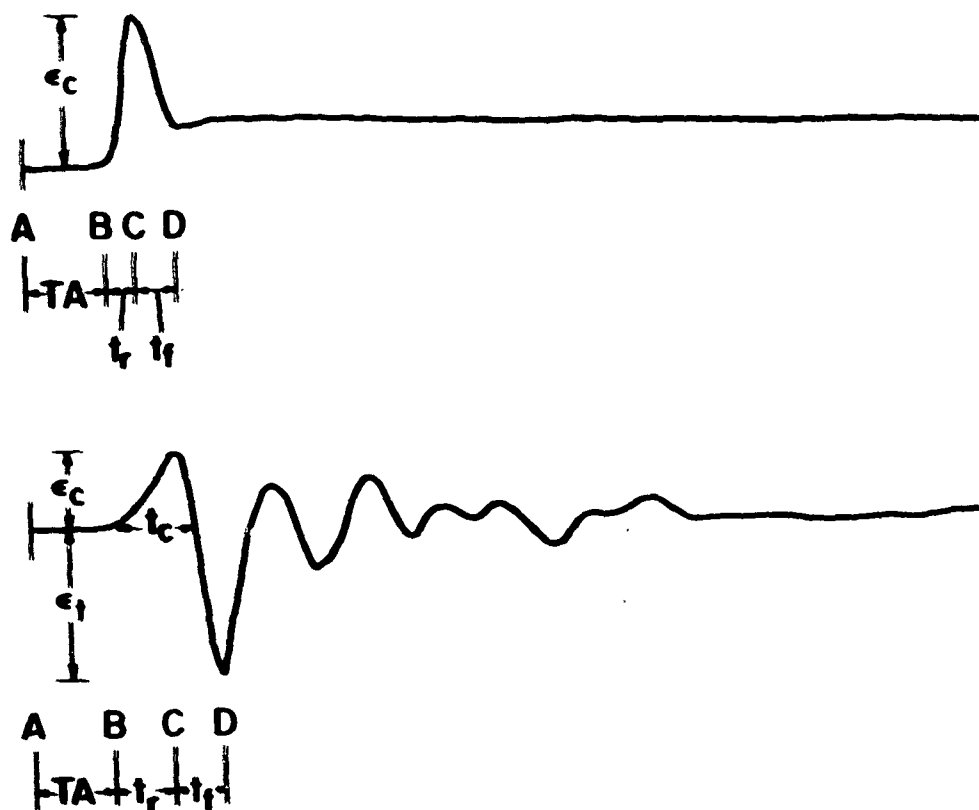
A. Detonation of charge
B. Start of pulse
C. First peak amplitude
D. End of fall time
TA. Arrival time for

t_r. Rise time
t_f. Fall time
t_c. Compression or positive time
ϵ_c. Peak positive amplitude
ϵ_t. Tensile or negative amplitude

Fig. 12 - Pulse Record Measurements.

44.

recorded strain to the strain value on the common slope line at each of the other gage positions for each array were obtained for each shot. The average ratio obtained for each gage was as follows: $\epsilon 1$-1.51, $\epsilon 2$-2.44, $\epsilon 3$-3.09, $\epsilon 4$-2.06, $\epsilon 5$-2.91, $\epsilon 6$- standard, $\epsilon 7$-1.53, $\epsilon 8$-3.01, $\epsilon 9$-standard, $\epsilon 10$-1.23, $\epsilon 11$-3.55, $\epsilon 12$-1.35, and these ratios were applied as a multiplying correction factor to the compressive and tensile amplitudes of each strain recording. The strain data, with adjusted amplitudes, are given in tables 9 to 12.

Plots of adjusted strain data versus scaled distance for each explosive are given in figures 13 to 16 and show that strain can be represented as a function of distance by the equation:

$$\epsilon = K \, (R/V^{\frac{1}{3}})^{m} \tag{1}$$

where

ϵ = peak compressive strain,

K = strain intercept constant at a scaled distance of 1,

R = shot-to-gage distance,

$V^{\frac{1}{3}}$ = cube root of the charge volume, scaling factor,

$R/V^{\frac{1}{3}}$ = scaled distance,

and

m = exponent or slope of the regression curve.

The tensile phase of the strain pulses was found to be comparatively larger than the compressive phase over most of the scaled distance range covered in these tests. This presented problems in determining gain settings for obtaining optimum records during the field program. Log-log coordinate plots of the adjusted tensile strain versus scaled distance are shown in figures 17 to 20. The tensile strain data were represented by the same function given by equation (1). Only the data represented by circles on each plot were used for the regression analysis.

The strain data represented by triangles indicates that the tensile phase of the strain pulse reaches a maximum at a scaled distance of about

TABLE 9.- Linear array strain data- Explosive AD-10

Shot designation, charge weight, charge volume, volume	Gage No.	Shot-to-gage distance R ft	Scaled distance R/V⅓ ft/ft⅓	Peak compressive strain ϵ_c in/in x10⁻⁶	Tensile strain ϵ_t in/in x10⁻⁶	Rise time t_r sec x10⁻³	Full compression time t_f sec x10⁻³	Compression time t_e sec x10⁻³	Arrival time t_A sec x10⁻³
5-B10 W=26.6 lb V=412 cu ft V⅓=.745 ft	ε-7	35	47.0	21.6	26.2	2.083	2.020	3.472	----
	ε-8	45	60.4	12.1	17.6	2.336	2.778	3.662	1.515
	ε-9	55	73.8	6.59	13.5	3.329	2.952	4.585	3.015
	ε-10	70	93.9	4.39	9.37	3.329	2.952	4.899	5.779
	ε-11	80	107.0	4.05	4.54	3.894	3.078	5.465	7.726
	ε-12	90	121.0	4.55	7.03	4.609	2.967	6.187	9.407
9-B13 W=26.6 lb V=412 cu ft V⅓=.745 ft	ε-7	60	80.5	7.73	14.2	3.000	2.875	4.375	8.500
	ε-8	50	67.1	7.77	12.1	2.904	2.715	4.104	6.944
	ε-9	40	53.7	15.5	31.4	3.157	2.083	3.914	5.429
	ε-10	25	33.6	35.1	42.2	1.515	2.336	2.778	2.778
	ε-11	15	20.1	87.7	21.9	1.515	*	*	1.010
	ε-12	5	6.71	1032	0	2.525	*	*	----
12-B1 W=26.6 lb V=412 cu ft V⅓=.745 ft	ε-1	50	67.1	15.0	24.3	2.652	2.904	4.040	----
	ε-2	60	80.5	9.59	19.0	2.875	2.750	4.063	1.750
	ε-3	70	93.9	6.40	11.5	2.750	2.563	4.063	3.625
	ε-4	85	114	3.96	7.52	3.580	2.701	4.711	5.967
	ε-5	95	127	*	*	*	*	*	*
	ε-6	105	141	8.47	4.15	4.146	2.764	5.528	9.548
17-B6 W=26.6 lb V=412 cu ft V⅓=.745 ft	ε-1	75	101	5.72	10.3	4.356	2.399	5.556	9.154
	ε-2	65	87.8	10.6	12.1	3.032	2.490	5.151	6.910
	ε-3	55	73.8	9.61	14.4	3.015	2.575	4.209	5.465
	ε-4	40	53.7	20.0	29.7	2.399	2.462	3.598	3.329
	ε-5	30	40.3	34.6	43.7	2.210	2.210	3.283	1.326
	ε-6	20	26.8	66.7	46.3	1.452	2.083	2.715	----

*= No data.   ----= Gage used as reference for arrival time measurement.

TABLE 10.- Tamped entry strain data- Explosive AD 20A

Shot designation, charge weight, charge volume	Gage No.	Shot-to-gage distance R ft	Scaled distance R/√³ ft/ft	Peak compressive strain ε_c in/in x10^-6	Tensile strain ε_t in/in x10^-6	Rise time t_r sec x10^-3	Fall time t_f sec x10^-3	Compression time t_c sec x10^-3	Arrival time T_A sec x10^-3
4- S16 W=21.7 lb V_s=412 cu ft V#=.745 ft	-7	105	141	2.94	4.48	5.088	2.575	6.344	9.611
	-8	95	127	3.55	4.94	3.625	2.625	5.000	8.438
	-9	85	114	3.61	6.09	3.788	2.462	4.924	5.808
	-10	70	93.9	6.22	14.6	4.334	2.513	5.653	3.141
	-11	60	80.5	9.59	21.1	3.141	2.513	4.334	1.759
	-12	90	67.1	17.8	28.5	3.266	2.764	4.523	----
8- S11 W=21.7 lb V_s=412 cu ft V#=.745 ft	-7	80	26.8	56.2	26.8	1.908	2.387	3.141	----
	-8	30	40.3	24.4	13.5	1.759	2.324	3.141	1.570
	-9	40	53.7	16.2	31.1	2.513	2.513	3.706	3.204
	-10	55	73.8	7.75	15.9	3.266	3.015	4.523	5.528
	-11	65	87.2	5.93	12.7	3.392	3.015	4.648	7.726
	-12	75	101	5.63	9.10	3.518	3.078	5.025	9.234
16- S7 W=21.7 lb V_s=412 cu ft V#=.745 ft	-1	90	121	2.87	7.50	4.774	2.638	6.281	8.794
	-2	80	107	4.95	8.42	3.957	2.450	5.151	*
	-3	70	93.9	3.83	10.7	3.832	2.513	5.025	5.528
	-4	55	73.8	7.81	21.2	3.455	2.575	4.648	3.266
	-5	45	60.4	13.2	30.3	2.952	2.513	4.083	.942
	-6	35	47.0	32.0	46.8	2.513	2.324	3.643	----
19- S4 W=21.7 lb V_s=412 cu ft V#=.745 ft	-1	5	6.71	2344	0	1.914	*	*	----
	-2	15	20.1	96.1	7.39	1.563	3.125	4.188	1.313
	-3	25	33.6	52.2	23.8	1.938	2.125	3.313	3.188
	-4	40	93.7	18.6	34.0	2.188	2.688	3.438	5.375
	-5	50	67.1	13.4	22.7	3.125	2.813	4.438	7.438
	-6	60	80.5	7.27	14.9	3.750	3.125	5.063	8.125

*= No data. ---- = Gage used as reference for arrival time measurement.

TABLE 11.- Linear array strain data, Explosive AD-2

Shot designation, charge weight, charge volume	Gage No.	Shot-to gage distance R ft	Scaled distance $R/W^{1/3}$ ft/ft	Peak compressive strain ε_c in/in x10^-6	Tensile strain ε_t in/in x10^-6	Rise time t_r sec x10^-3	Fall time t_f sec x10^-3	Compression time t_c sec x10^-3	Arrival time T_A sec x10^-3
6- 815 $W=19.6$ lb $V_q=.412$ cu ft $V^{1/3}=.745$ ft	6-7	80	121	3.01	7.74	4.375	2.500	5.563	9.500
	6-8	80	107	5.21	6.05	3.750	2.625	5.188	*
	6-9	70	93.9	4.67	12.0	3.875	2.688	5.125	5.938
	6-10	55	73.8	8.43	21.8	3.313	2.750	4.563	3.125
	6-11	45	60.4	*	*	*	*	*	*
	6-12	35	47.0	35.9	55.8	2.475	2.601	3.617	----
10- 812 $W=19.6$ lb $V_q=.412$ cu ft $V^{1/3}=.745$ ft	10-7	5	6.71	1060	0	2.136	*	*	----
	10-8	15	20.1	104	49.7	1.884	3.706	4.397	1.570
	10-9	25	33.6	40.6	33.6	1.633	2.261	2.952	3.141
	10-10	40	53.7	14.3	24.1	2.625	2.750	3.894	6.100
	10-11	50	67.1	*	*	*	*	*	*
	10-12	60	80.5	3.51	7.01	3.141	3.141	4.271	8.920
14- 88 $W=19.6$ lb $V_q=.412$ cu ft $V^{1/3}=.745$ ft	14-1	105	141	2.43	5.41	4.837	2.261	5.967	9.296
	14-2	95	127	3.96	9.08	4.209	2.450	5.528	*
	14-3	85	114	3.68	6.77	3.706	2.575	5.025	*
	14-4	70	93.9	5.13	13.6	3.706	2.575	4.962	3.518
	14-5	60	80.5	8.26	15.0	3.141	2.638	4.523	1.131
	14-6	50	67.1	11.9	19.0	3.015	2.764	4.271	----
18- 83 $W=19.6$ lb $V_q=.412$ cu ft $V^{1/3}=.745$ ft	18-1	20	26.8	77.6	36.4	1.452	2.588	2.841	----
	18-2	30	40.3	41.7	31.2	2.146	2.273	3.409	1.389
	18-3	40	53.7	25.9	25.9	2.399	2.146	3.598	3.409
	18-4	55	73.8	11.7	17.7	3.455	2.638	4.585	5.025
	18-5	65	87.2	7.30	11.9	4.230	2.778	5.492	7.386
	18-6	75	101	4.65	7.53	4.375	2.875	5.688	8.750

*= No data. ---- =Gage used as reference for arrival time measurement.

TABLE 12.- Linear array strain data—Explosive 80 45

Shot designation, charge weight, charge volume, volume f	Gage No.	Shot-to gage distance R ft	Scaled distance R/V⅓ ft/ft	Peak compressive strain ε_c in/in x10^{-6}	Tensile strain ε_t in/in x10^{-6}	Rise time t_r sec x10^{-3}	Fall time t_f sec x10^{-3}	Compression time t_c sec x10^{-3}	Arrival time T_A sec x10^{-3}
2- 89 W=29.2 lb Vₛ=.412 cu ft V⅓ = .745 ft	-7	50	67.1	15.0	24.6	3.157	3.283	4.735	----
	-8	60	80.5	8.82	18.2	3.000	3.250	4.250	1.831
	-9	70	93.9	7.22	13.0	3.455	3.204	4.899	3.580
	-10	85	114	5.14	8.86	4.356	3.283	6.061	6.187
	-11	95	127	4.47	8.95	4.711	3.078	6.281	8.668
	-12	105	141	5.64	8.91	5.025	3.141	6.470	10.239
7- 814 W=29.2 lb Vₛ=.412 cu ft V⅓ = .745 ft	-7	75	101	6.67	12.6	3.769	3.015	5.214	8.543
	-8	65	87.2	10.7	9.36	3.000	2.500	4.250	7.938
	-9	55	73.8	11.3	27.8	3.455	3.204	5.025	5.779
	-10	40	53.7	19.8	38.1	2.688	2.313	4.188	2.813
	-11	30	40.3	37.3	46.9	1.750	2.313	3.000	1.625
	-12	20	26.8	68.0	17.0	1.445	2.638	3.518	----
15- 82 W=29.2 lb Vₛ=.412 cu ft V⅓ = .745 ft	-1	35	47.0	41.7	54.5	2.136	2.889	3.580	----
	-2	45	60.4	20.8	36.6	2.701	2.952	4.271	1.319
	-3	55	73.8	12.0	26.1	3.266	3.015	4.585	3.580
	-4	70	93.9	8.86	15.0	3.701	2.889	5.151	5.528
	-5	80	107	5.53	11.1	3.769	3.141	5.151	7.600
	-6	90	121	4.10	7.56	4.104	3.346	5.745	9.028
20- 85 W=29.2 lb Vₛ=.412 cu ft V⅓ = .745 ft	-1	60	80.5	5.90	17.1	3.706	3.455	5.025	8.417
	-2	50	67.1	10.1	19.0	2.313	3.250	3.875	7.000
	-3	40	53.7	21.4	37.4	2.701	2.701	4.020	4.523
	-4	25	33.6	48.0	34.8	2.073	2.513	3.643	2.575
	-5	15	20.1	119	3.26	*	*	*	1.250
	-6	5	6.71	2146	0	*	*	*	----

* = No data. ---- = Gage used as reference for arrival time measurement.

$$\epsilon_c = 5.86 \times 10^4 (R/V^{\frac{1}{3}})^{-2.03}$$

Figure 13 - Strain vs. Scaled Distance for Explosive AD 10
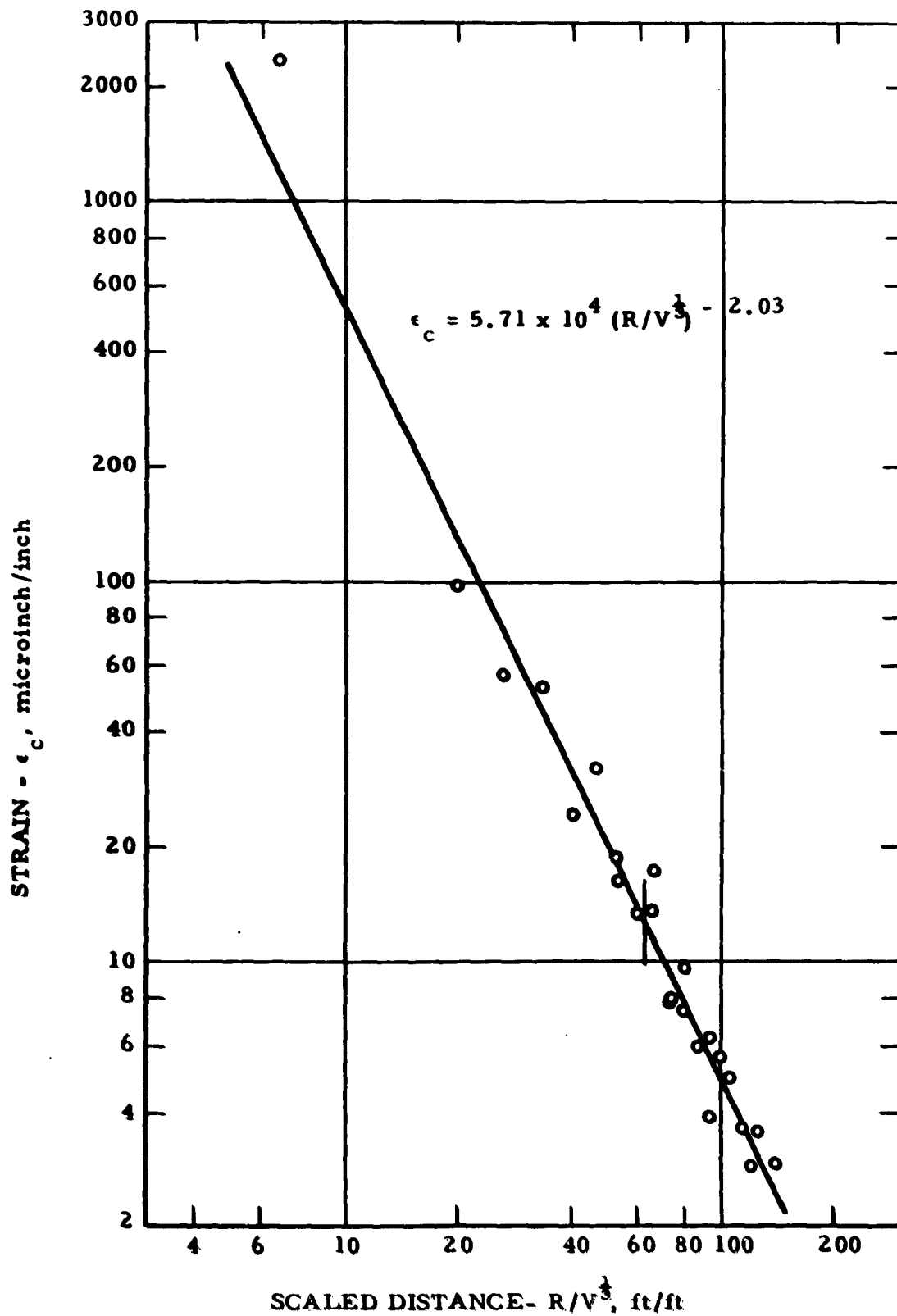
Figure 14 - Strain vs. Scaled Distance for Explosive AD 20A
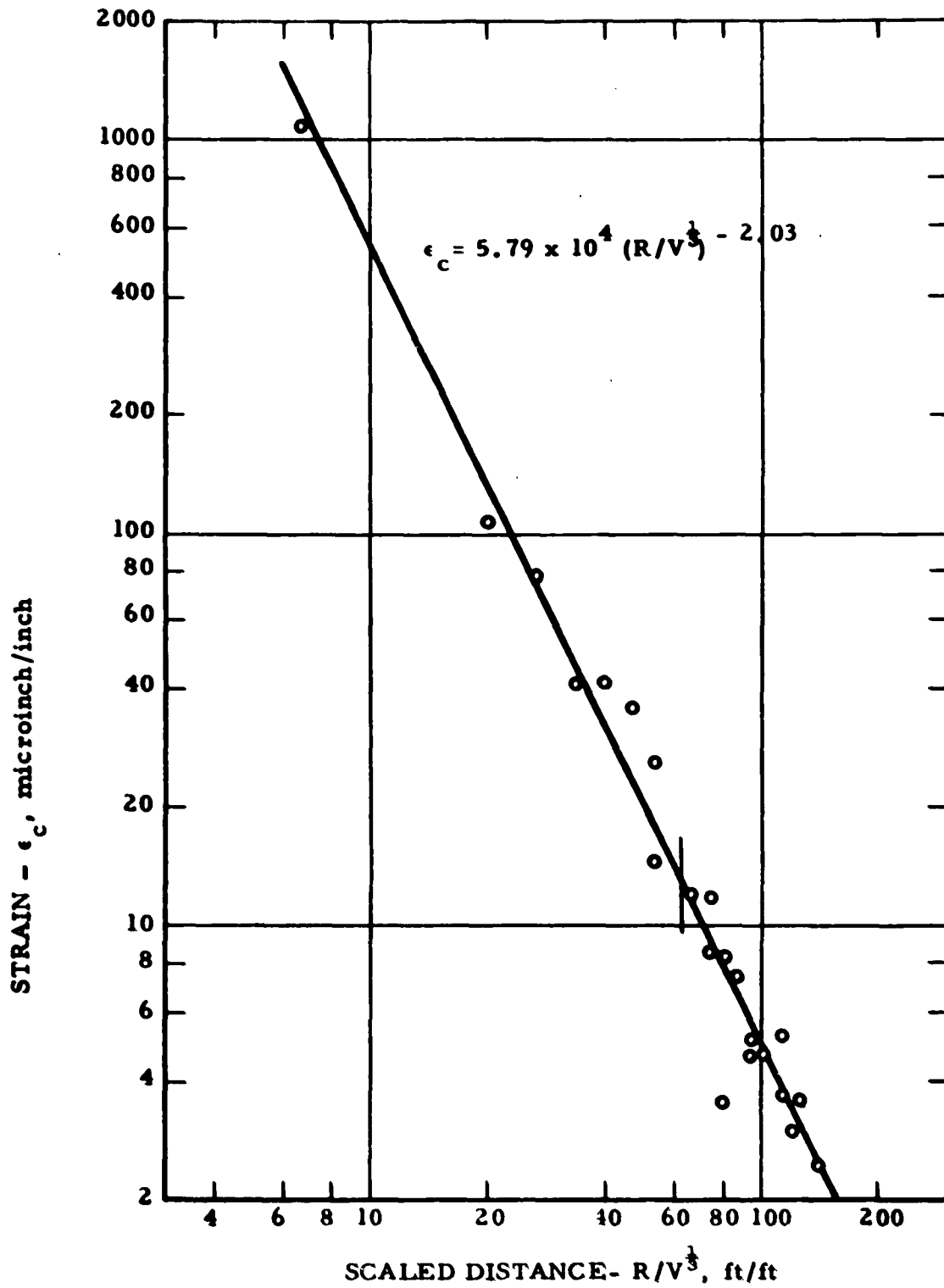
Figure 15 - Strain vs. Scaled Distance for Explosive AD-P

52.

$$\epsilon_c = 7.43 \times 10^4 \ R/V^{\frac{1}{3}})^{-2.03}$$

STRAIN - ϵ_c - microinch/inch

SCALED DISTANCE- $R/V^{\frac{1}{3}}$, ft/ft
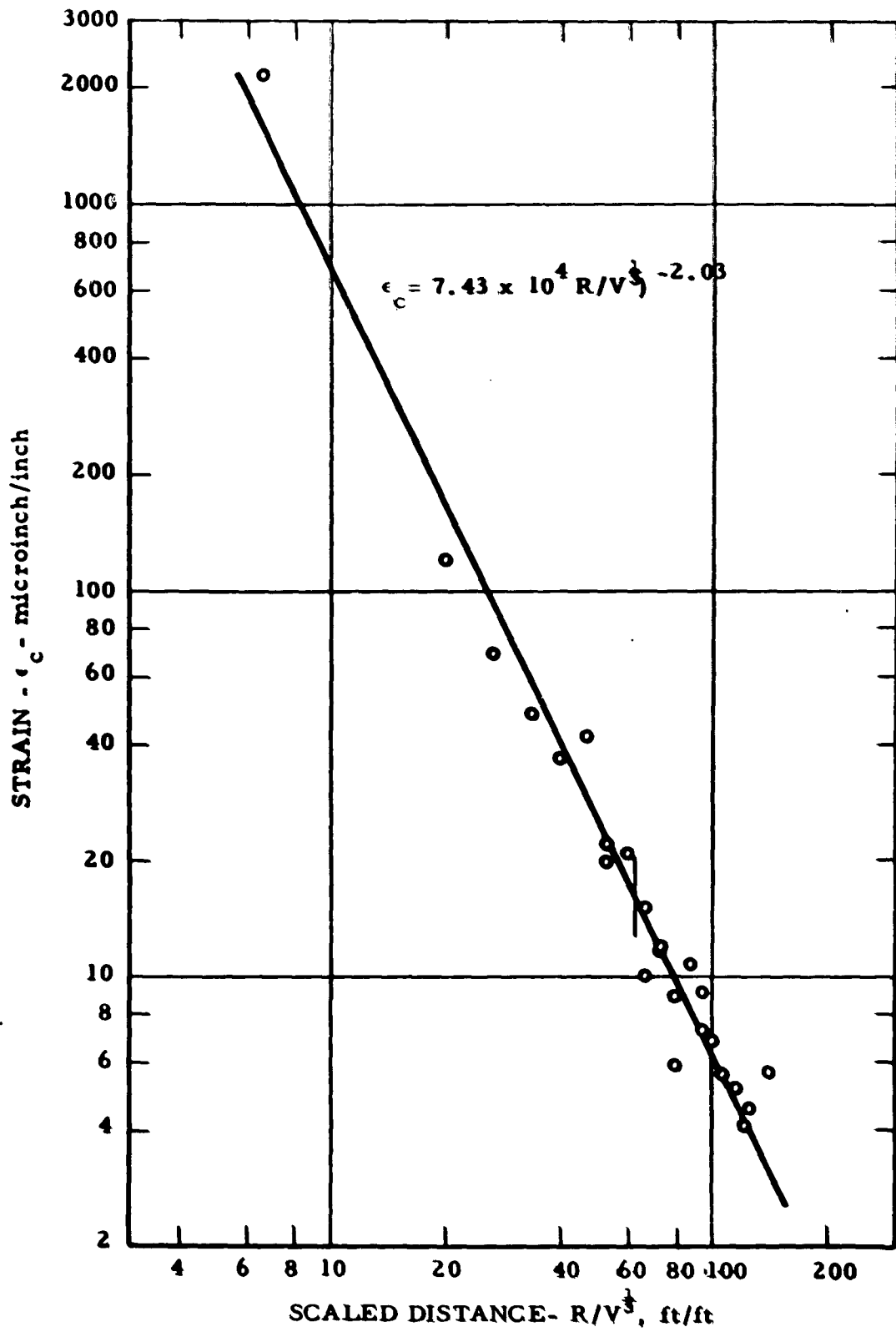
Figure 16 - Strain vs. Scaled Distance for Explosive SG 45

Fig. 18 – Tensile Strain vs. Scaled Distance for Explosive AD 20A

$\varepsilon_t = 4.83 \times 10^4 (R/V^{\frac{1}{3}})^{-1.83}$
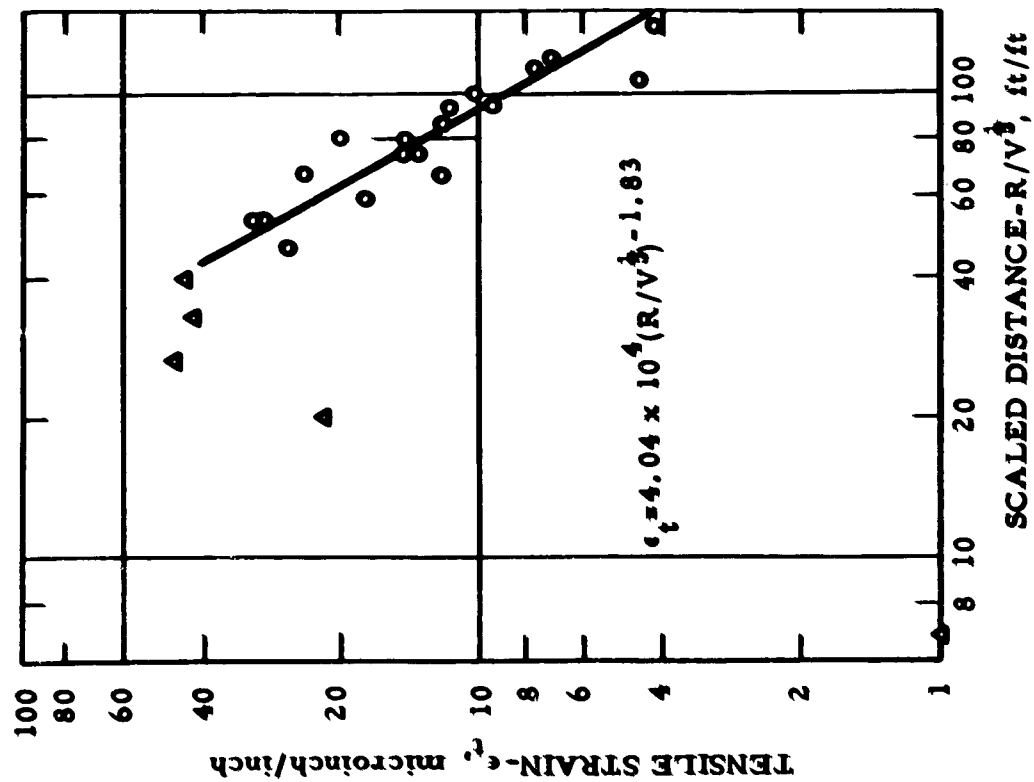
Fig. 17 – Tensile Strain vs. Scaled Distance for Explosive AD 10

$\varepsilon_t = 4.04 \times 10^4 (R/V^{\frac{1}{3}})^{-1.83}$

53.

54.

$$\epsilon_t = 5.74 \times 10^4 (R/V^{\frac{1}{3}})^{-1.83}$$
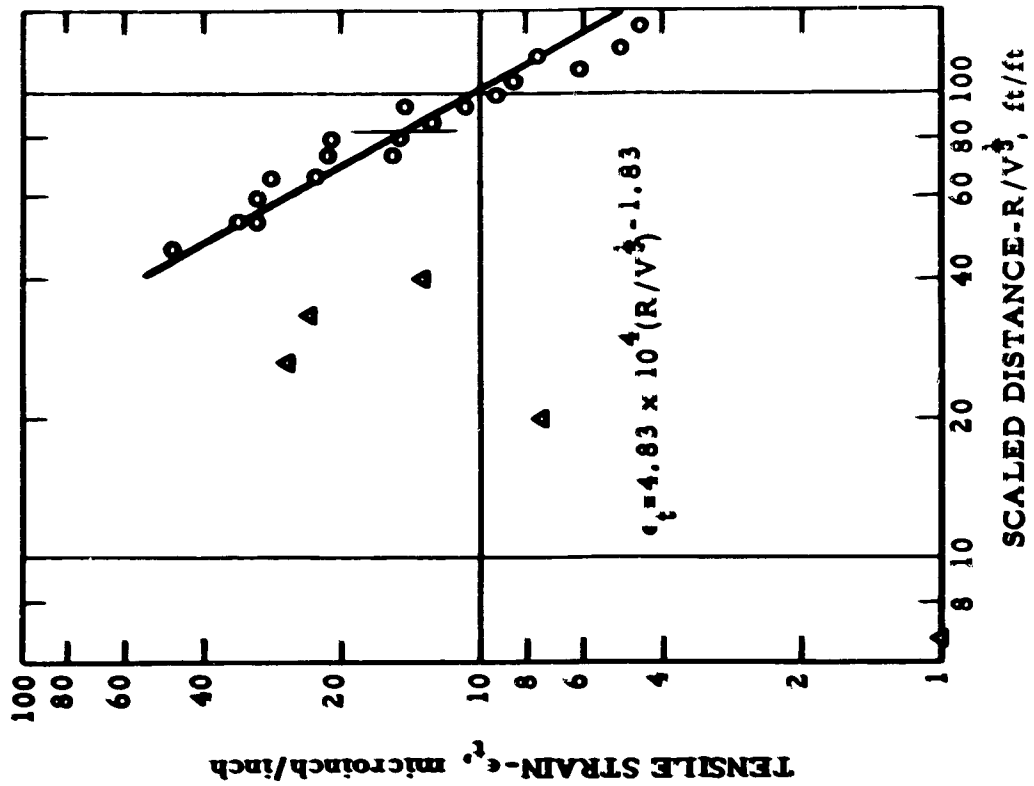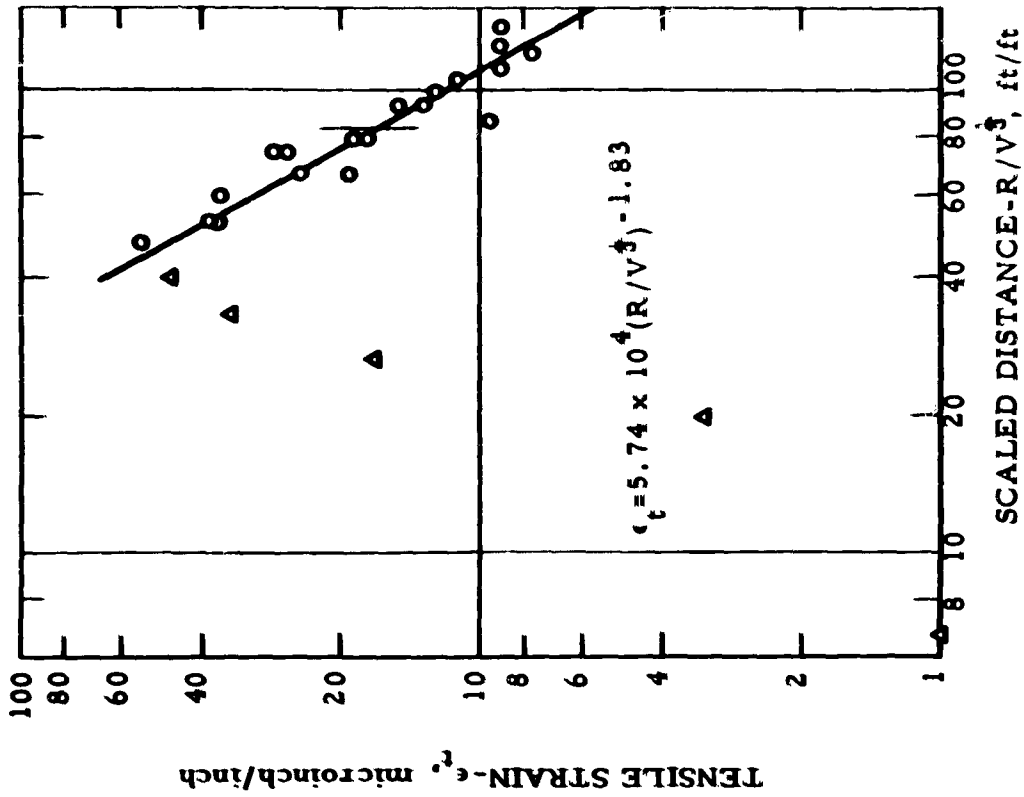
Fig. 20 - Tensile Strain vs. Scaled Distance for Explosive SG 45

$$\epsilon_t = 4.42 \times 10^4 (R/V^{\frac{1}{3}})^{-1.83}$$
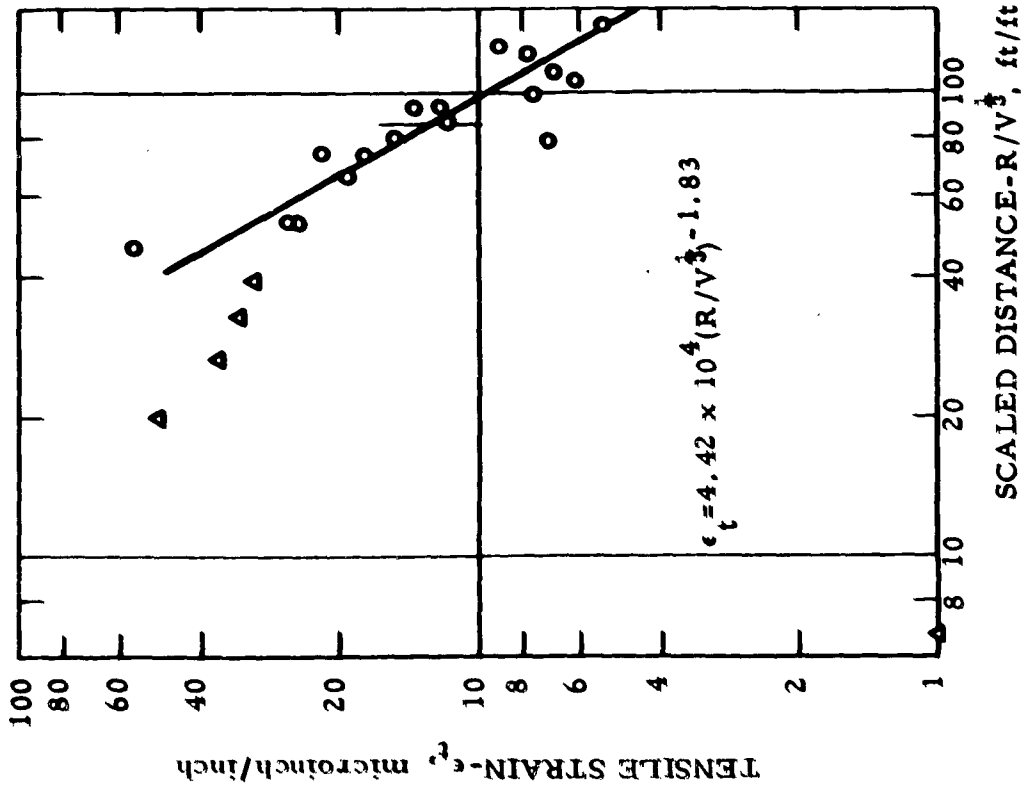
Fig. 19 - Tensile Strain vs. Scaled Distance for Explosive AD-P

40 ft/ft and then decreases with decreased shot-to-gage distance. At a
scaled distance of less than 6.7 ft/ft, no tensile phase exists within the
first 80 milliseconds after the arrival of the strain pulse. Similar results
have been noted in salt (Nicholls and Hooker, 1962a). Duvall (1953) has
shown that this phenomena is theoretically predicted. He stated "as the
distance from the cavity decreases, the oscillatory nature of the pulse de-
creases". In Duvall's paper, the strain-wave pulse becomes one-sided
(compression only) at a distance of from 2 to 5 times the cavity radius.
The cavity is the resultant cavity after detonation of the explosive charge.
Both compressive and tensile strain propagation law constants and their
standard deviations are given in table 13.

The radial strain energy radiated outward per unit area is given by the
equation:

$$E_a = \frac{\rho c^3}{2} \int_0^t \epsilon_r^2 \, dt \tag{2}$$

where

E_a = total radial strain energy per unit area,

ρ = rock density,

c = longitudinal propagation velocity of the rock,

ϵ_r = radial compressive strain,

and

t = time.

The method used for obtaining the integral portion of the energy equation
was to plot the square of the radial compressive strain as a function of
time and then evaluate the area under the curve by the trapezoidal rule
of approximation. The energy, E_a, the distance, R, and the scaled
quantities for each are summarized by explosive in tables 14 to 17. For
those records obtained over small shot-to-gage distances, where long
term compressive yielding or permanent deformation occurred (see the
upper trace of figure 12), no energy data could be calculated. Plots of
scaled energy versus scaled distance were made on log-log coordinate
paper as shown in figures 21 to 24. The linear grouping of the data indi-
cates that the propagation of scaled radial strain energy per unit area may
be represented by the equation:

TABLE 13. - Strain propagation law constants and standard deviations

Explosive	Compressive strain [1]		Tensile strain		Rise time		Fall time		Scaled energy	
	K μin/in $\times 10^4$	S_E [2] %	K μin/in $\times 10^4$	S_E %	K sec $\times 10^{-3}$	S_E %	K sec $\times 10^{-3}$	S_E %	K $\frac{\text{ft-lb/ft}^2}{\text{ft}}$ $\times 10^4$	S_E %
AD 10	5.86	30.7	4.04	29.7	.211	10.5	2.01	10.1	8.28	66.0
AD 20A	5.71	28.3	4.83	29.9	.224	11.0	2.02	10.0	9.52	65.7
AD-P	5.79	28.7	4.42	29.9	.223	10.7	2.00	10.1	9.18	65.7
SG 45	7.43	29.1	5.74	29.1	.219	10.8	2.29	10.1	16.0	65.9
Slope, n	-2.03		-1.83		0.68		0.13		-2.98	
S_n	$\pm$.04		$\pm$.10		$\pm$.03		$\pm$.02		$\pm$.11	

1/ K = intercept at $R/V^{\frac{1}{3}}$ = 1.0.

2/ S_E is the standard deviation about the mean.

TABLE 14.- Strain energy data- Explosive AD 10

Shot designation, charge weight, charge volume, volume$^{\frac{1}{3}}$	Shot-to-gage distance R ft	Scaled distance R/V$^{\frac{1}{3}}$ ft/ft	Energy per unit area E$_a$ ft-lb/ft^2 x 10^{-3}	Scaled energy per unit area E$_a$/V$^{\frac{1}{3}}$ ft-lb/ft^2/ft x 10^{-3}
5- S10	35	47.0	613	822
W=26.6 lb	45	60.4	233	313
V=.412 cu ft	55	73.8	132	177
V$^{\frac{1}{3}}$= .745 ft	70	93.9	61.7	82.8
	80	107	24.8	33.2
	90	121	45.6	61.2
9- S13	60	80.5	147	197
W=26.6 lb	50	67.1	124	166
V=.412 cu ft	40	53.7	605	812
V$^{\frac{1}{3}}$= .745 ft	25	33.6	1409	1891
	15	20.1	5364	7200
	5	6.71	*	*
12- S1	50	67.1	489	657
W=26.6 lb	60	80.5	273	366
V=.412 cu ft	70	93.9	101	136
V$^{\frac{1}{3}}$= .745 ft	85	114	35.6	47.7
	95	127	*	*
	105	141	13.2	17.8
17- S6	75	101	70.9	95.1
W=26.6 lb	65	87.2	157	210
V=.412 cu ft	55	73.8	187	251
V$^{\frac{1}{3}}$= .745 ft	40	53.7	638	857
	30	40.3	1444	1938
	20	26.8	2968	3984

*= no data

TABLE 15.- Strain energy data- Explosive AD 20A

Shot designation, charge weight, charge volume, volume$^{\frac{1}{3}}$	Shot-to-gage distance R ft	Scaled distance R/V$^{\frac{1}{3}}$ ft/ft	Energy per unit area E$_a$ ft-lb/ft^2 x 10^{-3}	Scaled energy per unit area E$_a$/V$^{\frac{1}{3}}$ ft-lb/ft^2/ft x 10^{-3}
4- S16	105	141	16.3	21.9
W=21.7 lb	95	127	20.2	27.1
V=.412 cu ft	85	114	26.6	35.7
V$^{\frac{1}{3}}$= .745 ft	70	93.9	130	174
	60	80.5	269	361
	50	67.1	686	921
8- S11	20	26.8	1949	2616
W=21.7 lb	30	40.3	361	484
V=.412 cu ft	40	53.7	688	924
V$^{\frac{1}{3}}$= .745 ft	55	73.8	188	252
	65	87.2	135	182
	75	101	72.3	97.1
16- S7	90	121	32.8	44.0
W=21.7 lb	80	107	47.2	63.3
V=.412 cu ft	70	93.9	67.8	91.0
V$^{\frac{1}{3}}$= .745 ft	55	73.8	297	398
	45	60.4	563	755
	35	47.0	1688	2266
19- S4	5	6.71	*	*
W=21.7 lb	15	20.1	7165	9618
V=.412 cu ft	25	33.6	1642	2204
V$^{\frac{1}{3}}$= .745 ft	40	53.7	839	1126
	50	67.1	394	529
	60	80.5	155	208

* No data

TABLE 16.- Strain energy data- Explosive AD-P

Shot designation, charge weight, charge volume, volume$^{\frac{1}{3}}$	Shot-to-gage distance R ft	Scaled distance $R/V^{\frac{1}{3}}$ ft/ft	Energy per unit area E_a ft-lb/ft^2 x 10^{-3}	Scaled energy per unit area $E_a/V^{\frac{1}{3}}$ ft-lb/ft^2/ft x 10^{-3}
6- S15	90	121	33.5	45.0
W=19.6 lb	80	107	146	197
V=.412 cu ft	70	93.9	88.7	119
V$^{\frac{1}{3}}$= .745 ft	55	73.8	269	361
	45	60.4	*	*
	35	47.0	2539	3408
10- S12	5	6.71	68,070	91,400
W=19.6 lb	15	20.1	8836	11,860
V=.412 cu ft	25	33.6	1290	1732
V$^{\frac{1}{3}}$= .745 ft	40	53.7	183	246
	50	67.1	*	*
	60	80.5	39.8	53.4
14- S8	105	141	17.8	23.9
W=19.6 lb	95	127	49.0	65.8
V=.412 cu ft	85	114	25.5	34.2
V$^{\frac{1}{3}}$= .745 ft	70	93.9	100	134
	60	80.5	165	221
	50	67.1	283	380
18- S3	20	26.8	3521	4726
W=19.6 lb	30	40.3	1487	1996
V=.412 cu ft	40	53.7	729	979
V$^{\frac{1}{3}}$= .745 ft	55	73.8	292	392
	65	87.2	133	179
	75	101	45.0	60.4

* No data

TABLE 17.- Strain energy data- Explosive SG 45

Shot designation, charge weight, charge volume, volume$^{\frac{1}{3}}$	Shot-to-gage distance R ft	Scaled distance R/V$^{\frac{1}{3}}$ ft/ft	Energy per unit area E$_a$ ft-lb/ft^2 x 10^{-3}	Scaled energy per unit area E$_a$/V$^{\frac{1}{3}}$ ft-lb/ft^2/ft x 10^{-3}
2- S9	50	67.1	515	691
W=29.2 lb	60	80.5	264	354
V=.412 cu ft	70	93.9	143	192
V$^{\frac{1}{3}}$= .745 ft	85	114	67.2	90.2
	95	127	65.8	88.3
	105	141	75.1	101
7- S14	75	101	119	160
W=29.2 lb	65	87.2	120	162
V=.412 cu ft	55	73.8	535	717
V$^{\frac{1}{3}}$= .745 ft	40	53.7	1109	1489
	30	40.3	1963	2635
	20	26.8	2937	3942
15- S2	35	47.0	2995	4020
W=29.2 lb	45	60.4	1209	1623
V=.412 cu ft	55	73.8	551	740
V$^{\frac{1}{3}}$= .745 ft	70	93.9	202	271
	80	107	92.9	125
	90	121	45.7	61.4
20- S5	60	80.5	156	210
W=29.2 lb	50	67.1	255	342
V=.412 cu ft	40	53.7	1012	1358
V$^{\frac{1}{3}}$= .745 ft	25	33.6	1843	2474
	15	20.1	12,176	16,340
	5	6.71	*	*

* No data

$$E_a/V^{\frac{1}{3}} = 8.28 \times 10^4 (R/V^{\frac{1}{3}})^{-2.98}$$

SCALED ENERGY PER UNIT AREA-$E_a/V^{\frac{1}{3}}$, $\dfrac{\text{ft-lb/ft}^2}{\text{ft}}$

SCALED DISTANCE-R/$V^{\frac{1}{3}}$, ft/ft
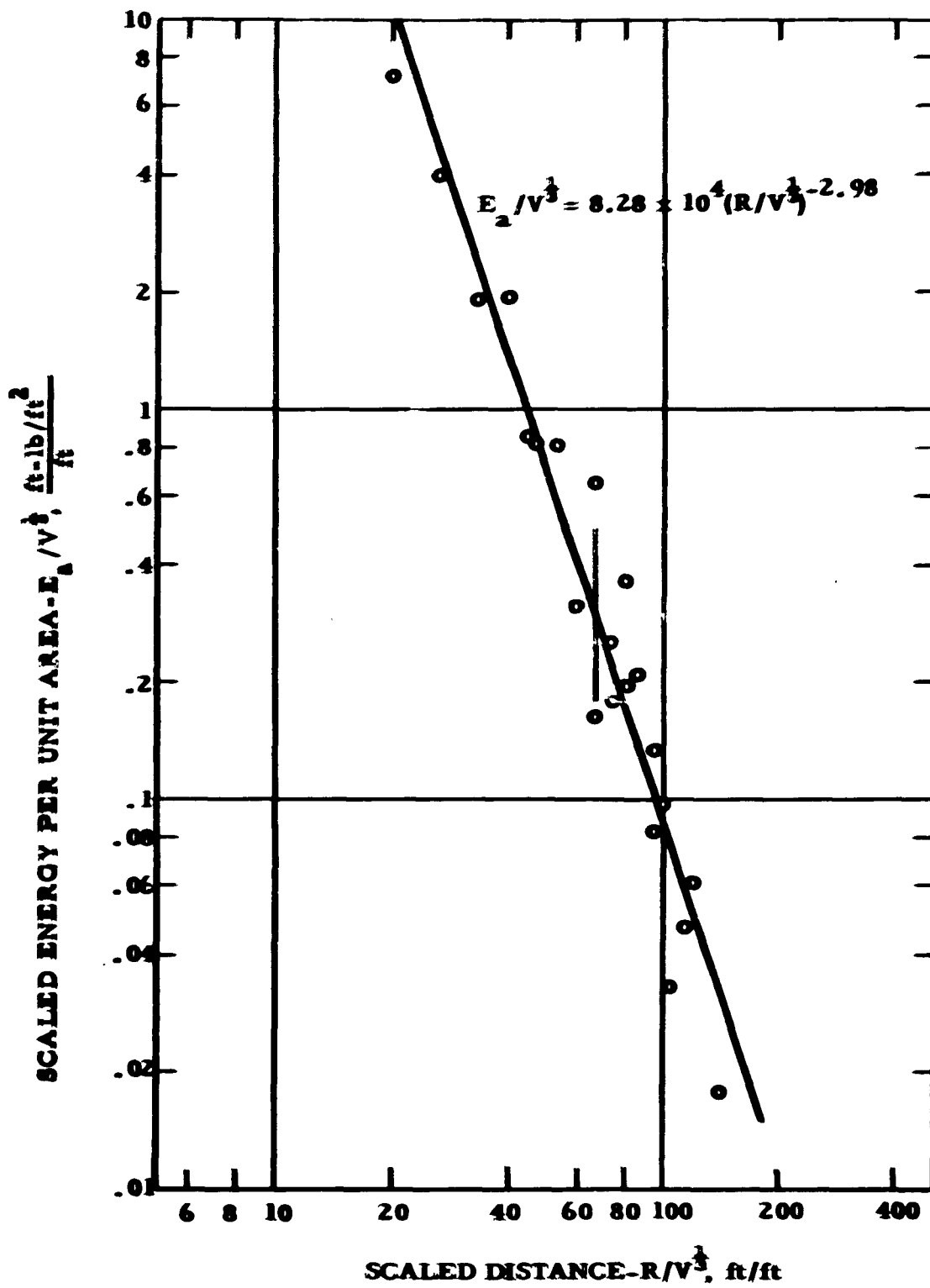
Figure 21 -Scaled Energy vs. Scaled Distance for
Explosive AD 10

The graph shows: $E_a/V^{\frac{1}{3}} = 9.52 \times 10^4 (R/V^{\frac{1}{3}})^{-2.98}$

Y-axis: SCALED ENERGY PER UNIT AREA- $E_a/V^{\frac{1}{3}}$, $\frac{ft\text{-}lb/ft^2}{ft}$

X-axis: SCALED DISTANCE- $R/V^{\frac{1}{3}}$, ft/ft
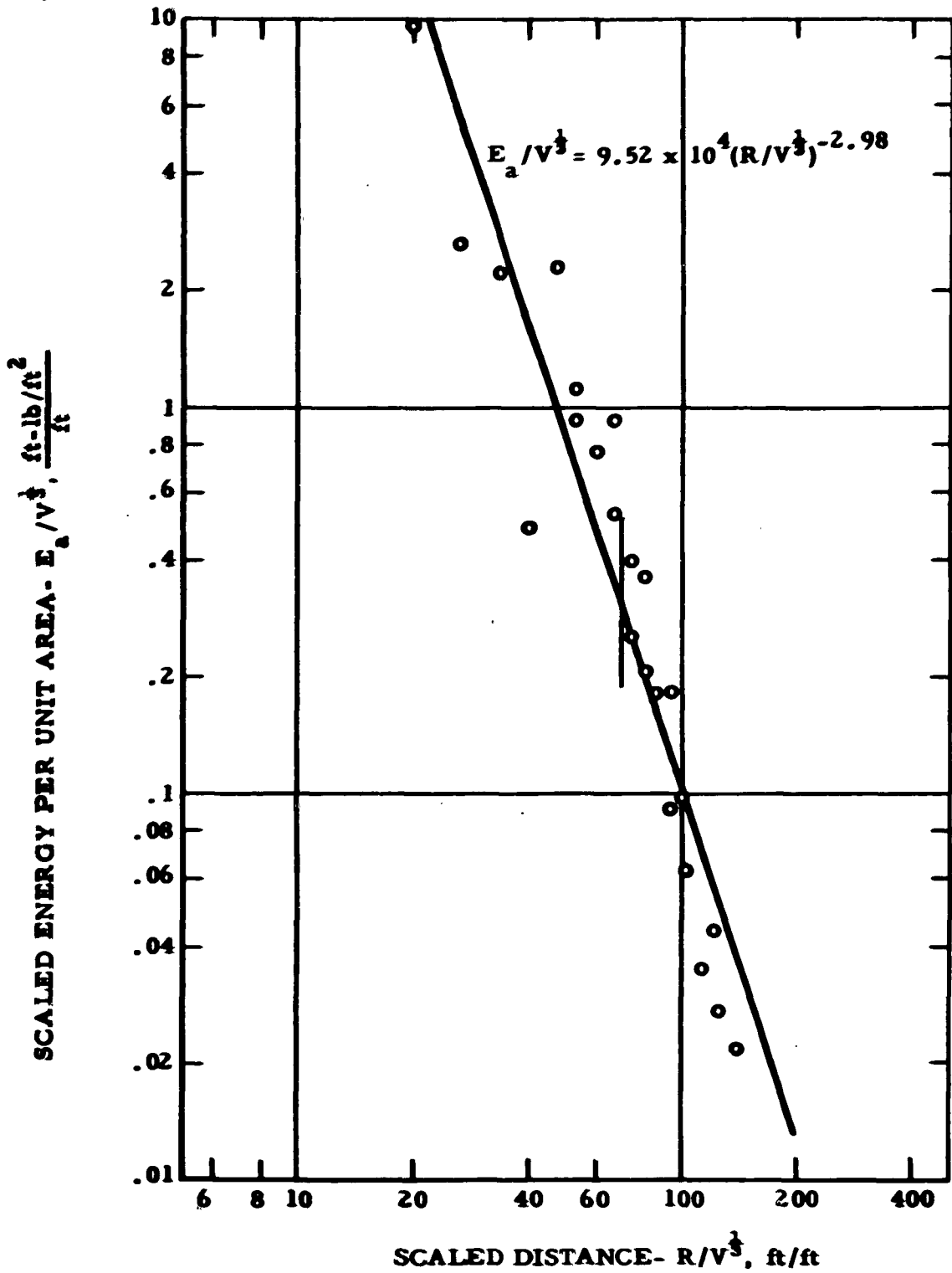
Figure 22- Scaled Energy vs. Scaled Distance for
Explosive AD 20 A

$$E_a/V^{\frac{1}{3}} = 9.18 \times 10^4 (R/V^{\frac{1}{3}})^{-2.98}$$

SCALED ENERGY PER UNIT AREA-$E_a/V^{\frac{1}{3}}$, $\dfrac{\text{ft-lb/ft}^2}{\text{ft}}$

SCALED DISTANCE- $R/V^{\frac{1}{3}}$, ft/ft
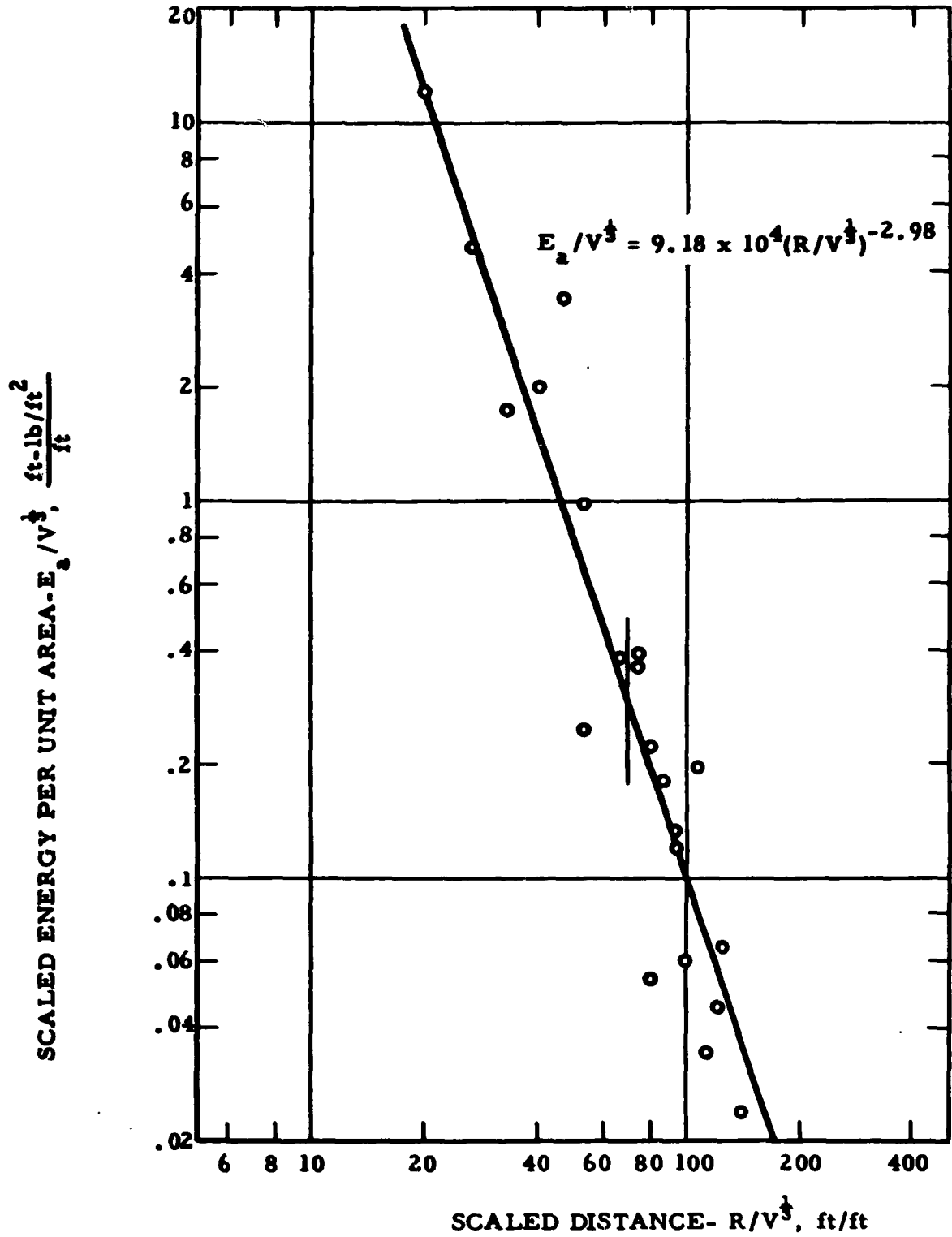
Figure 23-   Scaled Energy vs. Scaled Distance for
Explosive AD-P

64.

$$E_a / V^{\frac{1}{3}} = 16.0 \times 10^4 (R/V^{\frac{1}{3}})^{-2.98}$$

SCALED ENERGY PER UNIT AREA-$E_a/V^{\frac{1}{3}}$, $\dfrac{\text{ft-lb/ft}^2}{\text{ft}}$

20
10
8
6
4
2
1
.8
.6
.4
.2
.1
.08
.06
.04
.02

6   8   10   20   40   60 80 100   200   400

SCALED DISTANCE-$R/V^{\frac{1}{3}}$, ft/ft

Figure 24 - Scaled Energy vs. Scaled Distance for
Explosive SG 45

$$E_a / V^{\frac{1}{3}} = K \left(R / V^{\frac{1}{3}} \right)^{n} \tag{3}$$

where

$\qquad$ K = strain energy intercept constant,

and $\qquad$ n = strain energy decay exponent or slope.

The values of K and n are given in table 13.

Particle Acceleration

Particle acceleration data are given in tables 18 to 21. Amplitude and time measurements were the same as the measurements of strain records. Positive acceleration is defined as motion radially outward from the shotpoint and negative acceleration as radial motion toward the shotpoint.

Scaled peak positive acceleration distance was plotted versus scaled distance as shown in figures 25 to 28. Plots of scaled peak negative acceleration data versus scaled distance are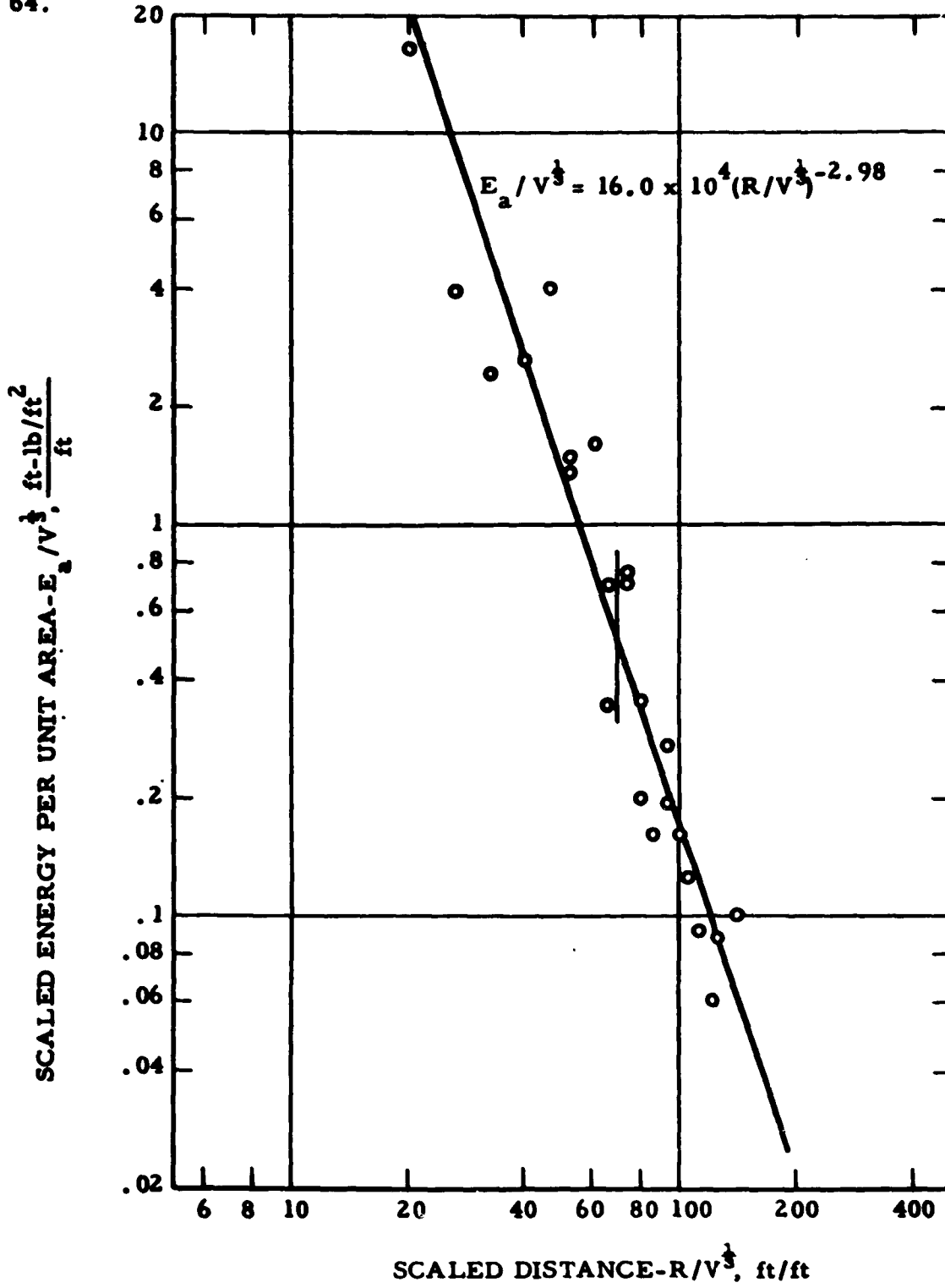 shown in figures 29 to 32. The vertical line through each set of data represents one standard deviation unit about the mean of the data. Because the plots are linear on log-log coordinate plots, particle acceleration can be represented by the following equation:

$$A \, V^{\frac{1}{3}} = K \left(R / V^{\frac{1}{3}} \right)^{n} \tag{4}$$

where

$\qquad$ A = peak acceleration,

$\qquad$ $A \, V^{\frac{1}{3}} =$ scaled acceleration,

$\qquad$ K = intercept at scaled distance of 1,

$\qquad$ $R / V^{\frac{1}{3}} =$ scaled distance,

and $\qquad$ n = slope or decay exponent.

Statistical methods were used to calculate the value of n and four values of K (one for each explosive) for positive acceleration and corresponding values for negative acceleration. The values of K and n and the standard deviations are given in table 22.

66.

TABLE 18.- Linear array particle acceleration data-Explosive AD 10

Shot designation, charge weight, charge volume, volume$^{\frac{1}{3}}$	Gage No.	Shot-to-gage distance R ft	Scaled distance $R/V^{\frac{1}{3}}$ ft/ft	Peak positive acceleration A g's	Scaled positive acceleration $A\,V^{\frac{1}{3}}$ g's x ft
5- S10	A7	35	47.0	*	*
W=26.6 lb	A8	45	60.4	*	*
V=.412 cu ft	A9	55	73.8	*	*
V$^{\frac{1}{3}}$= .745 ft	A10	70	93.9	*	*
	A11	80	107	*	*
	A12	90	121	*	*
9-S13	A7	60	80.5	.498	.371
W=26.6 lb	A8	50	67.1	.992	.739
V=.412 cu ft	A9	40	53.7	1.74	1.30
V$^{\frac{1}{3}}$= .745 ft	A10	25	33.6	8.12	6.05
	A11	15	20.1	22.6	16.8
	A12	5	6.71	300	224
12- S1	A1	50	67.1	1.55	1.15
W=26.6 lb	A2	60	80.5	1.11	.827
V=.412 cu ft	A3	70	93.9	1.12	.834
V$^{\frac{1}{3}}$= .745 ft	A4	85	114	.305	.227
	A5	95	127	.286	.213
	A6	105	141	*	*
17- S6	A1	75	101	.312	.232
W=26.6 lb	A2	65	87.2	.264	.197
V=.412 cu ft	A3	55	73.8	.727	.542
V$^{\frac{1}{3}}$= .745 ft	A4	40	53.7	2.13	1.59
	A5	30	40.3	4.52	3.37
	A6	20	26.8	*	*

* No data

TABLE 18.- Linear array particle acceleration data-Explosive AD 10

Negative accele- ration	Peak positive velocity	Negative velocity	Acceleration rise time	Acceleration fall time	Velocity rise time	Velocity fall time
A $g's$	V in/sec	V in/sec	t_r sec $\times 10^{-3}$	t_f sec $\times 10^{-3}$	t_r sec $\times 10^{-3}$	t_f sec $\times 10^{-3}$
*	*	*	*	*	*	*
*	*	*	*	*	*	*
*	*	*	*	*	*	*
*	*	*	*	*	*	*
*	*	*	*	*	*	*
*	*	*	*	*	*	*
2.99	.144	.803	2.625	2.625	3.000	2.625
3.97	.267	1.01	2.399	2.336	2.588	2.588
5.84	.433	1.58	2.020	2.525	2.336	2.652
14.9	1.38	3.46	1.136	2.146	1.389	2.399
24.0	2.97	5.76	.568	2.210	1.199	2.146
244	37.6	51.5	1.389	1.515	1.452	1.957
4.64	.337	1.19	1.894	2.588	2.273	2.904
3.54	*	*	2.375	2.125	*	*
1.53	.343	.363	2.125	2.250	2.688	2.188
1.48	.0664	.365	3.078	2.638	2.827	3.015
1.18	.0857	.366	3.455	2.827	3.329	3.078
*	*	*	*	*	*	*
1.87	.0789	.502	3.598	2.336	3.788	2.525
2.00	.0839	.558	3.266	2.575	3.329	2.764
2.59	.228	.836	2.827	2.387	3.141	2.387
5.33	.544	1.46	2.146	2.210	2.210	2.336
10.1	.925	2.65	1.389	2.146	1.515	2.146
*	*	*	*	*	*	*

* No data

TABLE 19.- <u>Linear array particle acceleration data-Explosive AD 20A</u>

Shot designation, charge weight, charge volume, volume$^{\frac{1}{3}}$	Gage No.	Shot-to-gage distance R ft	Scaled distance R/V$^{\frac{1}{3}}$ ft/ft	Peak positive acceleration A g's	Scaled positive acceleration A V$^{\frac{1}{3}}$ g's x ft
4- S16	A7	105	141	.261	.194
W=21.7 lb	A8	95	127	.263	.196
V=.412 cu ft	A9	85	114	.297	.221
V$^{\frac{1}{3}}$= .745 ft	A10	70	93.9	.642	.478
	A11	60	80.5	.938	.669
	A12	50	67.1	1.14	.849
8- S11	A7	20	26.8	11.3	8.42
W=21.7 lb	A8	30	40.3	5.56	4.14
V=.412 cu ft	A9	40	53.7	2.13	1.59
V$^{\frac{1}{3}}$ .745 ft	A10	55	73.8	.929	.692
	A11	65	87.2	.524	.390
	A12	75	101	.422	.314
16- S7	A1	90	121	.172	.128
W=21.7 lb	A2	80	107	.205	.153
V=.412 cu ft	A3	70	93.9	.312	.232
V$^{\frac{1}{3}}$ .745 ft	A4	55	73.8	.689	.513
	A5	45	60.4	1.40	1.04
	A6	35	47.0	*	*
19- S4	A1	5	6.71	194	145
W=21.7 lb	A2	15	20.1	26.7	19.9
V=.412 cu ft	A3	25	33.6	7.56	5.63
V$^{\frac{1}{3}}$ .745 ft	A4	40	53.7	2.37	1.77
	A5	50	67.1	.698	.520
	A6	60	80.5	*	*

* No data

TABLE 19.- Linear array particle acceleration data-Explosive AD 20A

Negative acceleration	Peak positive velocity	Negative velocity	Acceleration rise time	Acceleration fall time	Velocity rise time	Velocity fall time
A $g's$	V in/sec	V in/sec	t_r sec $\times 10^{-3}$	t_f sec $\times 10^{-3}$	t_r sec $\times 10^{-3}$	t_f sec $\times 10^{-3}$
1.17	.0560	.296	4.711	2.261	5.025	2.387
1.43	.0530	.374	3.313	2.313	3.750	2.387
1.91	.0714	.479	3.157	2.399	3.472	2.336
2.82	.205	.643	3.769	2.450	3.957	2.701
4.07	.224	.983	2.638	2.513	2.952	2.198
4.57	.271	1.21	2.638	2.701	2.638	2.638
19.3	2.17	4.62	.879	2.513	1.193	2.450
13.3	1.29	3.43	1.068	2.513	1.382	2.513
6.56	.600	1.84	1.884	2.513	2.261	2.575
3.13	.324	.991	2.638	2.701	3.078	2.889
2.10	.142	.610	3.266	2.638	3.580	2.827
1.44	.0909	.374	3.141	2.701	3.643	2.638
1.23	.0541	.295	4.083	2.827	3.392	2.952
1.20	.0797	.260	2.953	3.015	3.141	3.015
1.99	.0850	.457	3.141	2.952	3.141	3.015
3.14	.192	.752	3.015	2.387	3.015	2.513
5.08	.334	1.18	2.513	2.198	2.701	2.324
*	*	*	*	*	*	*
101	39.5	*	1.094	.781	1.382	.691
25.1	3.17	5.18	.500	2.188	1.000	2.188
13.7	1.43	3.03	1.250	2.250	1.563	2.313
6.35	.541	1.67	2.500	2.500	2.625	2.750
3.63	.190	1.04	2.688	2.500	2.688	2.938
*	*	*	*	*	*	*

* No data

TABLE 20.- Linear array particle acceleration data-Explosive AD-P

Shot designation, charge weight, charge volume, volume$^{\frac{1}{3}}$	Gage No.	Shot-to-gage distance R ft	Scaled distance $R/V^{\frac{1}{3}}$ ft/ft	Peak positive acceleration A g's	Scaled positive acceleration $A V^{\frac{1}{3}}$ g's x ft
6- S15	A7	90	121	.258	.192
W=19.6 lb	A8	80	107	.409	.305
V=.412 cu ft	A9	70	93.9	.543	.405
V$^{\frac{1}{3}}$= .745 ft	A10	55	73.8	.906	.675
	A11	45	60.4	1.84	1.37
	A12	35	47.0	3.16	2.35
10- S12	A7	5	6.71	153	114
W=19.6 lb	A8	15	20.1	10.2	7.60
V=.412 cu ft	A9	25	33.6	5.86	4.37
V$^{\frac{1}{3}}$= .745 ft	A10	40	53.7	*	*
	A11	50	67.1	.570	.425
	A12	60	80.5	*	*
14- S8	A1	105	141	.0928	.0691
W=19.6 lb	A2	95	127	.121	.0901
V=.412 cu ft	A3	85	114	.158	.118
V$^{\frac{1}{3}}$= .745 ft	A4	70	93.9	.386	.228
	A5	60	80.5	.603	.449
	A6	50	67.1	*	*
18- S3	A1	20	26.8	12.1	9.01
W=19.6 lb	A2	30	40.3	5.37	4.00
V=.412 cu ft	A3	40	53.7	2.34	1.74
V$^{\frac{1}{3}}$= .745 ft	A4	55	73.8	1.08	.805
	A5	65	87.2	.466	.347
	A6	75	101	*	*

* No data

TABLE 20.- Linear array particle acceleration data-Explosive AD-P

Negative accele-ration A g's	Peak positive velocity V in/sec	Negative velocity V in/sec	Acceleration rise time t_r sec $\times 10^{-3}$	Acceleration fall time t_f sec $\times 10^{-3}$	Velocity rise time t_r sec $\times 10^{-3}$	Velocity fall time t_f sec $\times 10^{-3}$
1.55	.0552	.455	4.063	2.500	4.063	2.750
1.87	.0929	.502	3.750	2.188	3.688	2.500
2.51	.105	.681	3.625	2.250	3.688	2.500
3.86	.199	1.13	2.813	2.500	3.125	2.500
5.53	.511	1.40	2.438	2.250	2.625	2.500
9.30	.761	2.33	1.840	2.221	2.010	2.387
69	38.2	38.2	1.319	1.696	1.633	1.822
30.7	3.00	7.67	.503	1.884	1.256	2.010
14.5	1.21	3.88	1.256	2.261	1.319	2.450
5.15	*	*	*	*	*	*
4.63	.144	1.20	2.375	2.313	2.938	2.438
5.65	*	1.53	*	*	*	*
1.04	.0152	.262	3.769	2.889	4.397	2.450
1.11	.0395	.276	3.141	2.952	3.140	3.015
1.66	.0450	.415	3.141	2.764	3.140	3.015
2.26	.0903	.591	3.141	2.513	3.141	2.827
2.58	.173	.637	2.827	2.324	3.141	2.450
*	*	*	*	*	*	*
20.6	2.51	4.41	.884	2.273	1.452	2.336
11.1	1.11	2.74	1.578	2.146	1.578	2.336
6.67	.570	1.68	1.957	2.020	2.083	2.525
3.36	.285	.889	3.141	2.136	3.141	3.078
2.08	.159	.530	3.346	2.588	3.409	2.967
*	*	*	*	*	*	*

* No data

TABLE 21. - <u>Linear array particle acceleration data-Explosive SG 45</u>

Shot designation, charge weight, charge volume, volume$^{\frac{1}{3}}$	Gage No.	Shot-to-gage distance	Scaled distance	Peak positive acceleration	Scaled positive acceleration
		R ft	R/V$^{\frac{1}{3}}$ ft/ft	A g's	AV$^{\frac{1}{3}}$ g's x ft
2- S9	A7	50	67.1	1.98	1.48
W=29.2 lb	A8	60	80.5	1.15	.857
V=.412 cu ft	A9	70	93.9	.607	.452
V$^{\frac{1}{3}}$ .745 ft	A10	85	114	.383	.285
	A11	95	127	.379	.282
	A12	105	141	.242	.180
7- S14	A7	75	101	.385	.287
W=29.2 lb	A8	65	87.2	.439	.327
V=.412 cu ft	A9	55	73.8	.763	.568
V$^{\frac{1}{3}}$ .745 ft	A10	40	53.7	2.25	1.68
	A11	30	40.3	5.62	4.19
	A12	20	26.8	14.6	10.9
15- S2	A1	35	47.0	4.18	3.11
W=29.2 lb	A2	45	60.4	2.10	1.56
V=.412 cu ft	A3	55	73.8	1.50	1.12
V$^{\frac{1}{3}}$ .745 ft	A4	70	93.9	.710	.529
	A5	80	107	.446	.332
	A6	90	121	*	*
20- S5	A1	60	80.5	.460	.343
W=29.2 lb	A2	50	67.1	.527	.393
V=.412 cu ft	A3	40	53.7	1.59	1.18
V$^{\frac{1}{3}}$ .745 ft	A4	25	33.6	6.55	4.88
	A5	15	20.1	24.5	18.3
	A6	5	6.71	*	*

* No data

TABLE 21. - <u>Linear array particle acceleration data-Explosive SG 45</u>

Negative accele- ration A	Peak positive velocity V in/sec	Negative velocity V in/sec	Acceleration rise time t_r sec x 10^{-3}	Acceleration fall time t_f sec x 10^{-3}	Velocity rise time t_r sec x 10^{-3}	Velocity fall time t_f sec x 10^{-3}
4.96	.488	1.42	2.778	2.904	2.841	2.841
3.29	.335	.740	2.500	2.688	2.375	2.841
2.23	.121	.727	3.266	2.764	3.266	3.266
1.80	.110	.509	4.040	3.030	4.040	3.535
1.78	.0875	.525	4.648	3.015	4.648	3.015
1.38	.0978	.349	4.585	2.764	4.585	3.015
2.62	.126	.728	3.329	2.952	3.329	3.015
3.51	.167	.925	3.438	2.688	3.750	2.625
4.88	.210	1.36	2.827	2.764	3.204	2.764
8.34	.646	2.16	2.500	2.625	2.688	2.875
14.1	1.16	3.97	1.375	2.438	1.438	2.563
21.2	2.41	5.47	.879	2.513	1.068	2.701
11.1	.947	2.81	1.822	2.575	1.947	2.952
6.01	.490	1.52	2.073	2.638	2.324	2.952
4.43	.372	1.17	2.513	2.575	2.638	2.952
2.53	.179	.712	3.141	2.701	3.266	3.141
1.68	.138	.459	3.141	3.141	3.266	3.141
*	*	*	*	*	*	*
2.99	.154	.731	2.513	3.015	2.764	3.455
3.90	.161	.994	2.375	3.250	1.938	3.313
6.08	.444	1.54	2.387	2.764	2.638	2.575
12.6	1.38	3.21	1.445	2.450	1.759	2.450
26.8	3.45	5.95	.750	2.438	1.125	2.625
*	*	*	*	*	*	*

* No data

74.

$$A V^{\frac{2}{3}} = 1.99 \times 10^4 (R/V^{\frac{1}{3}})^{-2.39}$$
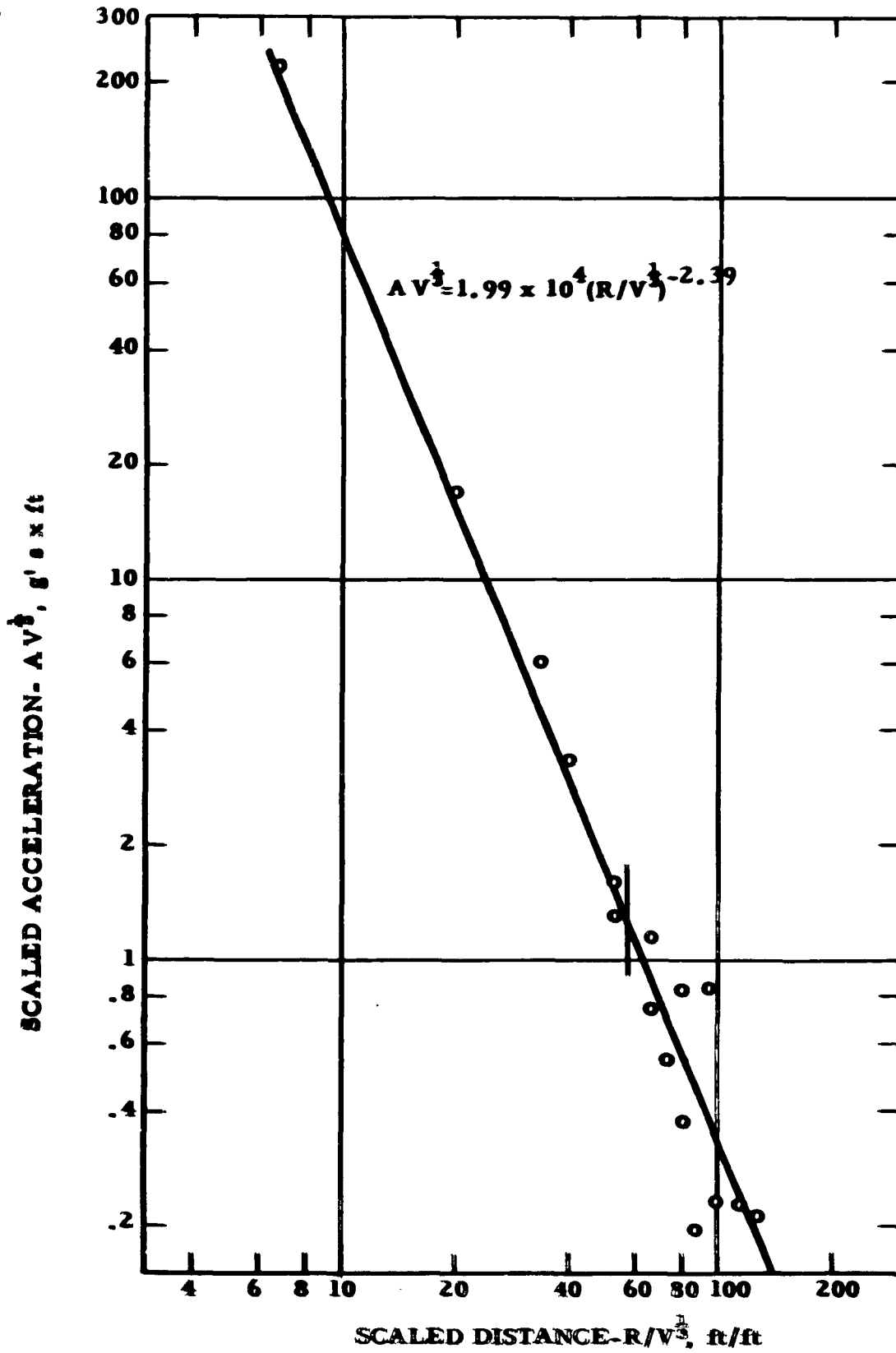
Fig. 25 - Scaled Acceleration vs. Scaled Distance for Explosive AD 10
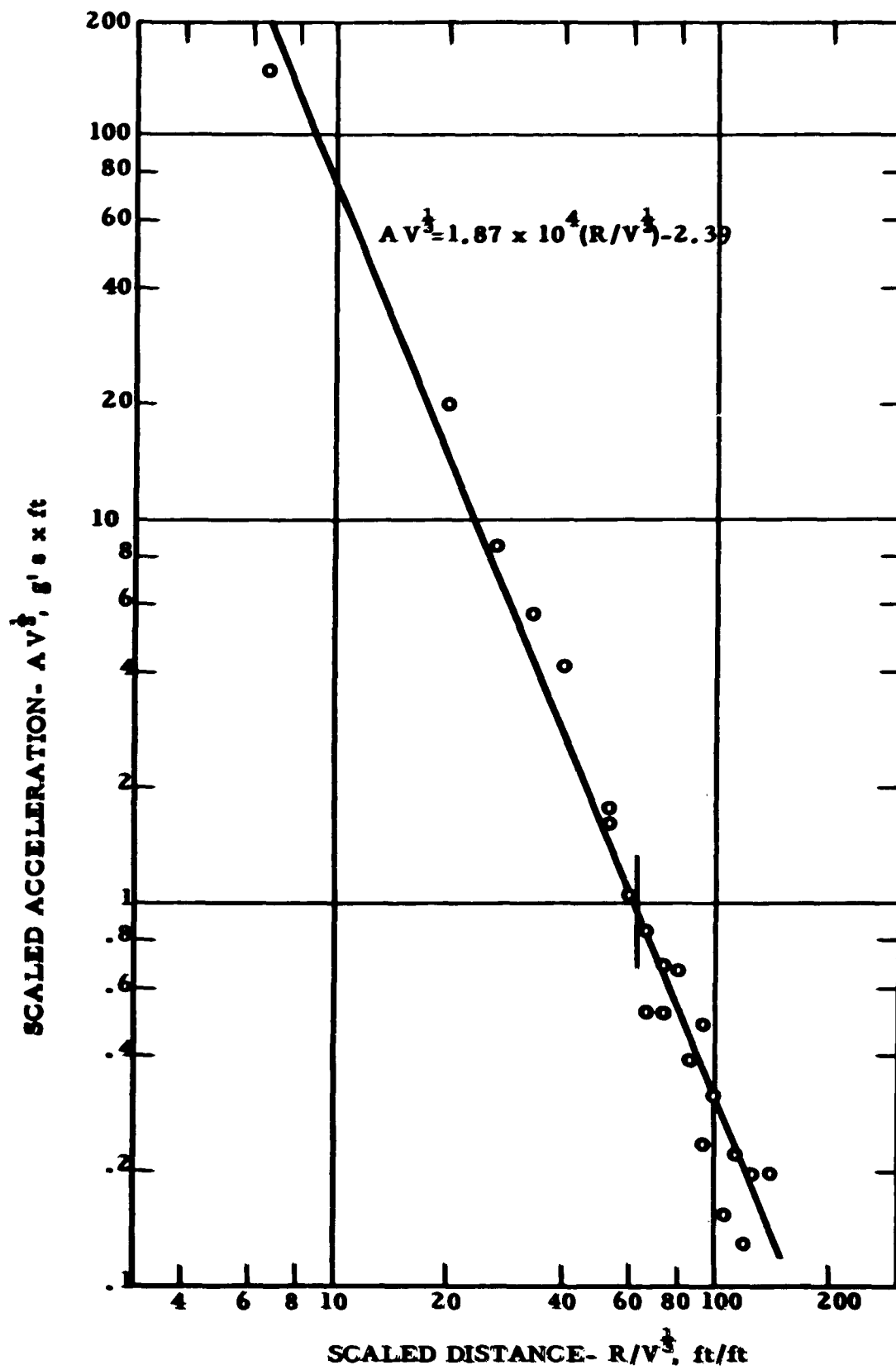
Fig.26 - Scaled Acceleration vs. Scaled Distance for Explosive AD 20A

76.

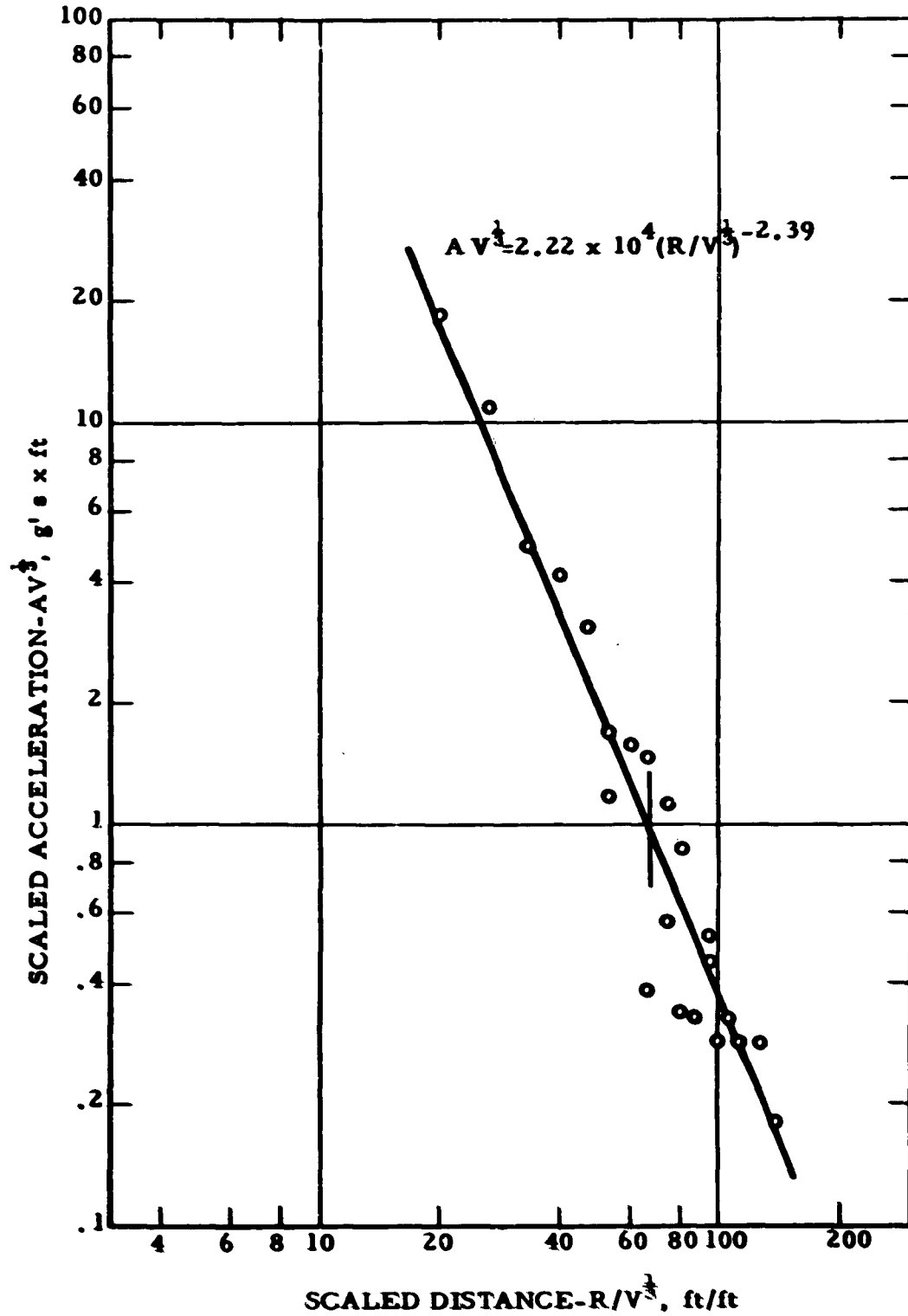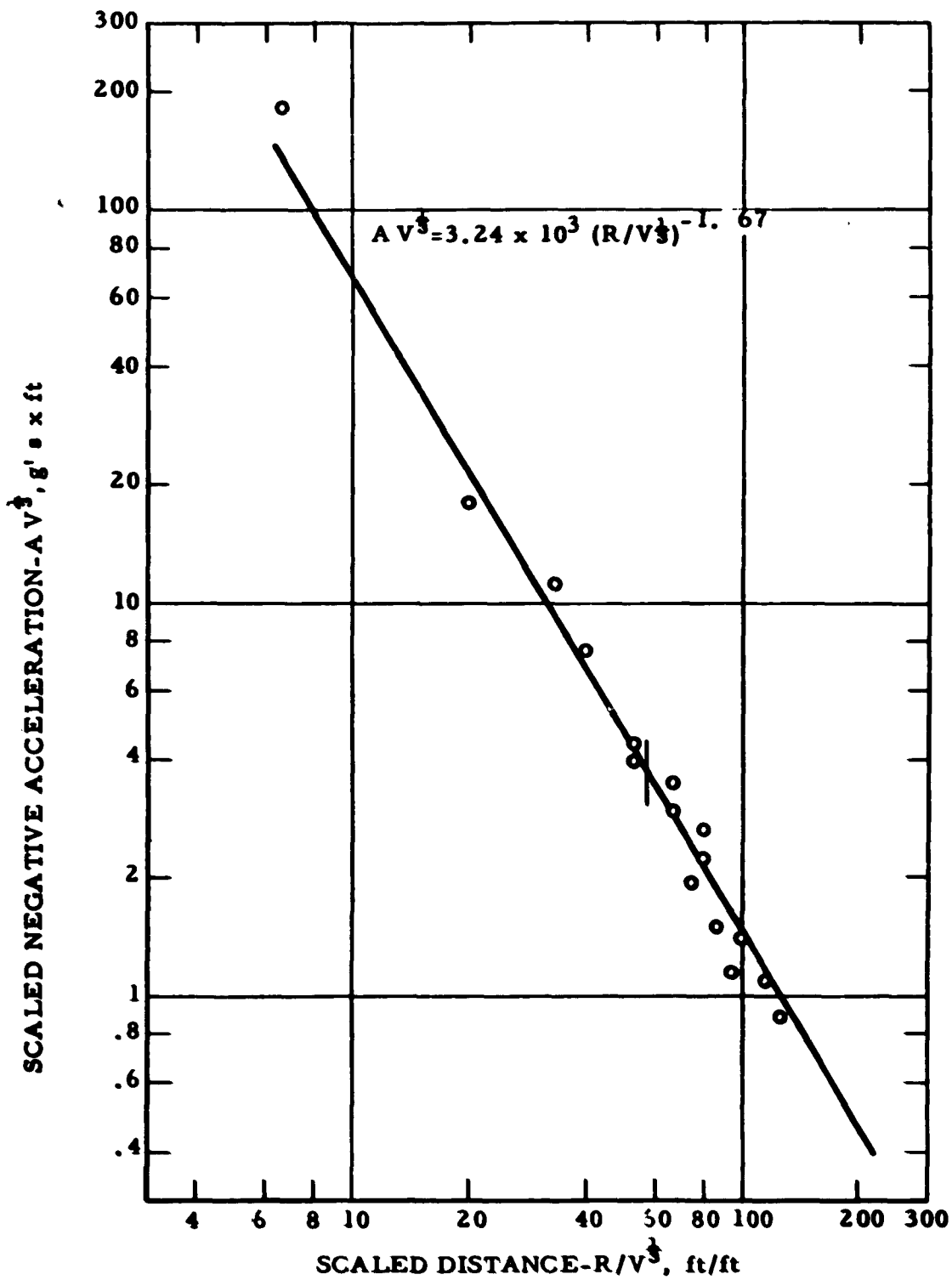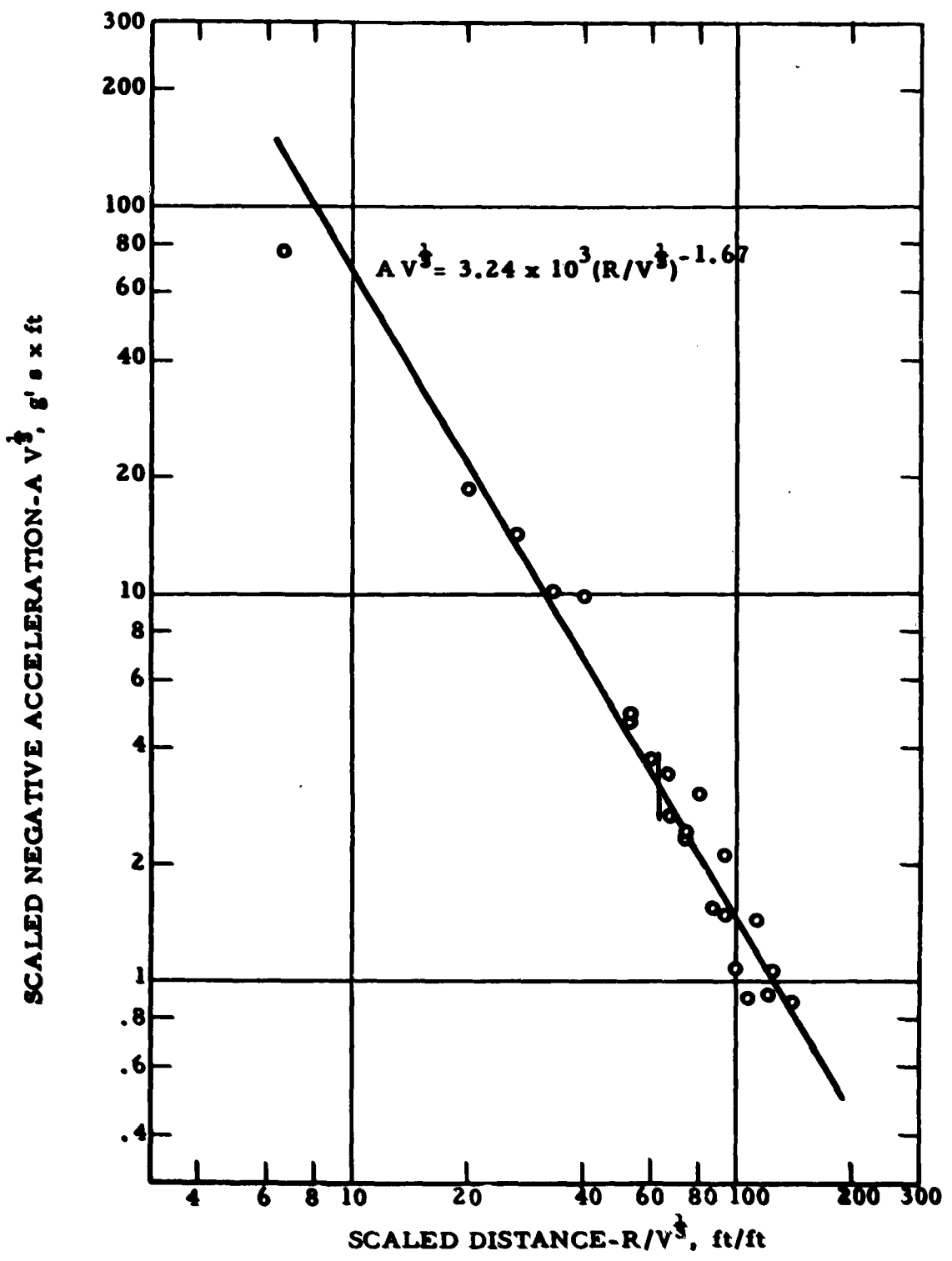
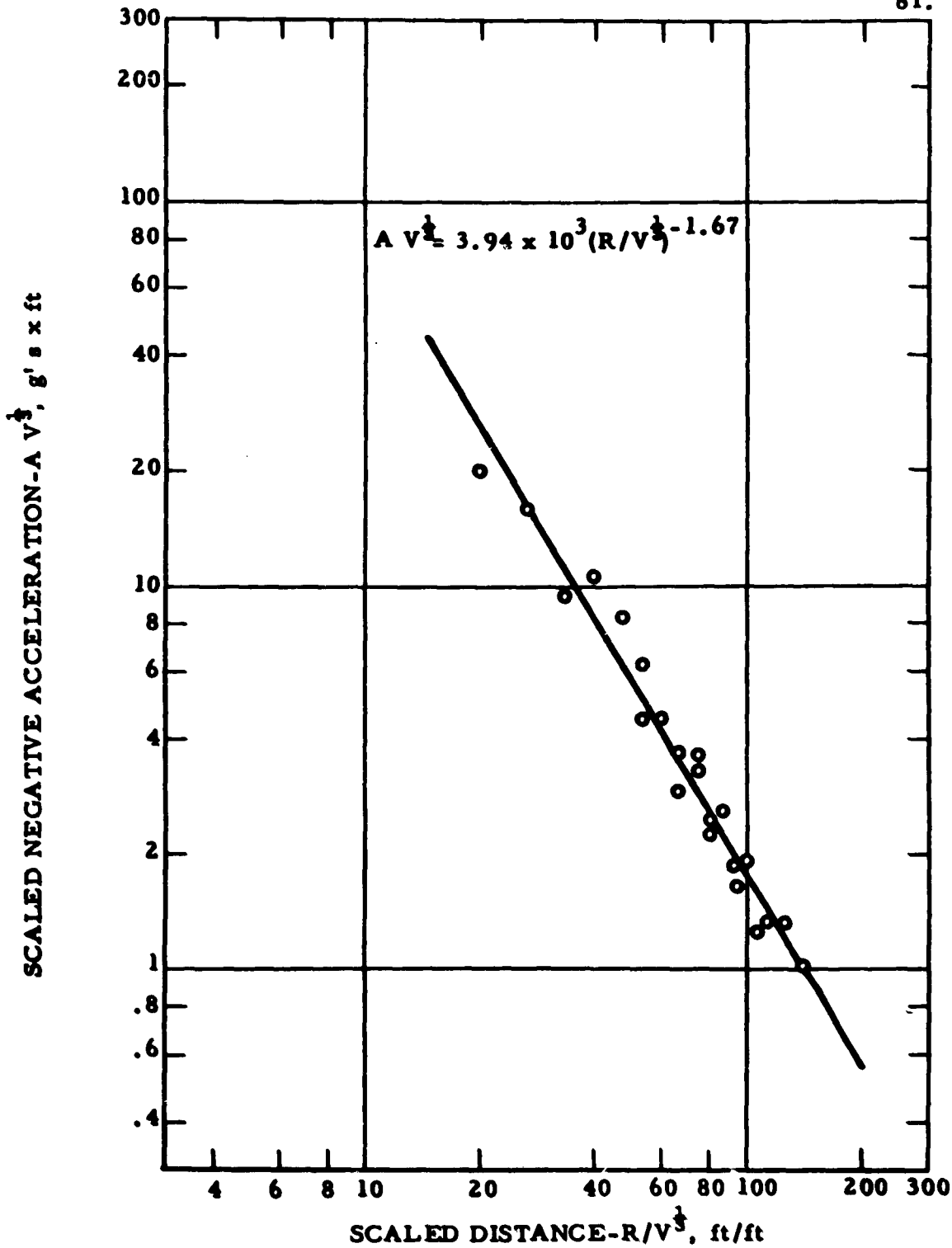$$A V^{\frac{1}{3}} = 1.83 \times 10^4 (R/V^{\frac{1}{3}})^{-2.39}$$
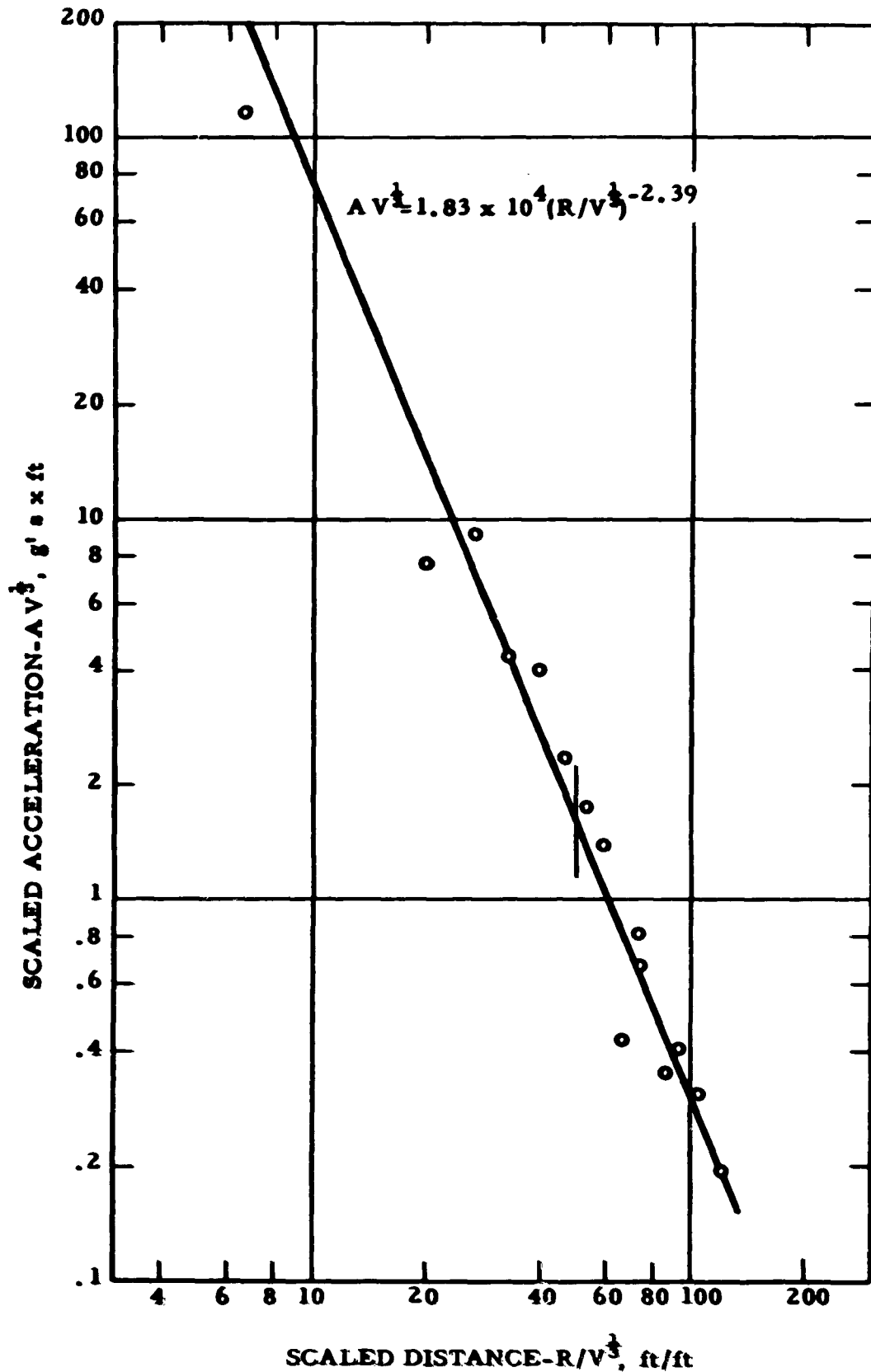
Fig. 27 - Scaled Acceleration vs. Scaled Distance for Explosive AD-P

$$A\,V^{\frac{1}{3}} = 2.22 \times 10^4 (R/V^{\frac{1}{3}})^{-2.39}$$

Fig.28 - Scaled Acceleration vs. Scaled Distance for Explosive SG 45

78.

$$A V^{\frac{1}{3}} = 3.24 \times 10^3 (R/V^{\frac{1}{3}})^{-1.67}$$

SCALED NEGATIVE ACCELERATION-$A V^{\frac{1}{3}}$, g's x ft

SCALED DISTANCE-$R/V^{\frac{1}{3}}$, ft/ft

Fig. 29 - Scaled Negative Acceleration vs. Scaled Distance for

Explosive AD 10

$$A V^{\frac{1}{3}} = 3.24 \times 10^3 (R/V^{\frac{1}{3}})^{-1.67}$$

Fig. 30 - Scaled Negative Acceleration vs. Scaled Distance for

Explosive AD 20A

80.
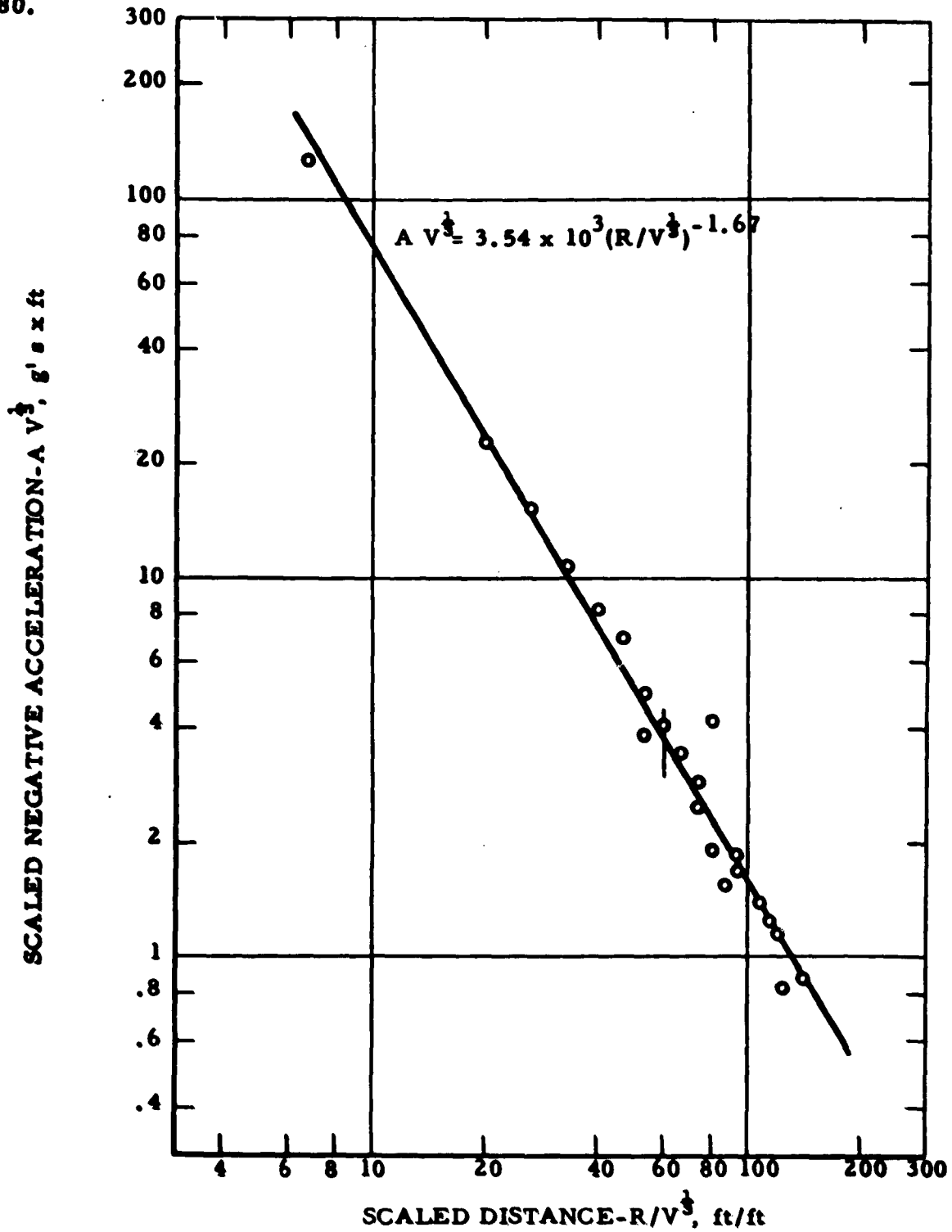
$$A V^{\frac{1}{3}} = 3.54 \times 10^3 (R/V^{\frac{1}{3}})^{-1.67}$$

Fig. 31- Scaled Negative Acceleration vs. Scaled Distance for
Explosive AD-P

$$A V^{\frac{1}{3}} = 3.94 \times 10^3 (R/V^{\frac{1}{3}})^{-1.67}$$

SCALED NEGATIVE ACCELERATION-A $V^{\frac{1}{3}}$, g' s x ft

SCALED DISTANCE-R/V$^{\frac{1}{3}}$, ft/ft

Fig. 32 - Scaled Negative Acceleration vs. Scaled Distance for

Explosive SG 45

TABLE 22. - Particle motion propagation law constants and standard deviations.

Explosive	Scaled positive acceleration		Scaled negative acceleration		Rise time		Fall time	
	$\underline{1/}$ K	$\underline{2/}$ S_E	K	S_E	K	S_E	K	S_E
	$g' s \times ft$ $\times 10^4$	%	$g' s \times ft$ $\times 10^4$	%	sec $\times 10^{-3}$	%	sec $\times 10^{-3}$	%
AD 10	1.99	40.5	.321	21.9	.0811	14.6	2.03	8.4
AD 20A	1.87	39.7	.324	21.7	.0860	14.8	2.13	8.2
AD-P	1.83	40.1	.354	21.5	.0868	15.0	2.01	8.1
SG 45	2.22	39.9	.394	21.8	.0887	14.9	2.34	8.1
Slope, n	-2.39		-1.67		.86		0.11	
S_n	$\pm.19$		$\pm.03$		$\pm.04$		$\pm.02$	

Explosive	Positive velocity		Negative velocity		Rise time		Fall time	
	K	S_E	K	S_E	K	S_E	K	S_E
	in/sec $\times 10^3$	%	in/sec $\times 10^3$	%	sec $\times 10^{-3}$	%	sec $\times 10^{-3}$	%
AD 10	2.62	39.9	1.03	23.5	.146	14.3	2.16	9.6
AD 20A	2.71	39.8	1.04	23.4	.156	14.1	2.15	9.3
AD-P	2.62	39.6	1.14	23.0	.155	14.1	2.18	9.5
SG 45	3.22	39.8	1.29	22.6	.154	14.2	2.47	9.4
Slope, n	-2.18		-1.65		0.74		0.11	
S_n	$\pm.06$		$\pm.04$		$\pm.04$		$\pm.02$	

$\underline{1/}$ K = intercept at $R/V^{\frac{1}{3}} = 1.0$. $\underline{2/}$ S_E = The standard deviation about the mean.

Particle Velocity

The particle velocity data were obtained by electronically integrating the acceleration records. A study of the acceleration records and the velocity indicates that the integration process was reliable. Furthermore, over most of the propagation distances in the test series, the shape of particle velocity and strain pulses should be identical if the direct, radial portion of each pulse is considered. Comparison of the pulses verified that the early portions were of the same shape. However, little correlation was expected or evidenced beyond the calculated time of arrival of surface reflected waves.

Peak positive velocity, negative velocity, and the associated rise and fall times as obtained from the integrated records are given in tables 18 to 21. Again, positive defines radial outward particle motion and negative defines radial inward particle motion. Positive and negative particle velocity have both been plotted as a function of scaled distance for each explosive. The plots on log-log coordinates are shown in figures 33 to 40. Particle velocity data have been fitted to the following equation:

$$v = K (R/V^{\frac{1}{3}})^n \tag{5}$$

where

$$v = \text{particle velocity.}$$

The values of n and K and the standard deviations are given in table 22.

Period Data

Rise and fall times were read from all records. These times for strain data are given in tables 9 to 12 and for acceleration and particle velocity in tables 18 to 21. The period data were scaled and plotted versus scaled distance on log-log coordinates as shown in figures 41 to 64. Rise and fall times were treated separately for each type of particle motion and for each explosive. The scaled data are represented by the following equation:

$$t/V^{\frac{1}{3}} = K (R/V^{\frac{1}{3}})^n \tag{6}$$

where

$$t = \text{time, either rise time, } t_r, \text{ or} \\ \text{fall time, } t_f.$$

$$V = 2.62 \times 10^3 (R/V^{\frac{1}{3}})^{-2.18}$$
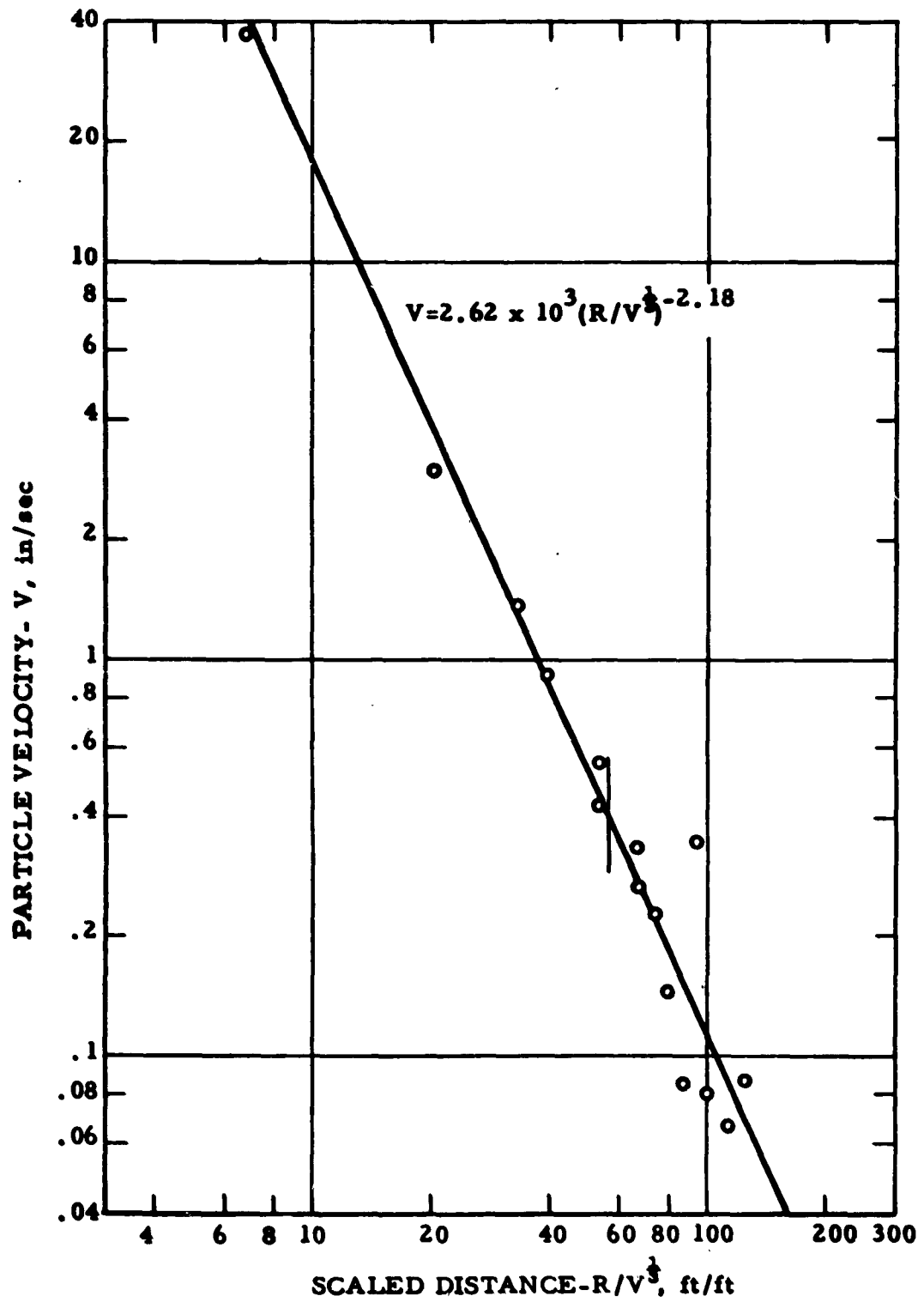
Fig. 33 - Particle Velocity vs. Scaled Distance for Explosive AD 10
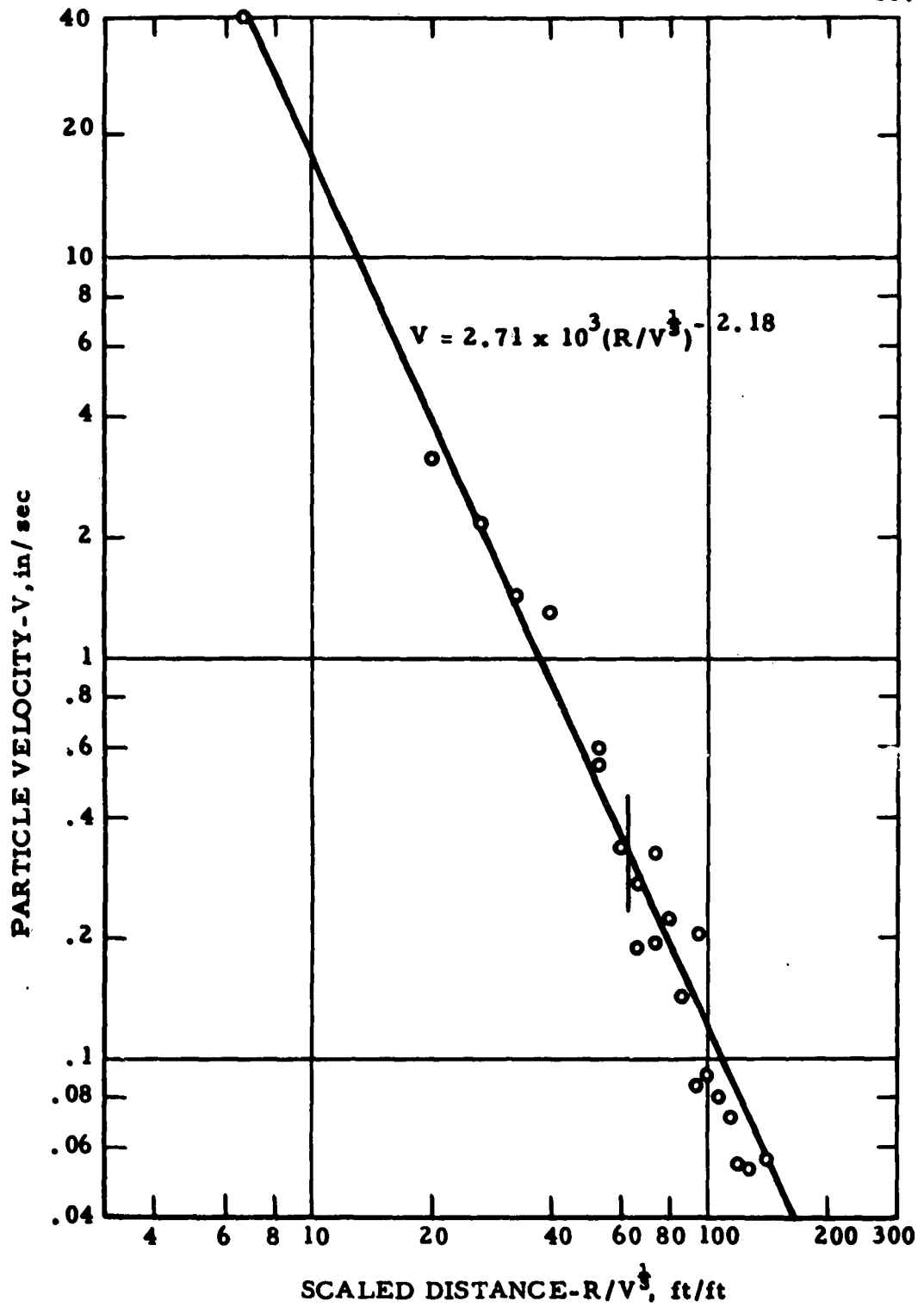
$$V = 2.71 \times 10^3 (R/V^{\frac{1}{3}})^{-2.18}$$

Fig. 34 - Particle Velocity vs. Scaled Distance for Explosive AD 20A

86.

$$V = 2.62 \times 10^3 (R/V^{\frac{1}{3}})^{-2.18}$$

PARTICLE VELOCITY-V, in/sec

SCALED DISTANCE-R/V$^{\frac{1}{3}}$, ft/ft

Fig.35 - Particle Velocity vs. Scaled Distance for Explosive AD-P

The line is labeled $V = 3.22 \times 10^3 (R/V^{\frac{1}{3}})^{-2.18}$

Y-axis: PARTICLE VELOCITY-V, in/sec

X-axis: SCALED DISTANCE-$R/V^{\frac{1}{3}}$, ft/ft
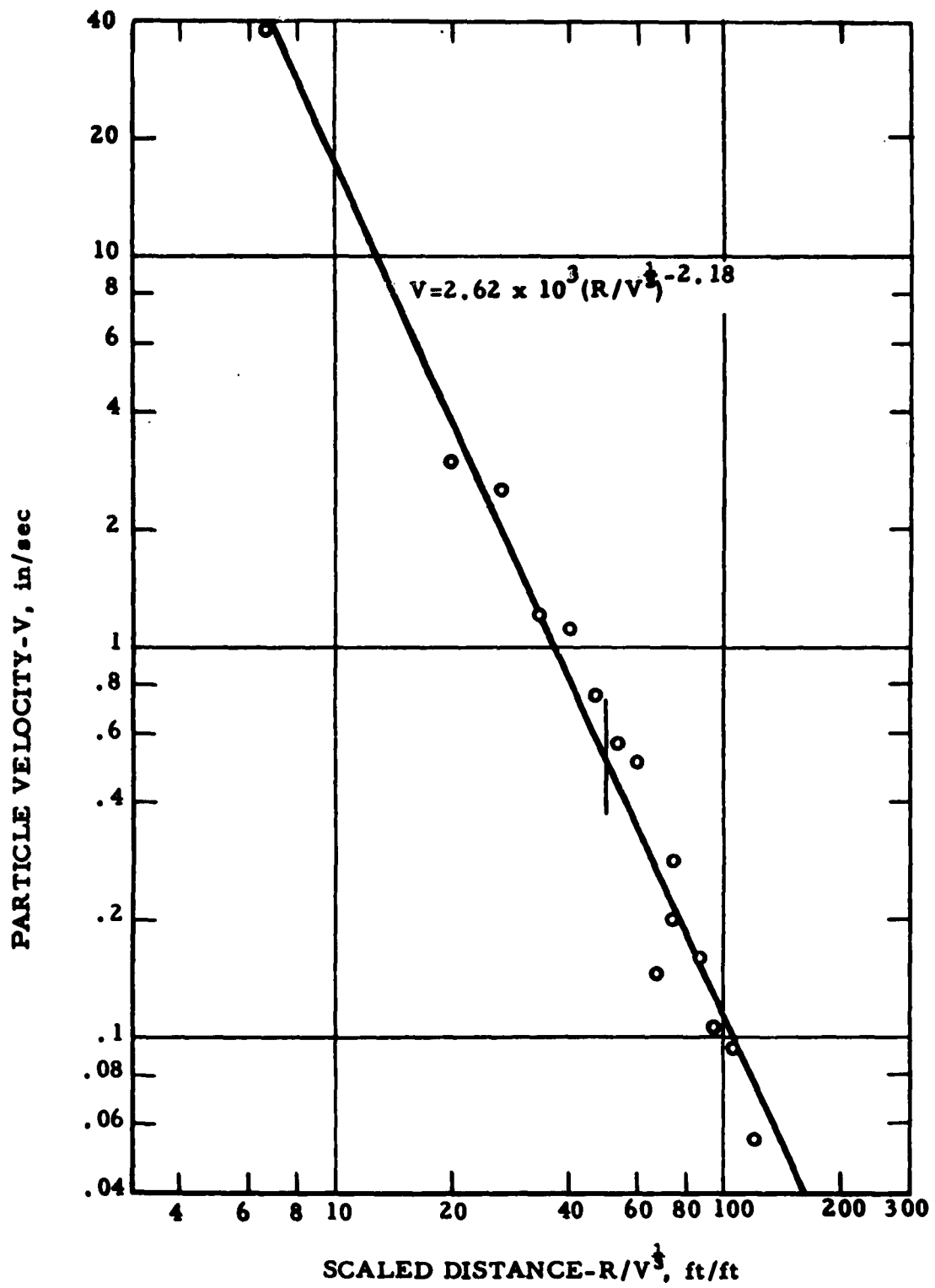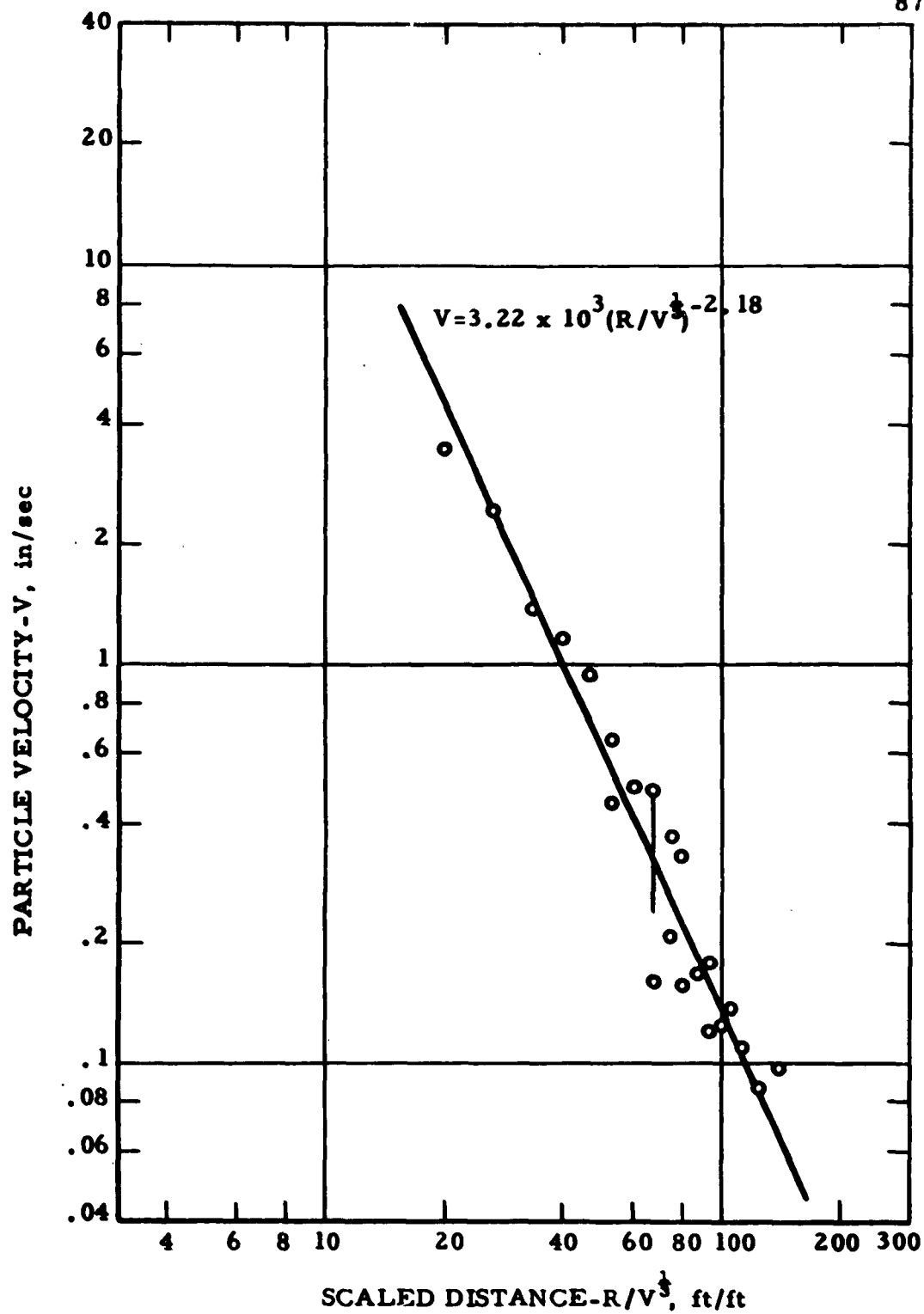
Fig.36 - Particle Velocity vs. Scaled Distance for Explosive SG 45

Fig. 37- Negative Velocity vs. Scaled Distance for Explosive AD 10

$$V = 1.04 \times 10^3 \ (R/V^{\frac{1}{3}})^{-1.65}$$

NEGATIVE VELOCITY-V, inches/second

SCALED DISTANCE- $R/V^{\frac{1}{3}}$, ft/ft

Fig. 38 - Negative Velocity vs. Scaled Distance for Explosive AD 20-A

$$V = 1.14 \times 10^3 (R/V^{\frac{1}{3}})^{-1.65}$$

NEGATIVE VELOCITY- V, inches/second

SCALED DISTANCE- $R/V^{\frac{1}{3}}$, ft/ft
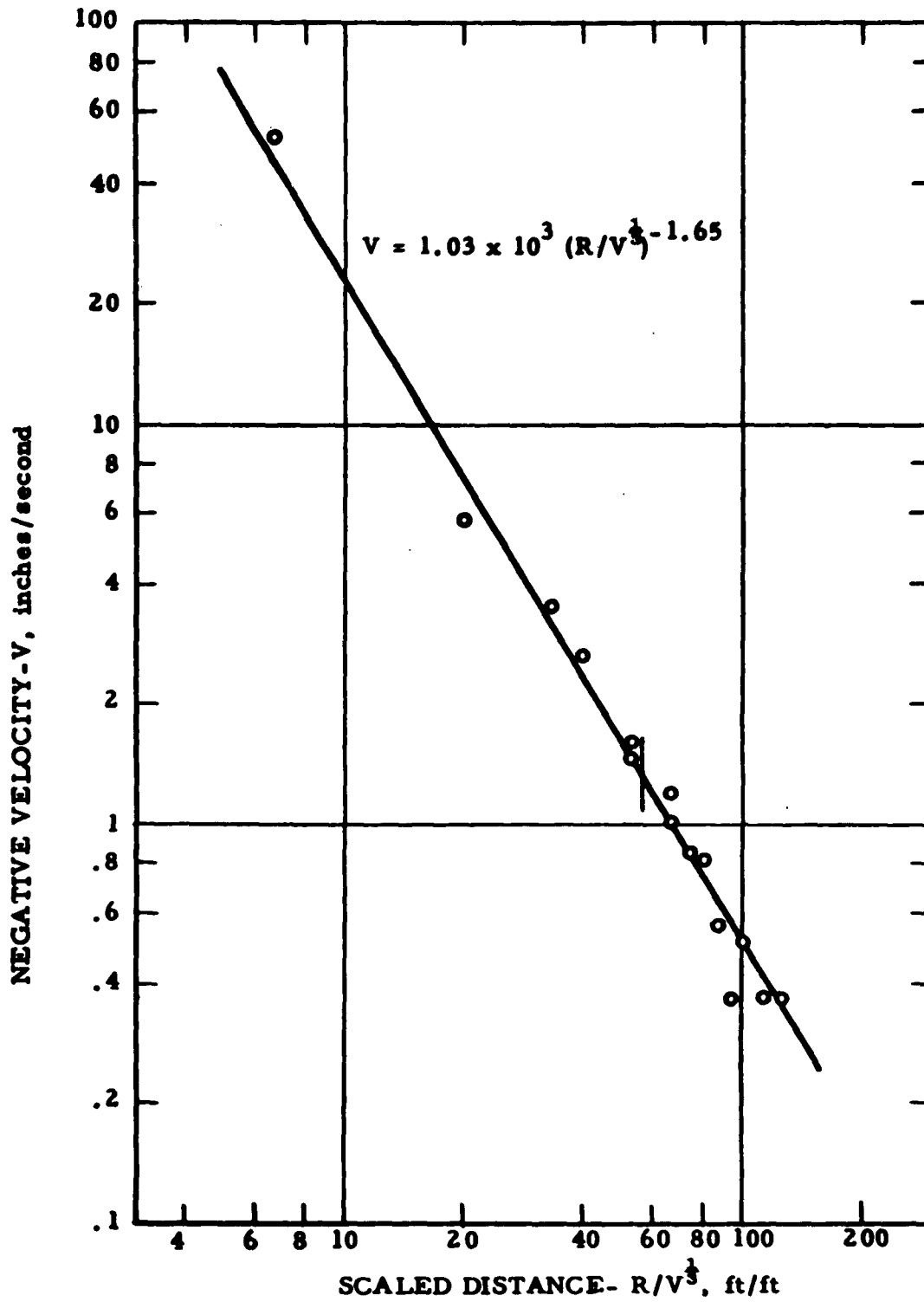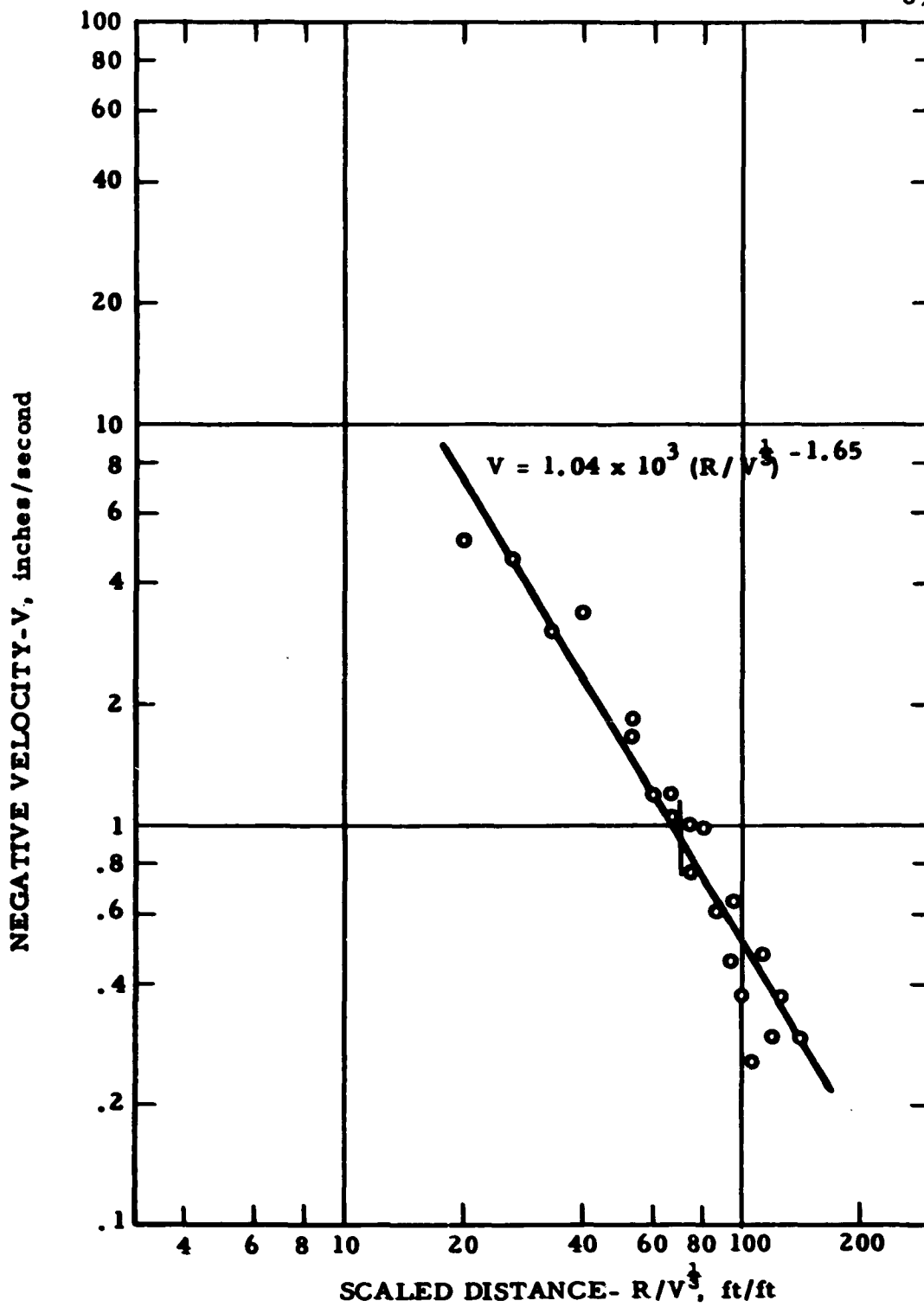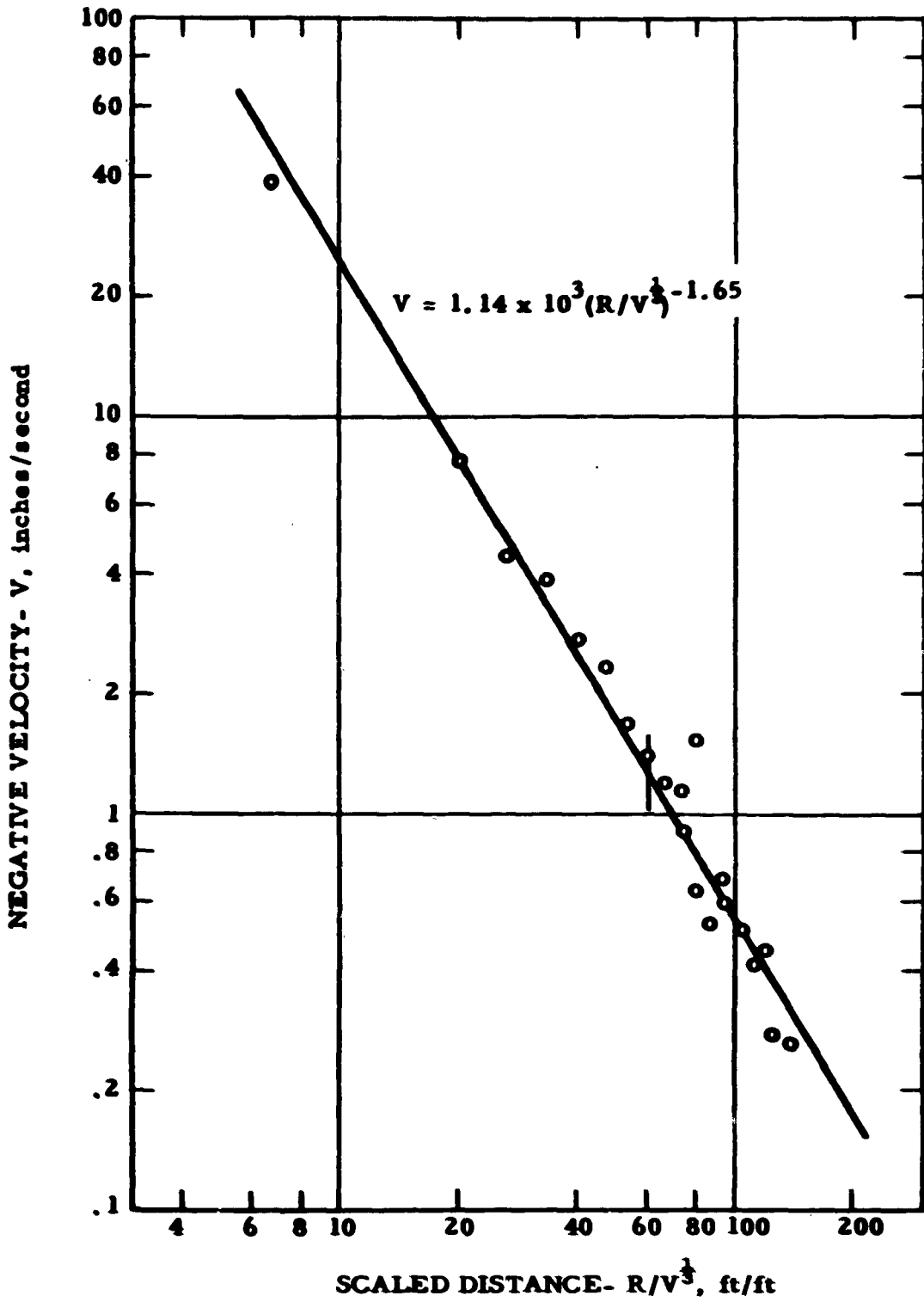
Fig. 39 - Negative Velocity vs. Scaled Distance for Explosive AD-P

$$V = 1.29 \times 10^3 \ (R/V^{\frac{1}{3}})^{-1.65}$$
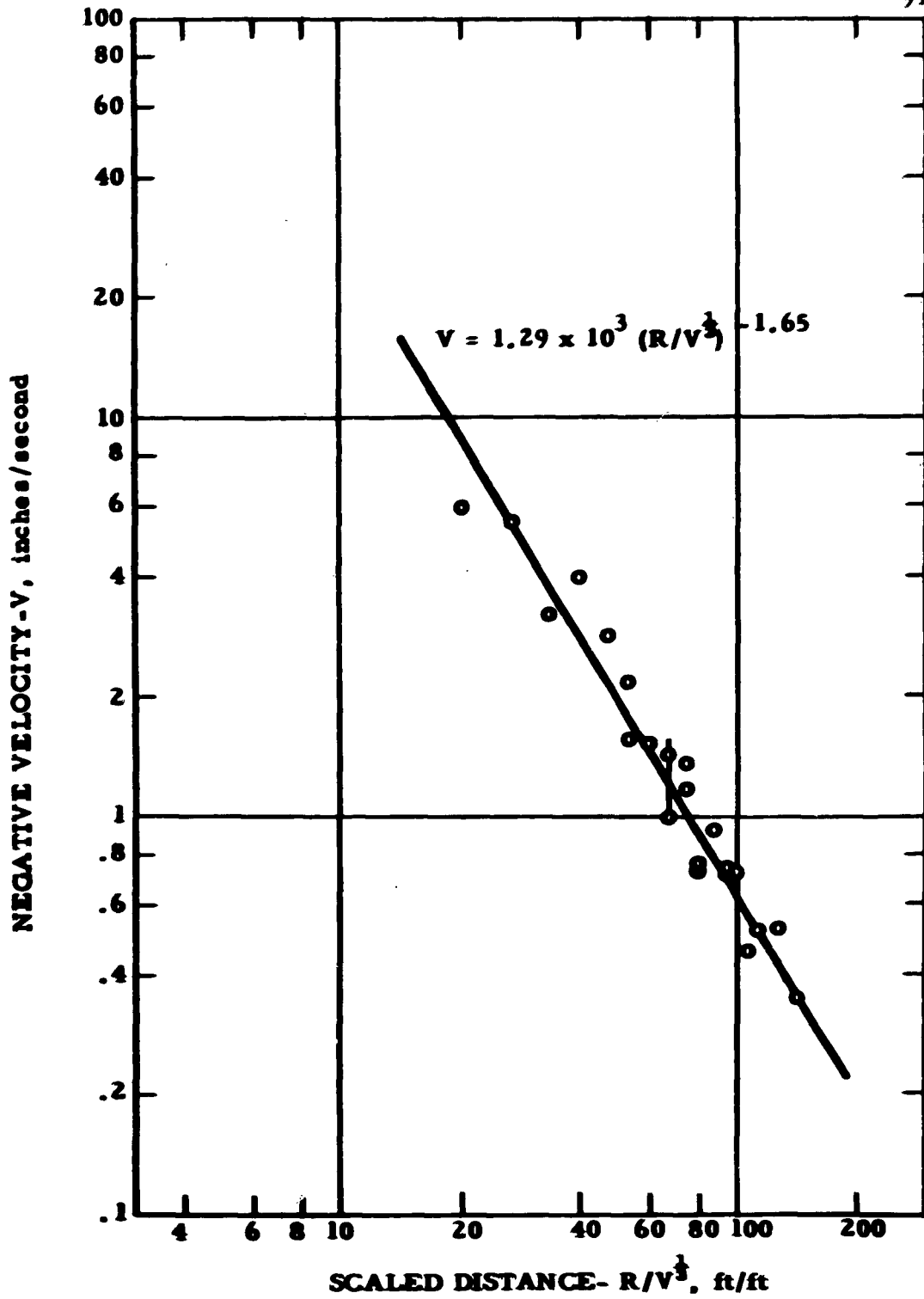
Fig. 40 - Negative Velocity vs. Scaled Distance for Explosive SG 45

92.

$t_r/V^{\frac{1}{3}} = 0.224(R/V^{\frac{1}{3}})^{0.68}$

SCALED DISTANCE–R/V$^{\frac{1}{3}}$, ft/ft

SCALED RISE TIME– $t_r/V^{\frac{1}{3}}$, sec/ft x 10^{-3}

Fig. 42 – Scaled Rise Time vs. Scaled Distance
for Strain Data– Explosive AD 20A

$t_r/V^{\frac{1}{3}} = 0.211(R/V^{\frac{1}{3}})^{0.68}$

SCALED DISTANCE– R/V$^{\frac{1}{3}}$, ft/ft

SCALED RISE TIME– $t_r/V^{\frac{1}{3}}$, sec/ft x 10^{-3}
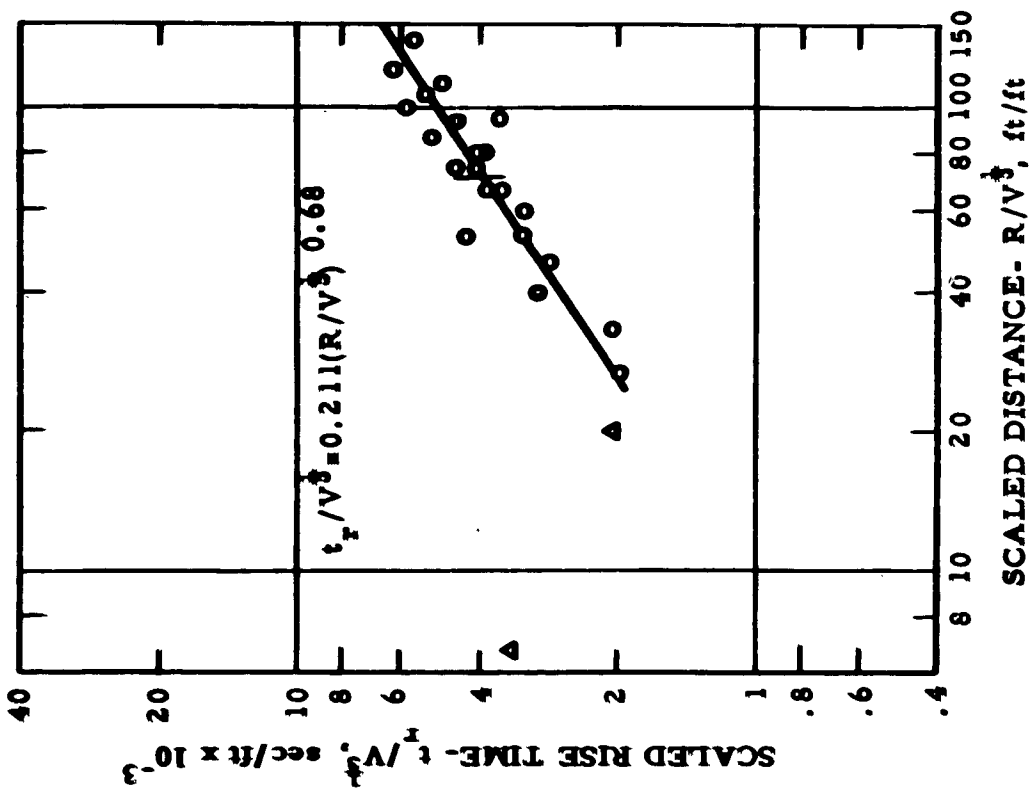
Fig. 41 – Scaled Rise Time vs. Scaled Distance
for Strain Data–Explosive AD 10

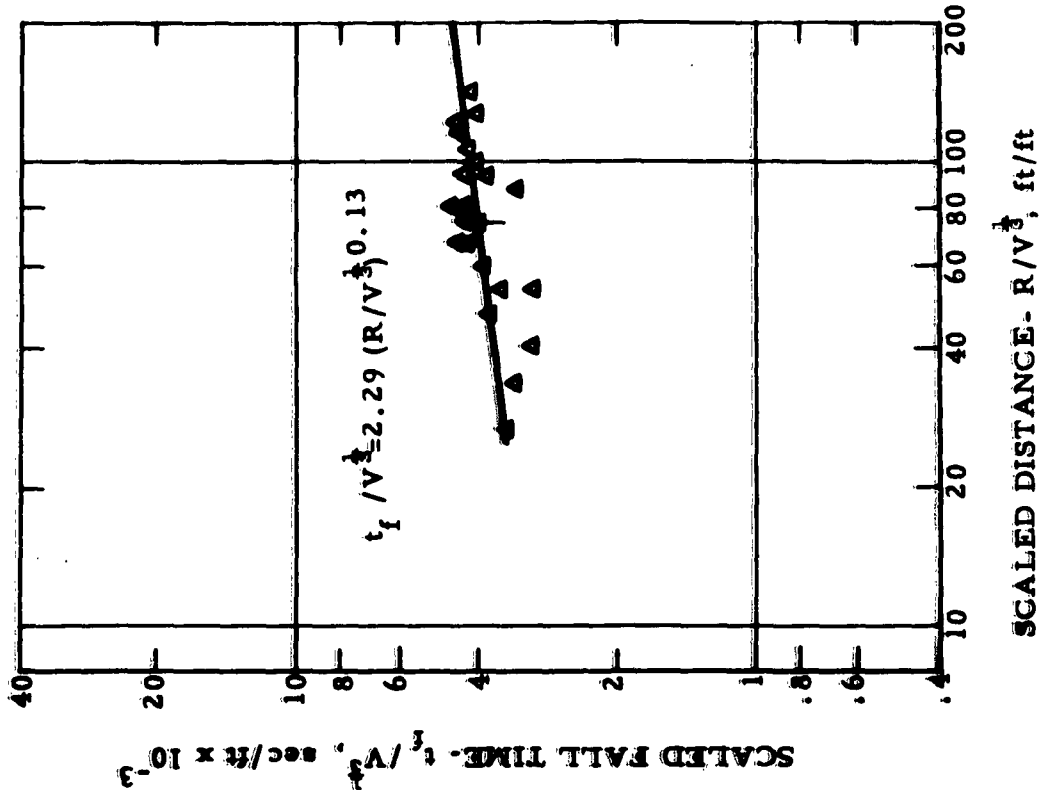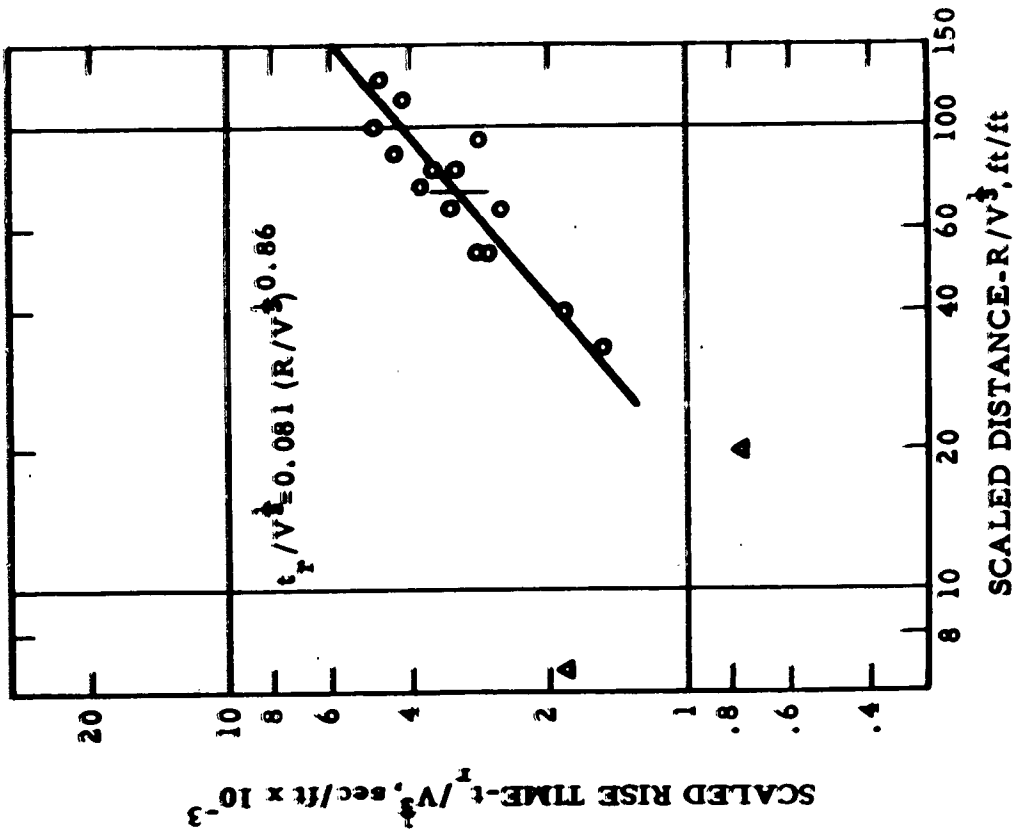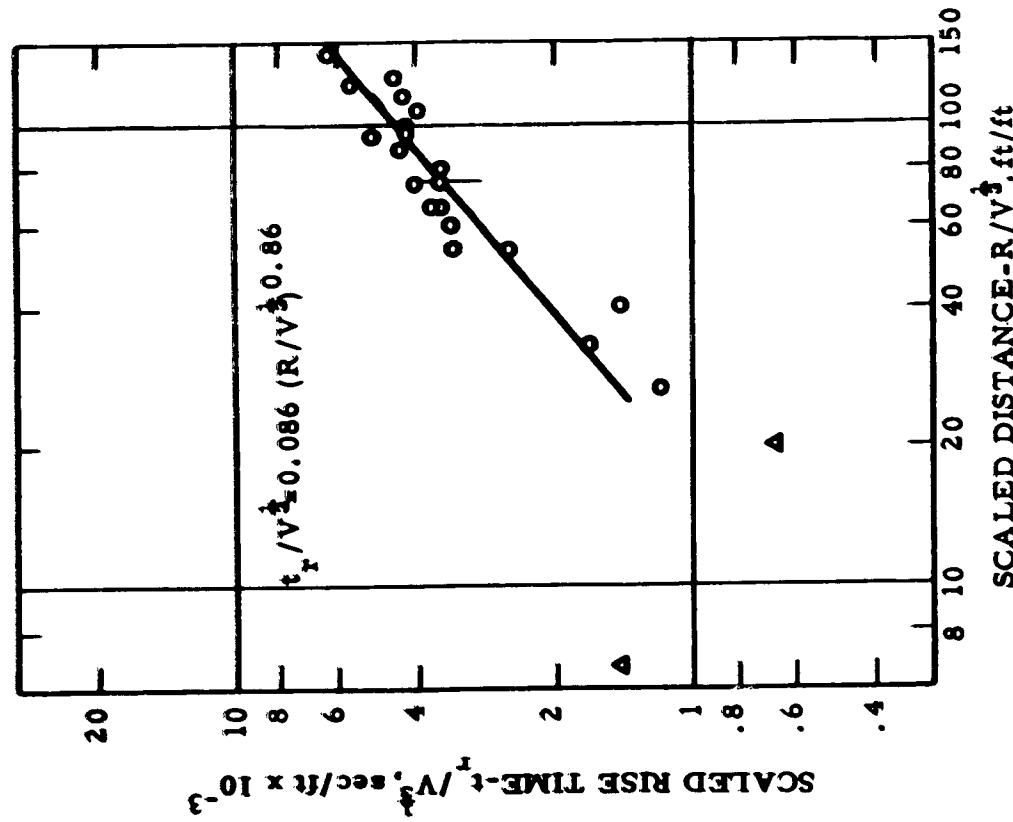Fig. 44 – Scaled Rise Time vs. Scaled Distance
for Strain Data- Explosive SG 45

$$t_r/V^{\frac{1}{3}} = 0.219 \, (R/V^{\frac{1}{3}})^{0.68}$$
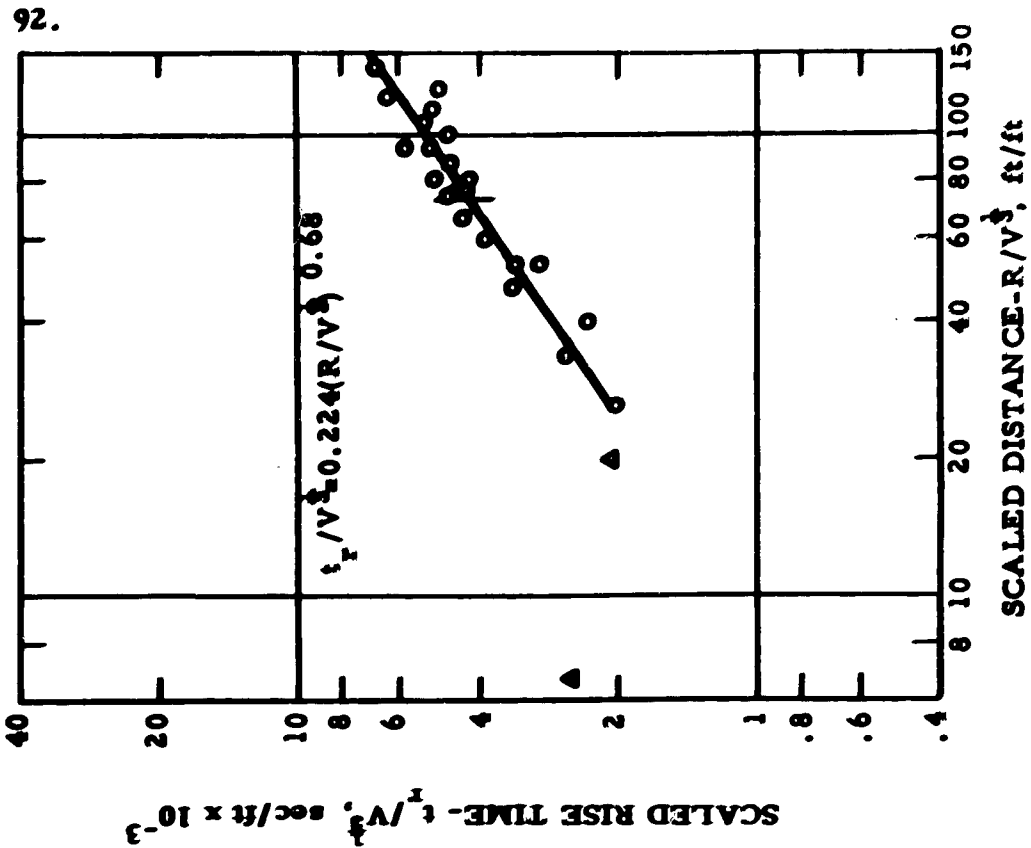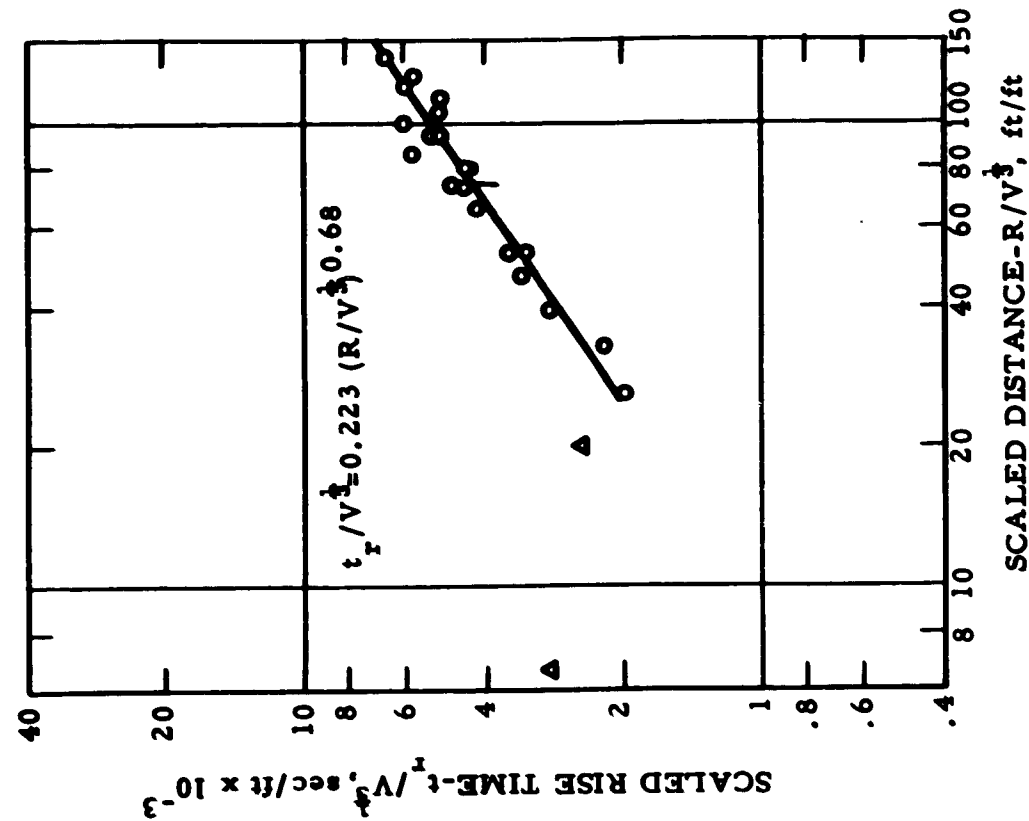
Fig. 43 – Scaled Rise Time vs. Scaled Distance
for Strain Data-Explosive AD-P
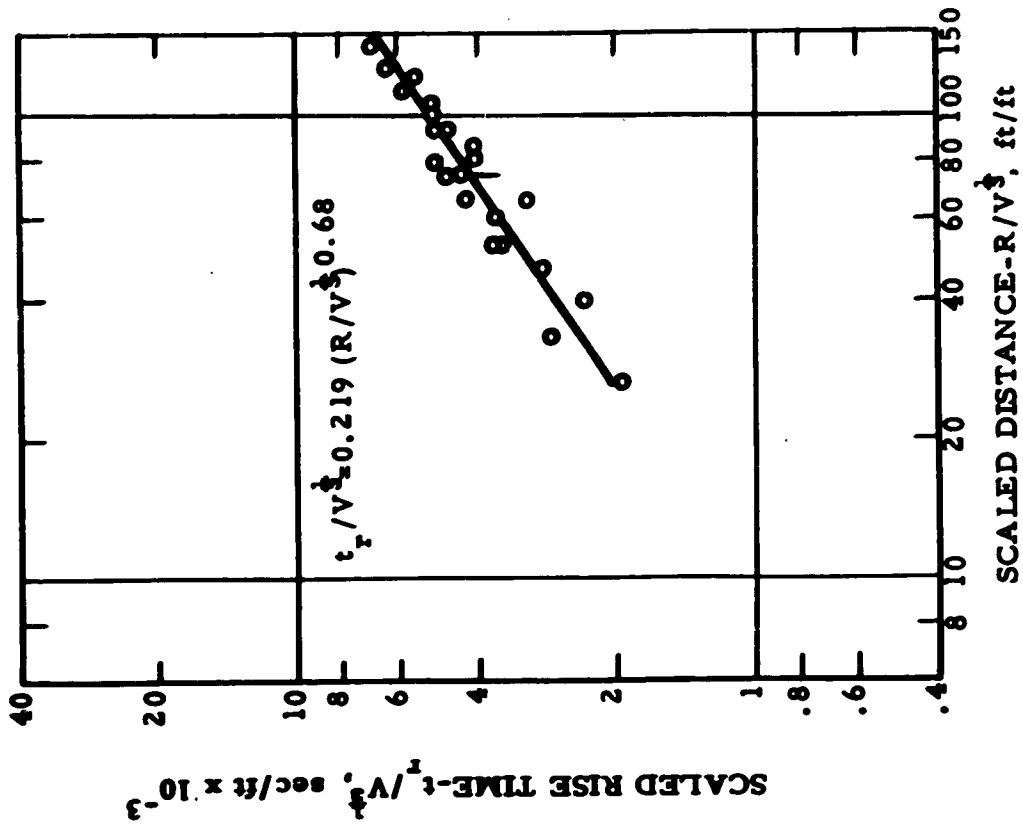
$$t_r/V^{\frac{1}{3}} = 0.223 \, (R/V^{\frac{1}{3}})^{0.68}$$

93.

$t_f/V^{\frac{1}{3}} = 2.02 (R/V^{\frac{1}{3}})^{0.13}$

SCALED DISTANCE-$R/V^{\frac{1}{3}}$, ft/ft

SCALED FALL TIME-$t_f/V^{\frac{1}{3}}$, sec/ft x 10^{-3}
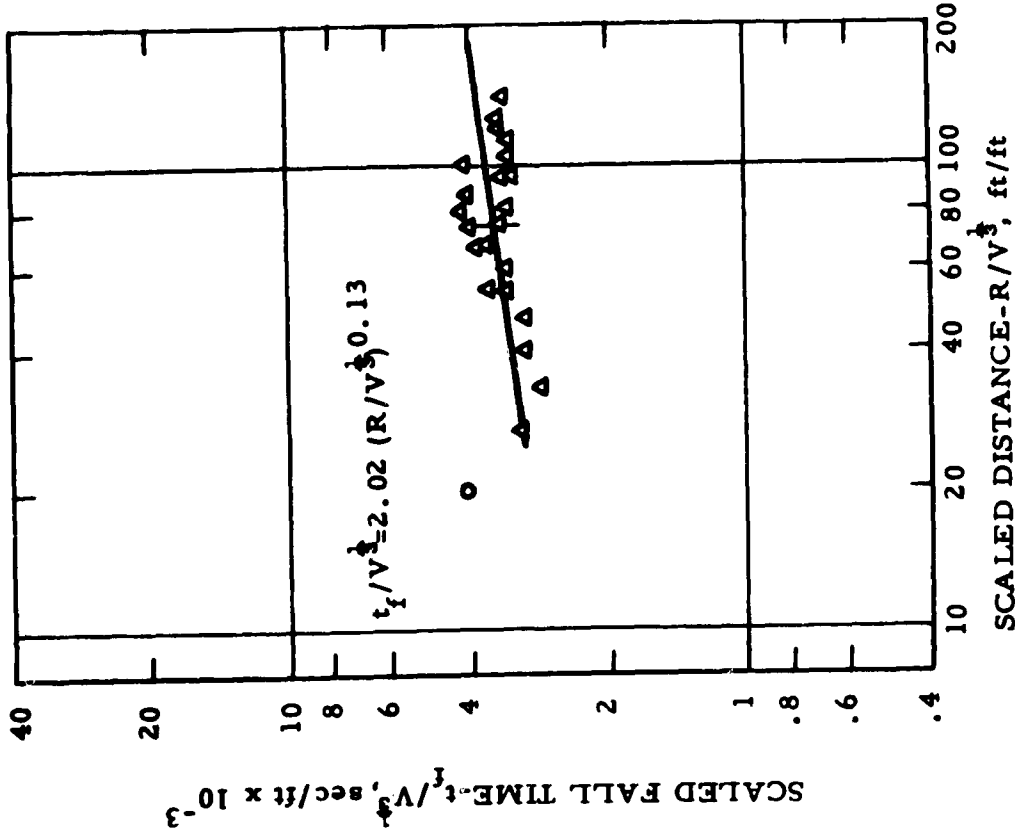
Fig. 46 - Scaled Fall Time vs. Scaled Distance
for Strain Data-Explosive AD 20A

$t_f/V^{\frac{1}{3}} = 2.01 (R/V^{\frac{1}{3}})^{0.13}$

SCALED DISTANCE-$R/V^{\frac{1}{3}}$, ft/ft

SCALED FALL TIME-$t_f/V^{\frac{1}{3}}$, sec/ft x 10^{-3}
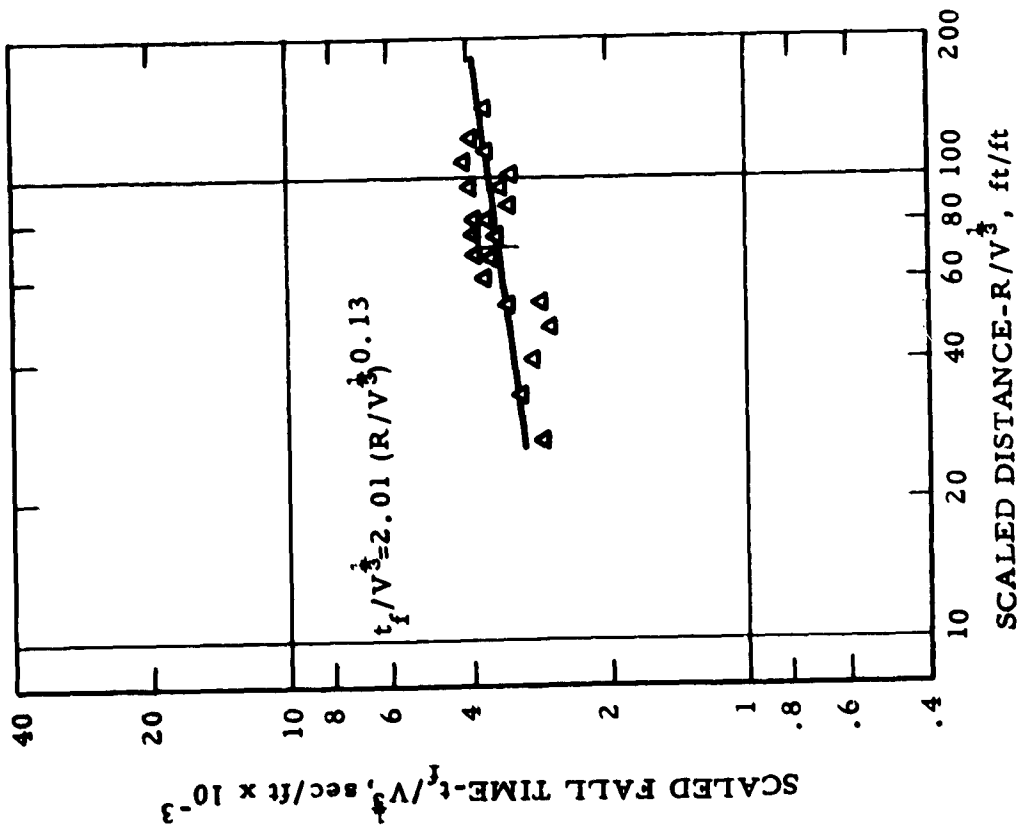
Fig. 45 - Scaled Fall Time vs. Scaled Distance for
Strain Data-Explosive AD 10

Fig. 48 - Scaled Fall Time vs. Scaled Distance
for Strain Data- Explosive SG 45

Fig. 47 - Scaled Fall Time vs. Scaled Distance
for Strain Data- Explosive AD-P

95.

Fig. 50 - Scaled Rise Time vs. Scaled Distance
for Acceleration Data-
Explosive AD 10

Fig. 49 - Scaled Rise Time vs. Scaled Distance for
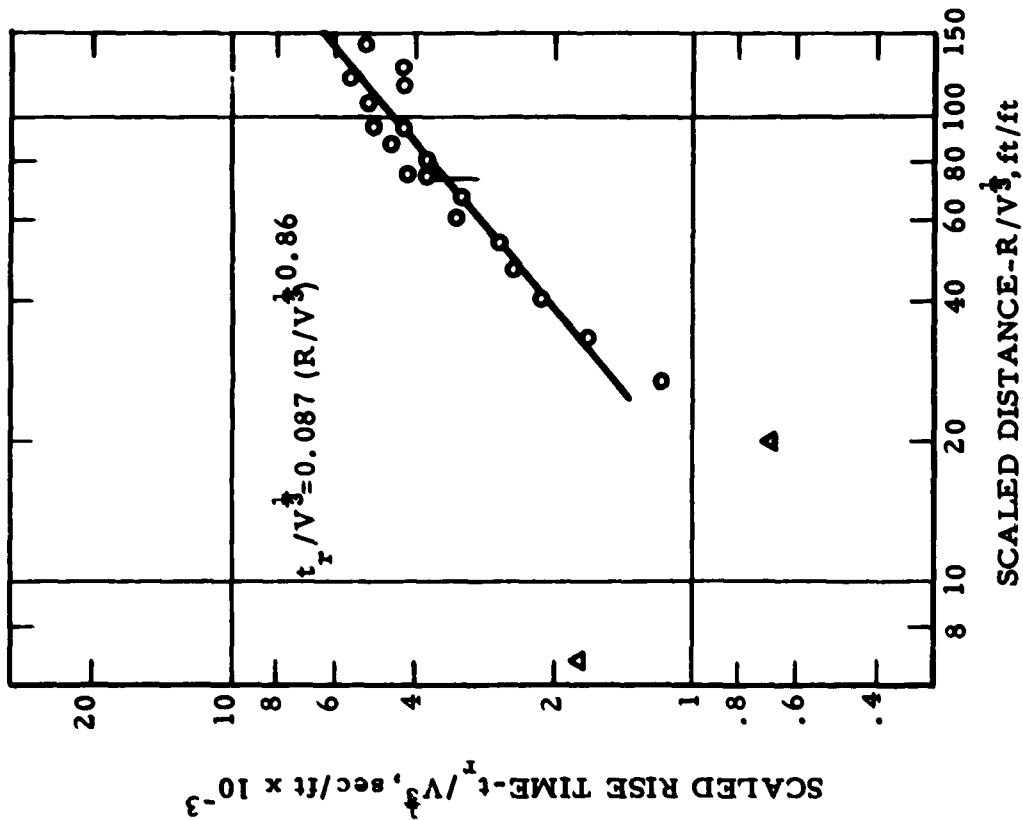Acceleration Data-
Explosive AD 20A

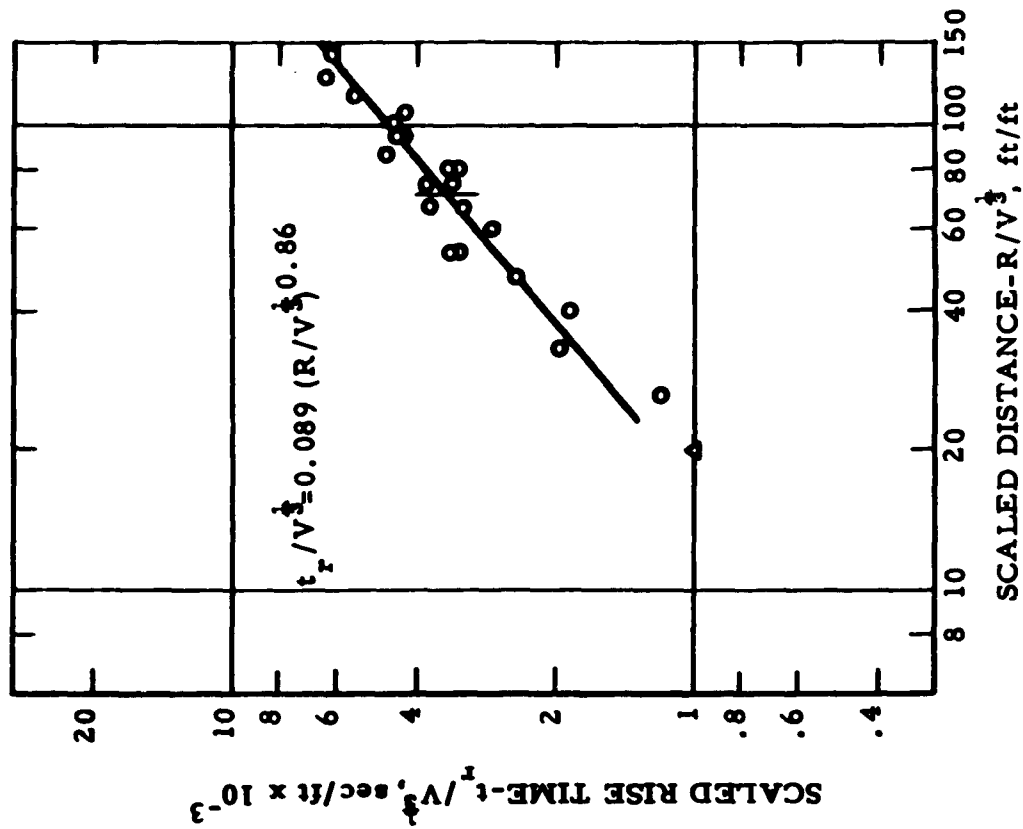Fig. 52 - Scaled Rise Time vs. Scaled Distance
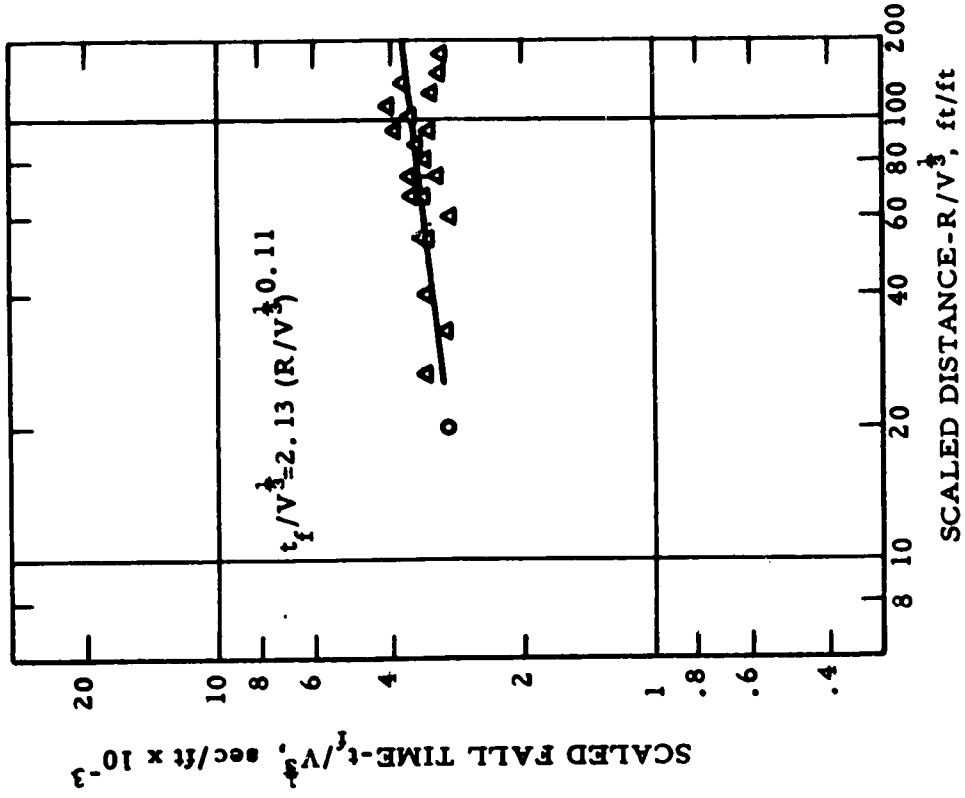for Acceleration Data-
Explosive SG 45

Fig. 51 - Scaled Rise Time vs. Scaled Distance for
Acceleration Data-
Explosive AD-P

97.

Fig. 54 – Scaled Fall Time vs. Scaled Distance
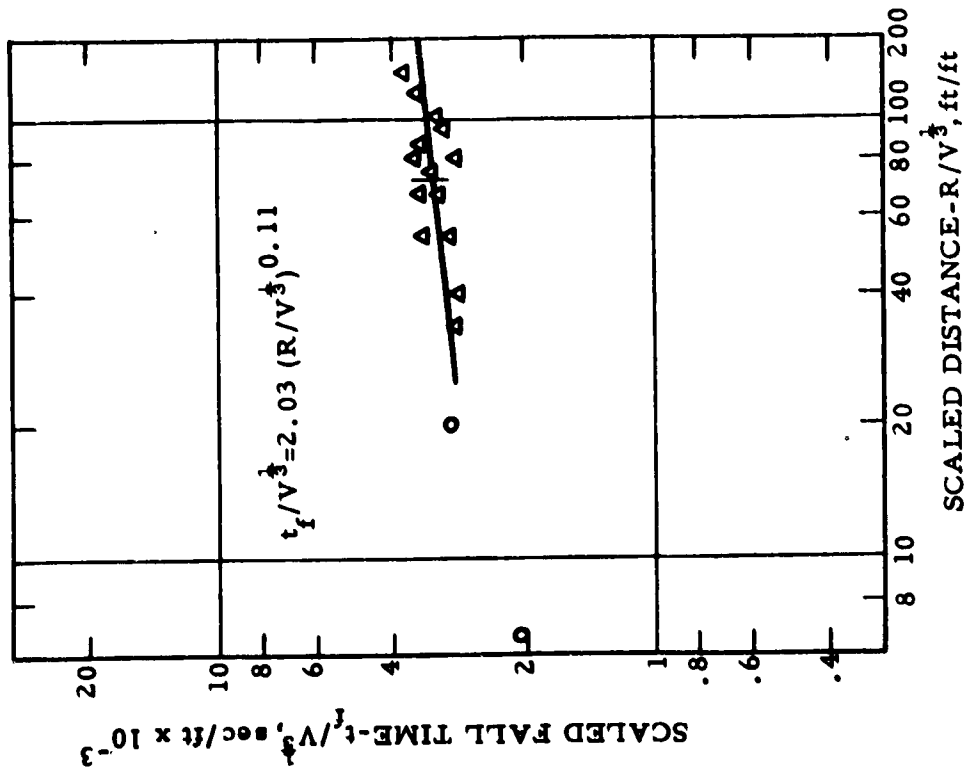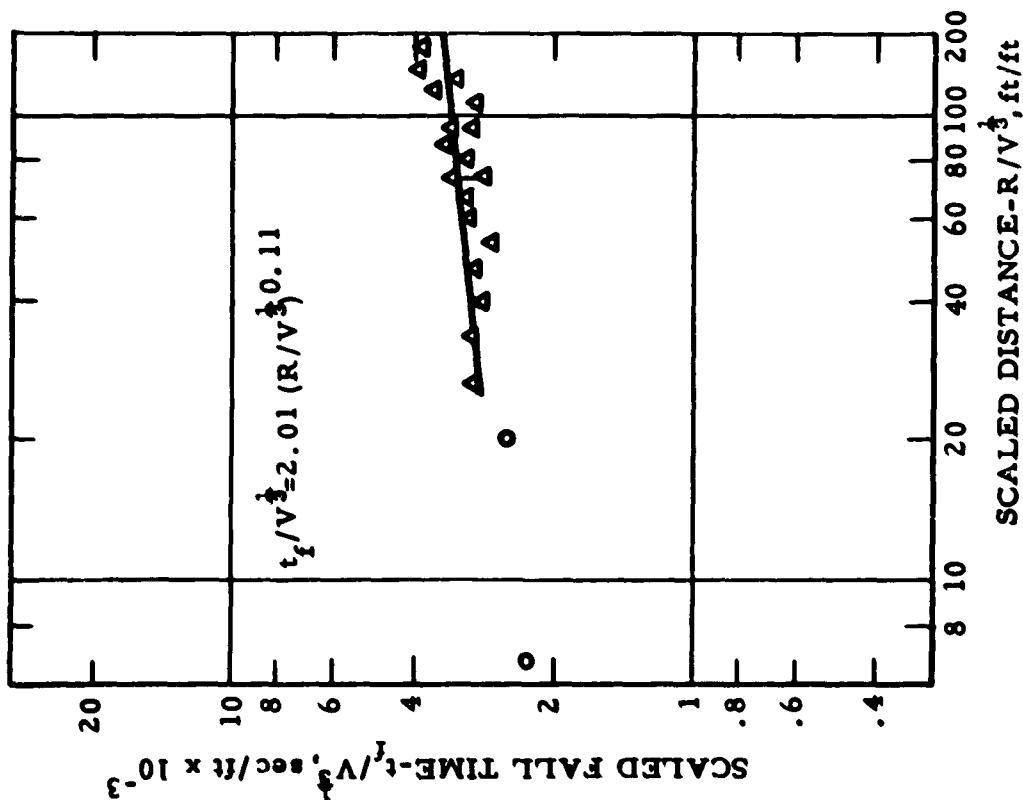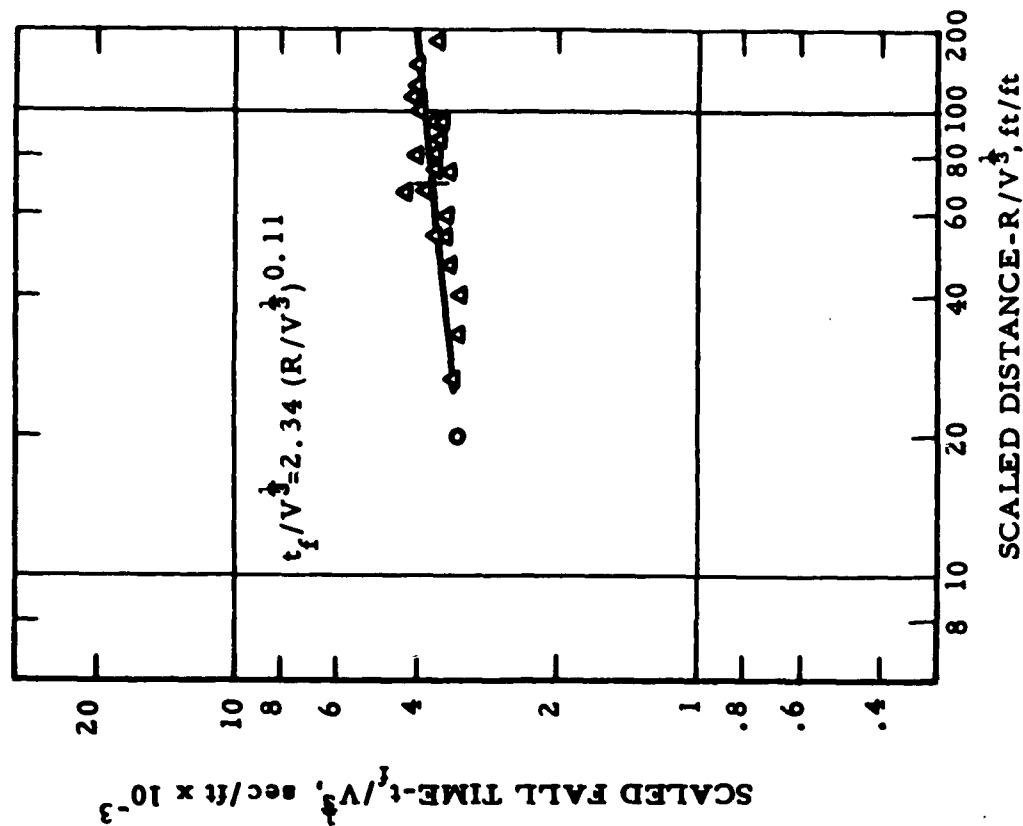for Acceleration Data-Explosive AD 20A

$$t_f/V^{\frac{1}{3}} = 2.13 \ (R/V^{\frac{1}{3}})^{0.11}$$

Fig. 53 – Scaled Fall Time vs. Scaled Distance for
Acceleration Data-Explosive AD 10

$$t_f/V^{\frac{1}{3}} = 2.03 \ (R/V^{\frac{1}{3}})^{0.11}$$

Fig. 56 - Scaled Fall Time vs. Scaled Distance for Acceleration Data- Explosive SG 45

$$t_f/V^{\frac{1}{3}} = 2.34 \, (R/V^{\frac{1}{3}})^{0.11}$$

Fig. 55 - Scaled Fall Time vs. Scaled Distance for Acceleration Data- Explosive AD-P

$$t_f/V^{\frac{1}{3}} = 2.01 \, (R/V^{\frac{1}{3}})^{0.11}$$

99.

$t_r/V^{\frac{1}{3}} = 0.156 \ (R/V^{\frac{1}{3}})^{0.74}$

Fig.58 - Scaled Rise Time vs. Scaled Distance for Particle Velocity Data-Explosive AD 20A
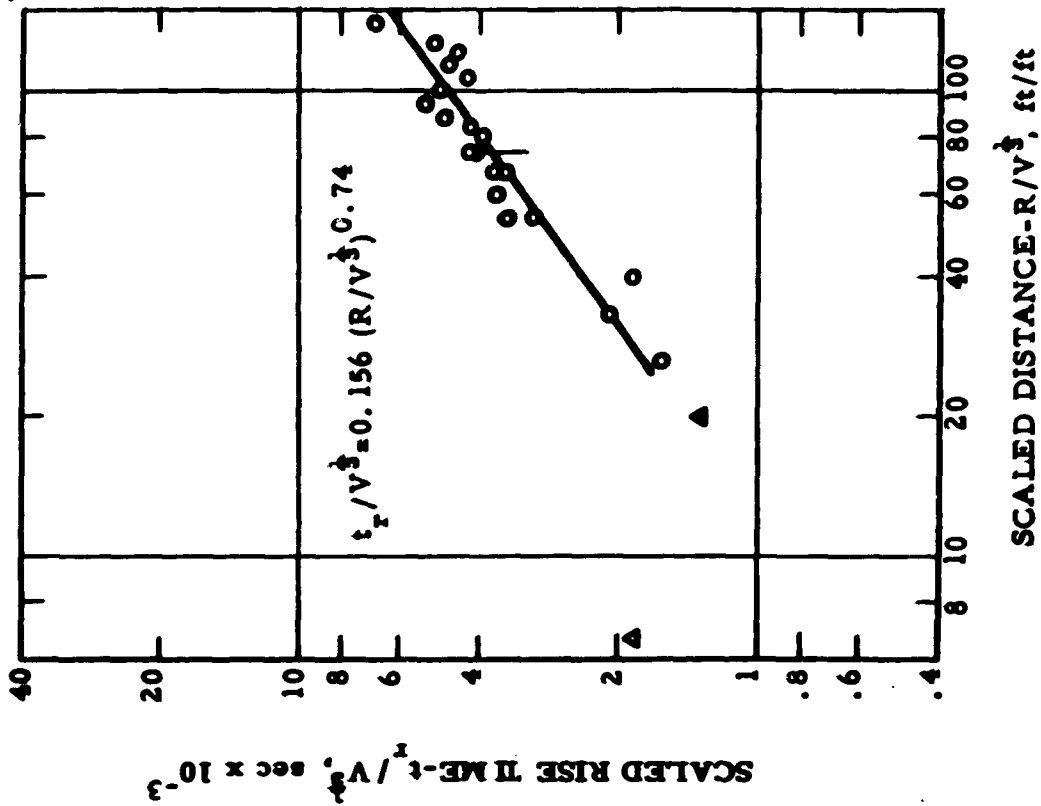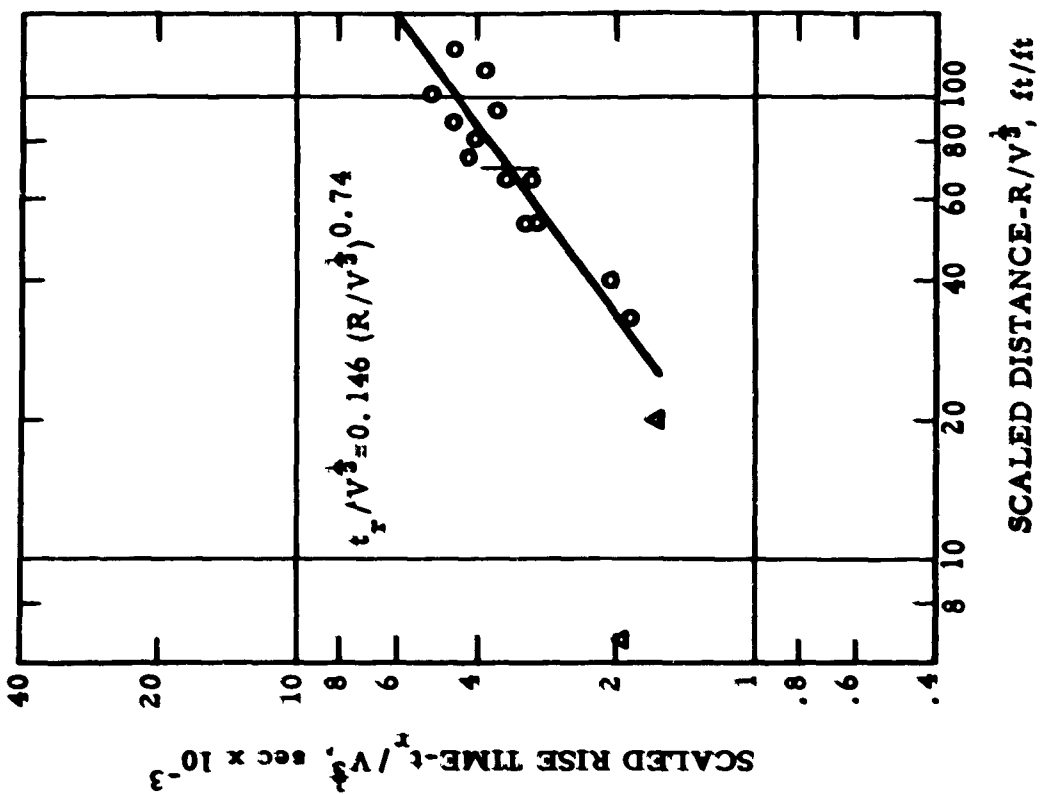
$t_r/V^{\frac{1}{3}} = 0.146 \ (R/V^{\frac{1}{3}})^{0.74}$

Fig. 57-Scaled Rise Time vs. Scaled Distance for Particle Velocity Data-Explosive AD 10

Fig. 60 - Scaled Rise Time vs. Scaled Distance
for Velocity Data-Explosive SG 45

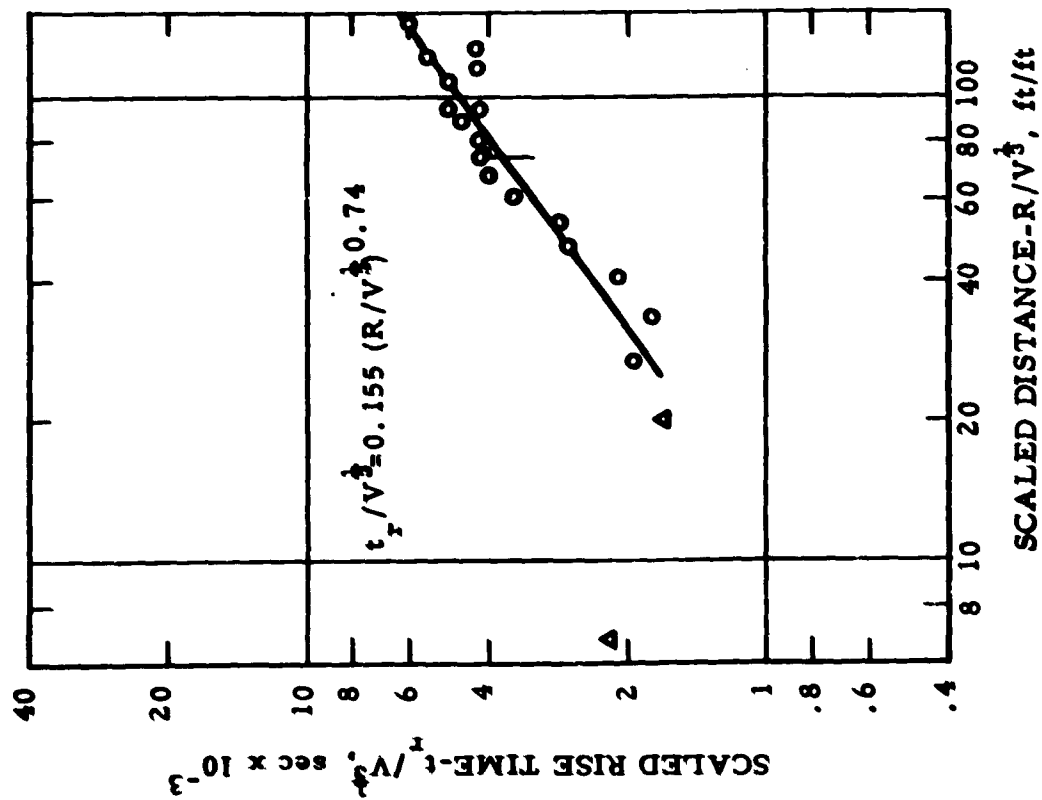Fig. 59 - Scaled Rise Time vs. Scaled Distance for
Velocity Data- Explosive AD-P

102.

$t_f/V^{\frac{1}{3}} = 2.15 (R/V^{\frac{1}{3}})^{0.11}$

SCALED DISTANCE-$R/V^{\frac{1}{3}}$, ft/ft

Fig. 62- Scaled Fall Time vs. Scaled Distance for
Velocity Data-Explosive AD 20A

$t_f/V^{\frac{1}{3}} = 2.16 (R/V^{\frac{1}{3}})^{0.11}$
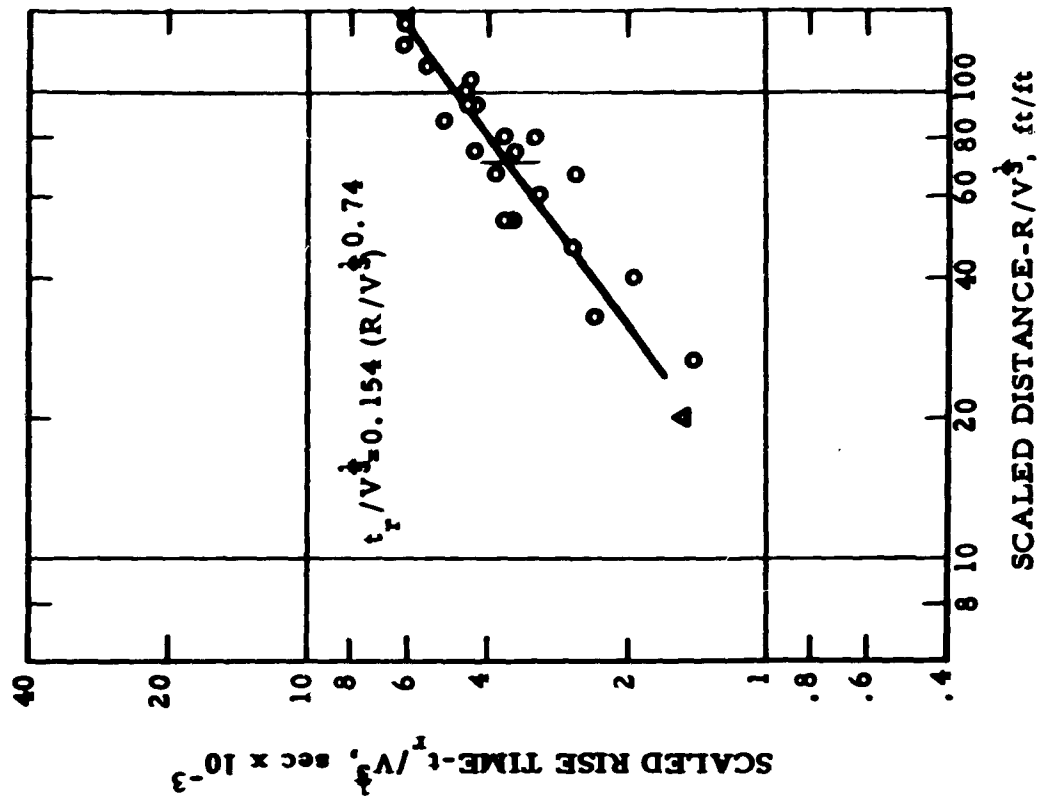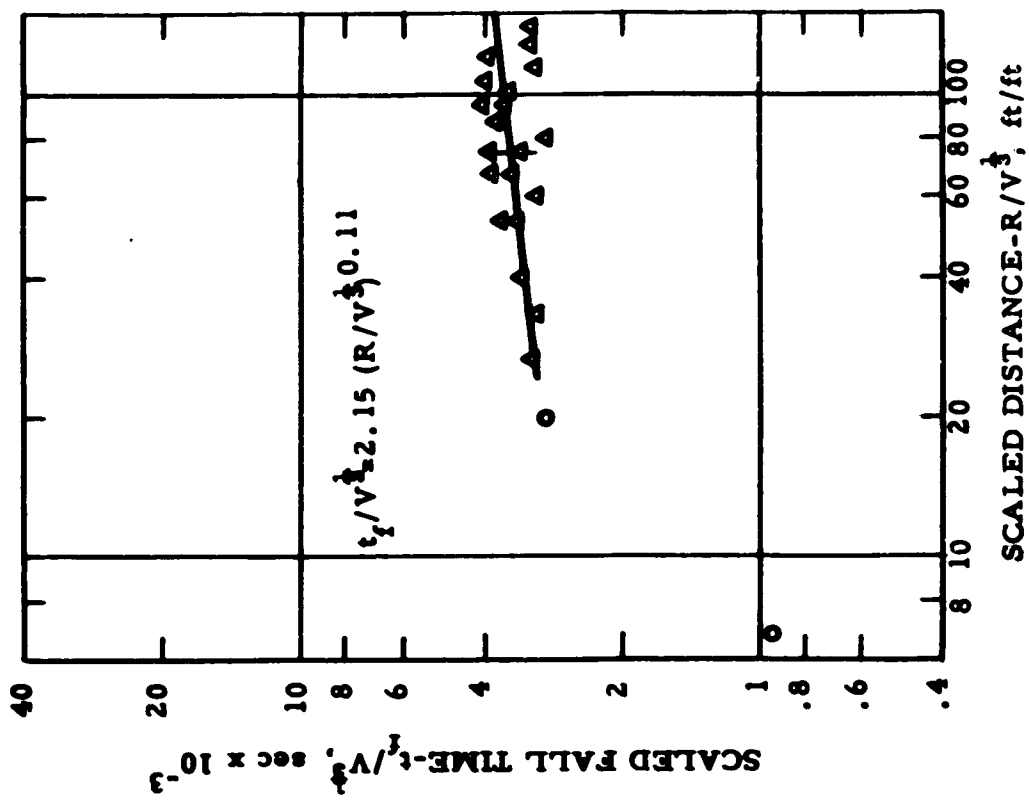
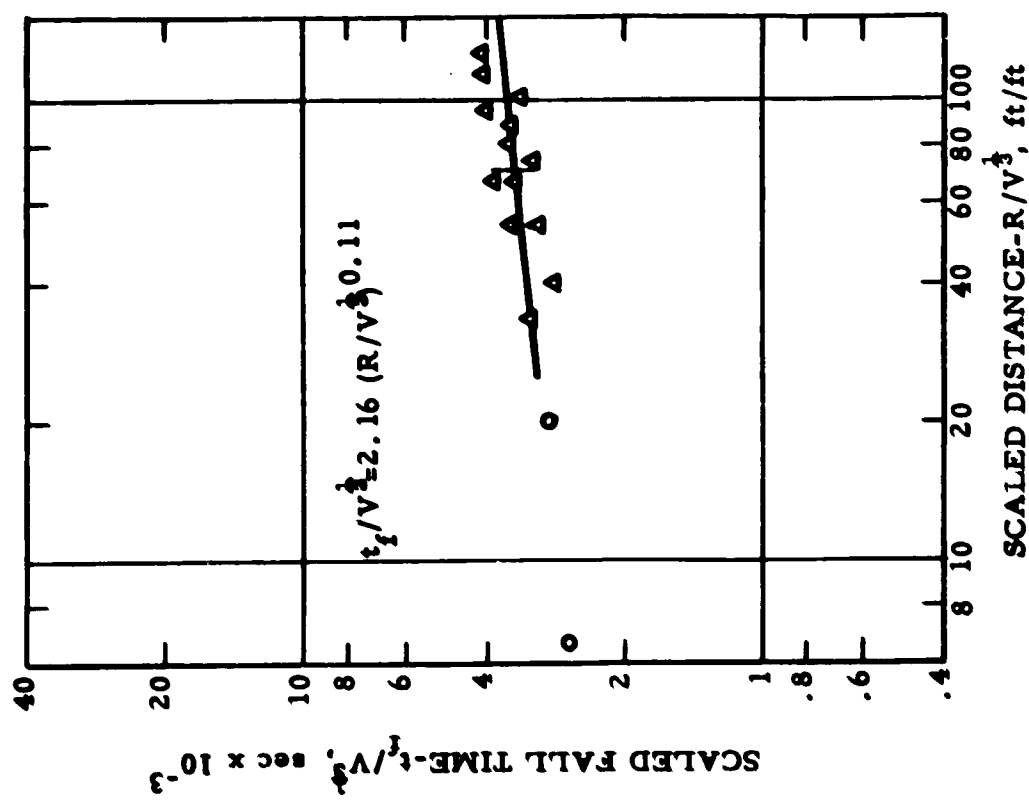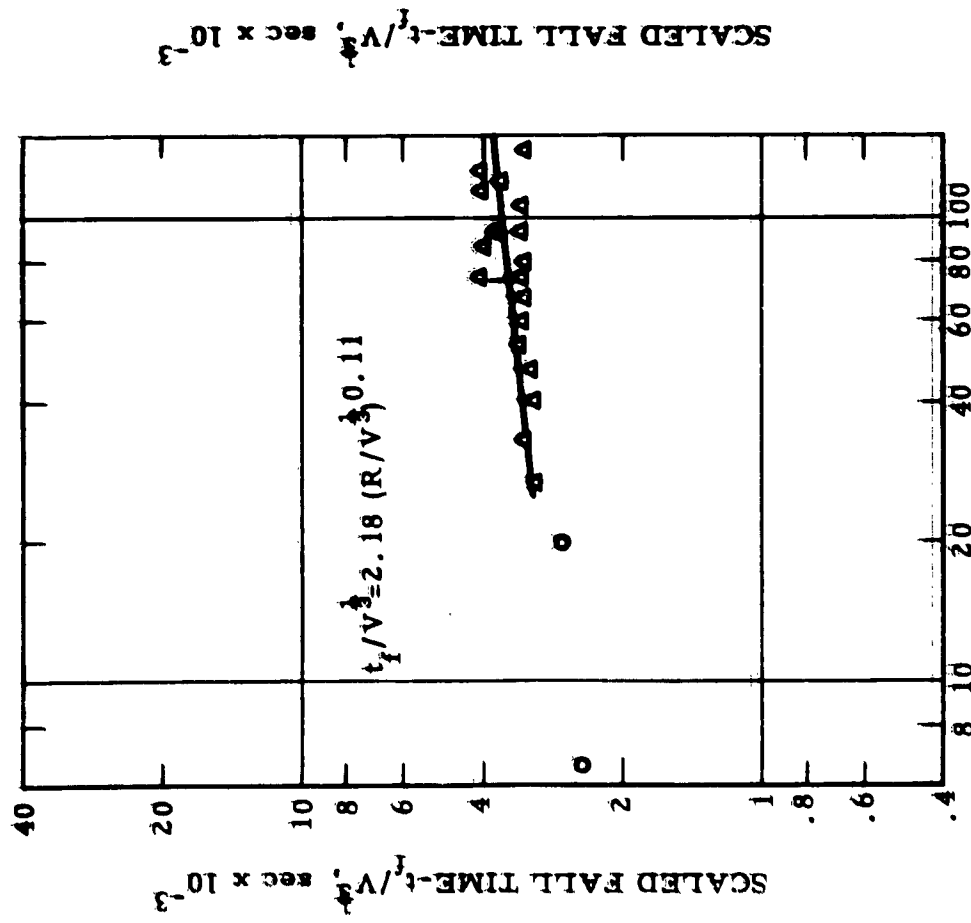SCALED DISTANCE-$R/V^{\frac{1}{3}}$, ft/ft

Fig. 61 - Scaled Fall Time vs. Scaled Distance for
Velocity Data- Explosive AD 10

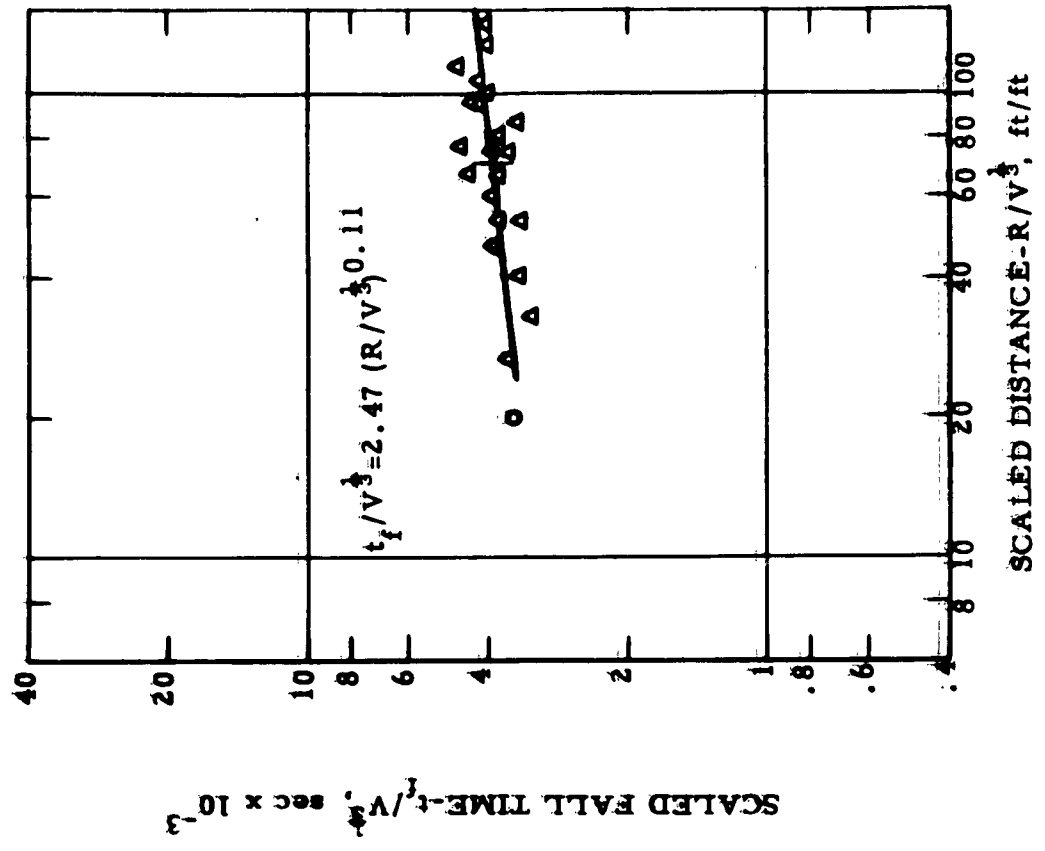Fig. 64 - Scaled Fall Time vs. Scaled Distance for Velocity Data-Explosive SG 45

$t_f/v^{\frac{1}{3}} = 2.47 (R/v^{\frac{1}{3}})^{0.11}$

Fig. 63 - Scaled Fall Time vs. Scaled Distance for Velocity Data-Explosive AD-P

$t_f/v^{\frac{1}{3}} = 2.18 (R/v^{\frac{1}{3}})^{0.11}$

103.

104.

The values of K and n for acceleration and velocity data are given in
table 22, and for strain data in table 13.

Several facts about the period data sets tuff apart from other rocks, or
at least from granite (Nicholls and Hooker, 1962). In tuff the detonation
time of the explosive was only a small fraction of the rise time. Rise
time was strongly dependent on travel distance, increasing with in-
creased travel distance. Fall times were very nearly independent of
travel distance. For a symmetrical pulse, rise time should be one-
half the fall time. The asymmetrical pulse in tuff yielded rise times
less than fall times for scaled distances less than 50 to 80 ft/ft. For
scaled distances greater than 50 to 80 ft/ft, rise times were greater
than fall times. The most powerful explosive, SG 45, generally yielded
longer rise and fall times than the other explosives did.

Crushed Zone Measurements

In the granite report, it was shown that the size of the cavity created by
an explosion in rock was directly related to the amount of strain gen-
erated. Similar measurements were conducted in tuff. After an explo-
sion in a shothole, a supply of compressed air was directed into the
hole. Material which had been crushed was ejected from the hole. The
size and shape of the cavity was then measured by adding known incre-
ments of sand and measuring the buildup in the hole. Shotholes 9 and 14
could not be measured because the sand stemming in the hole had com-
pacted so tightly during detonation that re-entry was impossible. Another
problem in cleaning the holes was that of possible enlargement of the
cavity. An over supply of compressed air or working the air hose too
vigorously in the cavity, was sufficient to break-up and eject unbroken
or uncrushed tuff. The volume of the crushed zone has been expressed
as a ratio of the original charge volume in table 23. The ratio varied
from 20.1 to 35.3 which represents cavity volumes of 8.33 and 14.55 cubic
feet created by charges with a volume of 0.41 cubic feet.

The crushed zone represents a 2.0 foot diameter cavity up to 5.0 feet in
height as compared to the original charge-hole dimensions of 0.55 foot in
diameter and 2.5 long. The most powerful explosive, SG 45, has the
largest average value of crushed zone volume/charge volume ratio as ex-
pected. However, only two values of crushed zone volume were obtained
for the SG 45 explosive.

TABLE 23.- Crushed zone volume/charge volume ratio

AB 10		AB 20A		AB-P		SG 45	
Shot No.	Crushed vol. / Charge vol.	Shot No.	Crushed vol. / Charge vol.	Shot No.	Crushed vol. / Charge vol.	Shot No.	Crushed vol. / Charge vol.
5=S10	34:3	4=S12	28:4	6=S15	26:3	2=S9	**
9=S13	23:4	8=S11	32:2	10=S12	26:5	7=S14	**
12=S1	25:1	16=S7	25:0	14=S8	25:0	15=S2	35:3
17=S6	20:1	19=S4	23:4	18=S3	22:4	20=S5	27:3
Average	25:7		27:3		25:1		31:3

** No data.

106.

Calibration and Other Data

Four charges of SRG 485 were detonated as calibration shots. These charges were 66.95 pounds each and were used to determine amplitude levels for the larger shots. The data from Shot 11-B3 was lost because amplifier gain settings were too low. Acceleration data from these shots are given in table 24. Additionally, data from Operation PLUMBBOB (Perret, 1957) are included in table 24 for subsequent use in this report.

Correlations and Discussion

Particle Motion

Throughout most of the particle velocity, acceleration, and strain data, the amplitude of the second peak is larger than the amplitude of the first peak. This is always the case for scaled distances greater than 400 ft/ft. For example, for strain data, the tensile amplitude may be as great as three times the compressive amplitude; for acceleration, the negative amplitude may be up to eleven times the positive amplitude; and for particle velocity, negative amplitude may be up to seventeen times the positive amplitude. In granite, the first peak amplitudes were larger than second peak amplitudes for 94% of the data. The theoretically derived particle velocity wavelets of Ricker (1942), bear a striking resemblance to the pulses obtained in tuff. This type of pulse may be characteristic of "soft", low velocity media such as tuff and the shale in which Ricker performed his tests.

Results from strain data were about as expected. The regression slope of −2.03 for compressive strains indicated a high rate of attenuation with distance. The most powerful explosive, SRG 485, generated the largest strains. Tensile strain was proportional to an inverse power of the scaled distance for scaled distances greater than 400 ft/ft. At smaller scaled distances, the tensile portion of the strain pulse became smaller by comparison. At small scaled distances, permanent compressive deformation occurred.

Because of the low propagation velocity, reflections from the surface were a major source of trouble. Based on an assumed velocity of 6000 ft/sec, and calculated rise and fall times, compressive peaks and

TABLE 24. — Subsurface particle acceleration data

Shot designation, charge weight, change volume, volume	Shot-to-gage distance R ft	Scaled distance $R/W^{\frac{1}{3}}$ ft/ft	Peak positive acceleration A g's	Scaled positive acceleration $AW^{\frac{1}{3}}$ g's x ft
Rainier	99	2.61	2550	96,645
W = 1.7 KT	99	2.61	3120	118,243
W = 54,487 cu ft	148	3.90	1510	57,229
$W^{\frac{1}{3}}$ = 37.9 ft	199	5.25	242	9,172
	199	5.25	191	7,239
	250	6.60	101	3,823
	300	7.92	41.2	1,561
	901	23.8	11.34	500.8
	1365	35.8	.67	25.4
	1365	35.8	.55	20.8
	1365	35.8	.55	20.8
3-B4	125	271	.00669	.00308
W = 6.95 lb	115	249	.00738	.00340
W = .0982 cu ft	105	228	.00848	.00391
$W^{\frac{1}{3}}$ = .461 ft	90	195	.00778	.00359
	80	174	.00914	.00421
	70	152	.1366	.0627
11-B1	70	152	.3444	.159
W = 6.95 lb	80	174	.1399	.0641
W = .0982 cu ft	90	195	.1226	.0581
$W^{\frac{1}{3}}$ = .461 ft	105	228	.0685	.0316
	115	249	.02833	.01130
13-B2	125	271	.01252	.01116
W = 6.95 lb	115	249	.02840	.01129
W = .0982 cu ft	105	228	.02011	.00927
$W^{\frac{1}{3}}$ = .461 ft	90	195	.05574	.0255
	80	174	.05778	.0266

tensile peaks were subjected to reflected energy interference at scaled distances greater than 40 ft/ft and 80 ft/ft, respectively. Although the appearance of the records was greatly affected by surface reflections (fig. 65), no appreciable effect was noted in plots of amplitude or rise and fall times versus scaled distance.

Three zones of propagation may be implied from the analysis of strain data. These three zones are directly comparable to those suggested by Chabai, et al (1962). The boundaries of the zones are arbitrary but meaningful. Chabai divides the area surrounding an explosive into five zones as follows: Zone I, acoustic; Zone II, semiacoustic or reversible; Zone III, crack zones, A and B; Zone IV, crushing; and Zone V, hydrodynamic. Experimental data permit identification of the boundary between Zones II and III, IIIA, and IIIB, and between III and IV. As shown in figure 66, Zones II and III are grouped, as are Zones IV and V, because experimental data do not provide adequate identification of separation. The boundary between Zones III and IIIA is the outer limit of cracking in the rock. As discussed by Chabai, the cracking considered is that caused by tensile "hoop" stresses. "These cracks will appear when the circumferential tension ("hoop" stress) of a wave first exceeds the tensor resultant of the ambient (compressive) stress, plus the tensile strength of the medium". Tuff is considered to have a negligible tensile strength. The ambient stress is:

$$P_I = \rho g h + P_B \tag{7}$$

where:

P_I = absolute ambient pressure,

ρ = density of medium,

g = acceleration due to gravity,

h = depth at which wave is propagated,

P_B = atmospheric pressure.

The tension character of P_I has been ignored. The value of P_I as calculated from a weight density of 106 lb/cu ft and a depth of 26 ft was approximately 34 psi. No tensile stress greater than 34 psi would then be expected to exist because tensile failure would occur and relieve the stress. The maximum tensile strain value recorded was 56 μ in/in.
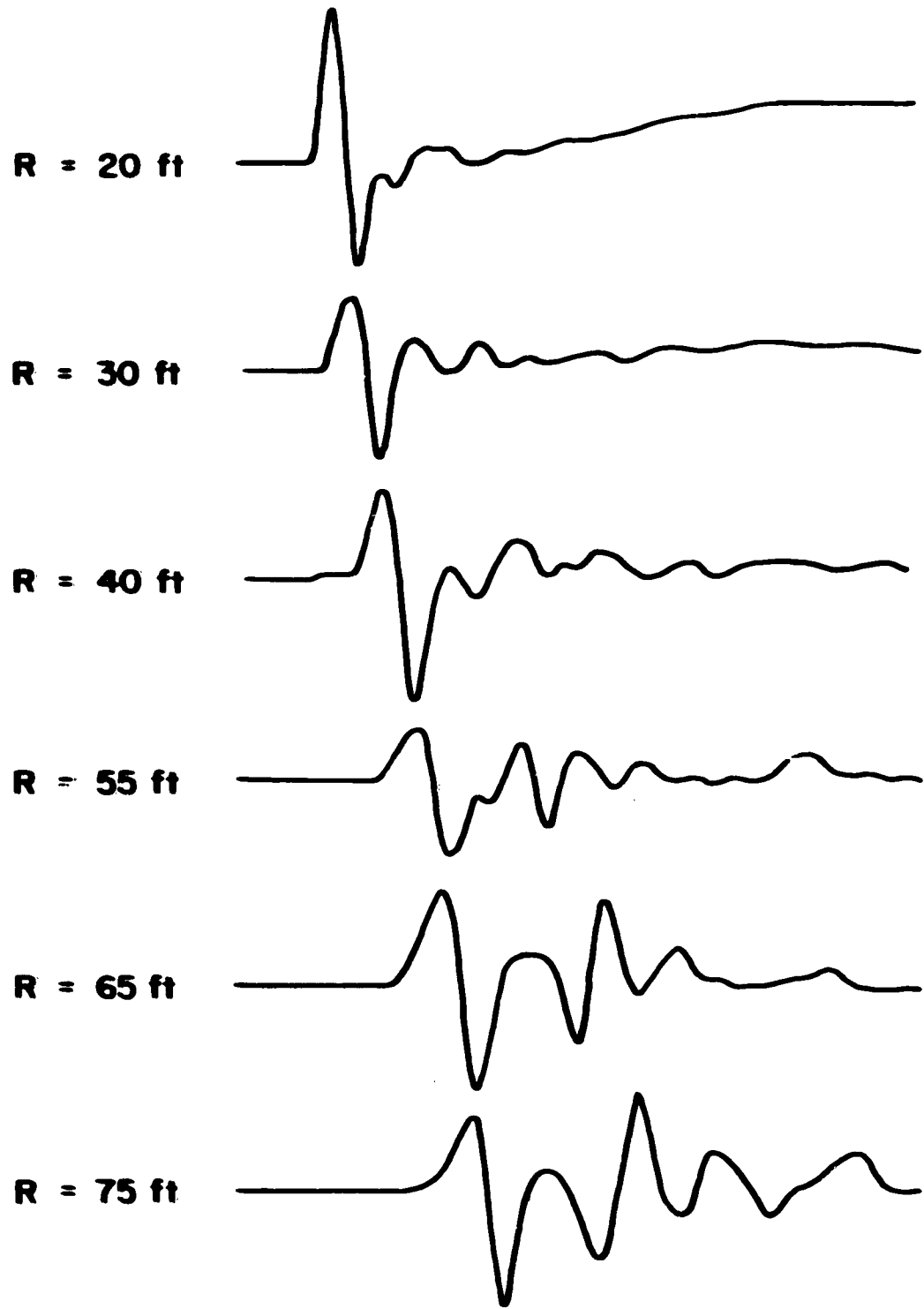
Fig. 65 - Strain-Shot 17-S6.

R = 20 ft

R = 30 ft
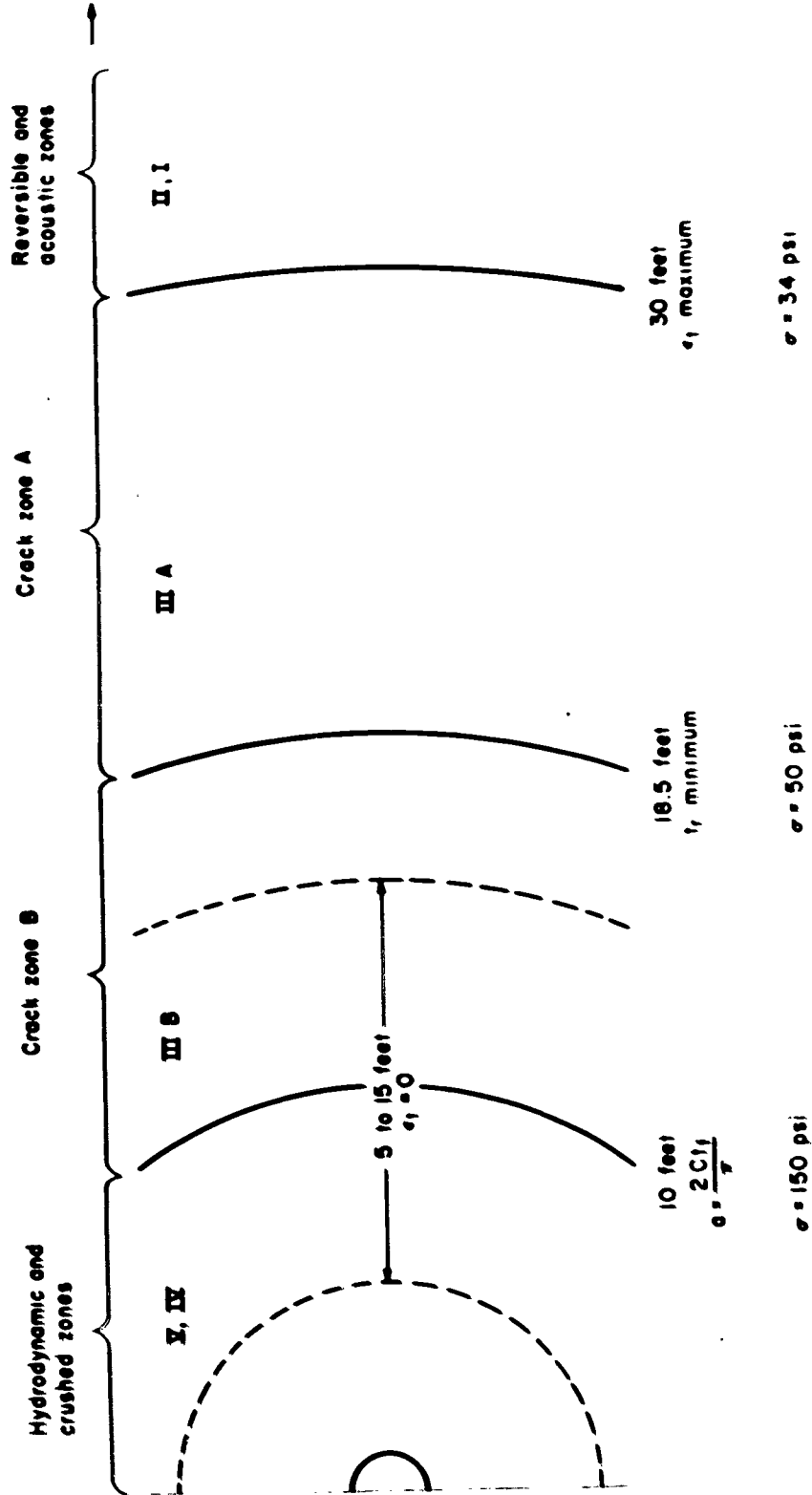
R = 40 ft

R = 55 ft

R = 65 ft

R = 75 ft

Fig. 66 - Zone Surrounding an Explosion in Rock.

The maximum calculated tensile stress was 34 psi based on a value of Young's modulus of 0.6×10^6 psi. The theoretical permissible tensile stress and the observed maximum tensile stress are in agreement and indicate that the outer limit of Zone IIIA, for the test series, about 30 feet from the center of the explosive charge.

In the discussion of Zone IIIB, Chabai points out that in this region, the "shock propagation velocity, U, decreases as pressure increases. This results in the well known 'elastic precursor'". A change in the pulse shape, particularly in the rise time portion of the pulse, could be expected under these conditions. The scaled rise time versus scaled distance plots from strain data (figures 41 to 44) show a marked change at a scaled distance of 25 ft/ft or a distance of 18.6 feet. A minimum value of rise time, t_r, occurs at this point with larger values of rise time occurring at both smaller and larger distances. This indication is proposed as the boundary between Zones IIIA and IIIB as shown in figure 66.

A third limit or boundary can be implied from the tensile strain data. This limit is between the crushed Zone IV and crack Zone IIIB. If the material being crushed is assumed to be permanently deforming in compression, no tensile strain would be expected to exist. An examination of the tensile strain versus scaled distance plots (figures 17 to 20) shows that tensile strain becomes zero at a distance somewhere between 5 and 15 feet from the charge. Additionally, period data may be used to estimate the limit of crushing. Assuming that the period of the pulse is controlled by the size of the cavity created, the following equation would be expected to hold: (Duvall, Atchison, 1950).

$$a = \frac{2 C t_f}{\pi} \tag{8}$$

where

a = radius of cavity, limit of crushing,

C = longitudinal propagation velocity,

and

t_f = fall time of strain pulse.

112.

The calculated cavity radius was about 10 feet which compares favorably with the estimated limit of crushing from zero tensile strain.

The estimated stresses as calculated from strain values and a Young's modulus of 6×10^6 psi were:

$$\sigma \text{ at Zone II, IIIA boundary} = 34 \text{ psi}$$

$$\sigma \text{ at Zone IIIA, IIIB boundary} = 50 \text{ psi}$$

$$\sigma \text{ at Zone IIIB, IV boundary} = 150 \text{ psi}$$

The average static compressive strength of four 2-1/2 inch long, 2-1/8 inch diameter tuff cores was 840 ± 155 psi, quite different from the 150 psi calculated at the limit of crushing. However, the value of Young's modulus is undoubtedly incorrect when measured in the acoustic zone and applied in the crushed zone.

Plots of scaled rise time versus scaled distance for acceleration and particle velocity data show the same minimum and change of slope that the plots from strain data do. However, the acceleration and particle velocity data do not show the maximum negative phase that tensile strain does. Nor do they show a negative phase approaching zero as tensile strain does. This is because of the nature of particle motion, motion and gage must both come to rest.

The slopes for the positive phase of strain, acceleration, and particle velocity are respectively -2.03, -2.39, and -2.18. Radial strain and particle velocity should attenuate the same and there is no significant difference in the data. Based upon Ricker's theory (1940), the slopes should be $-(1 + 3b)$, $-(1 + 4b)$ and $-(1 + 3b)$, respectively. Numerically, the slopes would then be -2.03, -2.37, and -2.03, assuming that $1 + 3b = 2.03$. The observed slopes are not significantly different than those predicted by Ricker. The presence of reflected waves undoubtedly has some effect on the slopes because the positive phase is subject to interference from reflections at scaled distances greater than about 60 ft/ft.

The slopes for the negative phase of strain, acceleration, and particle velocity are -1.83, -1.67, and -1.65, respectively. This relationship indicates that reflected waves do have a greater influence on velocity and acceleration amplitudes than on strain amplitudes.

The slope of the strain energy propagation law should be twice the slope of the strain propagation law if there is no broadening of the pulse with distance. The fact that the strain energy slope of -2.98 is much less than twice the strain slope of -2.03, indicates that there has been considerable absorption and broadening of the pulse as it traveled outward. Table 25 provides a comparison of strain and strain energy slopes and the absorption and broadening of the pulse in tuff, granite and salt.

TABLE 25. - Comparison of absorption- tuff, salt and granite

Rock	Strain slope N_ϵ	Energy slope N_E	2x strain slope $2 N_\epsilon$	Relative absorption $2N_\epsilon - N_E/2N_\epsilon$
Tuff	-2.03	-2.98	-4.06	.266
Granite	-1.80	-3.24	-3.60	.100
Salt	-1.25	-2.34	-2.50	.064

The column headed $2N_\epsilon$ is the energy slope which theoretically would exist in the absence of broadening and absorption. The column headed $2N_\epsilon - N_E/2N_\epsilon$ provides a comparison of the relative broadening and absorption in the three rock types which is obviously greatest in tuff and least in salt.

Although strain and particle velocity pulses have similar shapes as expected, and the decay exponent is not significantly different for their respective propagation laws, their relative amplitudes do not agree with theory. At relatively large distances, several charge radii, strain and particle velocity are related:

$$\epsilon = \frac{v}{C} \tag{9}$$

where

ϵ = strain,

v = particle velocity,

and

C = longitudinal propagation velocity.

Table 26 provides a comparison of observed compressive strain values versus compressive strain calculated from observed particle velocity and C = 6080 ft/sec. Values are from explosive SG 45.

TABLE 26. - Strain and particle velocity

Scaled distance	Observed particle velocity	Calculated strain	Observed strain
	in/sec	μ in/in	μ in/in
10	20	274	680
40	1	14	40
100	.135	1.9	6.2

Strain and particle velocity amplitudes differ by about a factor of three. If the propagation velocity were 2000 ft/sec, fair agreement would exist. However, this appears completely unrealistic. A more realistic approach suggests that strain amplitudes are not absolute because they are dependent upon the grout and the core on which they are mounted and could not therefore be considered as absolute values. If the Young's modulus of the core-grout inclusion is less than for the surrounding medium, the strain observed by the gage would be greater than the strain transmitted in the medium. Particle velocity amplitudes are considered to be more absolute than strain amplitudes.

Energy Transfer

The total radial strain energy, H, at any distance may be calculated from the scaled radial strain energy per unit area:

$$H = [E_a/V^{\frac{1}{3}}] \; 4 \pi [R/V^{\frac{1}{3}}]^2 \qquad (10)$$

where

H = total radial strain energy,

$E_a/V^{\frac{1}{3}}$ = radial strain energy radiating outward per unit area,

$4\pi[R/V^{\frac{1}{3}}]^2$ = surface area of a sphere with scaled radius of $R/V^{\frac{1}{3}}$

The total energy of an explosive may be estimated from $NRT/(\gamma - 1)$, where N is the moles of gaseous products of detonation per unit volume of explosive; R, the gas constant; T, the detonation temperature; and γ is the ratio of the specific heats. The percentage of the calculated explosive energy transferred to the rock as strain energy can then be expressed as the ratio of H to $NRT/(\gamma - 1)$ times 100%.

Table 27 gives the values of total radial strain energy and relative energy transferred to the rock for the four explosives used. The data are different in two respects than those reported from granite. First, the relative energy transferred in tuff was about 1.5% and ranged from 12 to 32% in granite. However, the percentages for granite were probably too large because of an apparent decrease in the slope of strain and strain energy propagation laws at small scaled distances which was not considered. Second, a threefold change in the percentages of relative strain energy transferred was observed in granite for six explosives covering a characteristic impedance ratio range from 0.16 to 0.52. Only about a 10% change was observed in tuff for the four explosives with characteristic impedance ratios ranging from 0.76 to 1.92. It had been shown previously in the granite report and from salt (Nicholls and Duvall, 1962), that explosives having characteristic impedances which closely matched the impedance of the rock, impedance ratio approaching 1.0, transfer a greater percentage of the available energy to the rock. The amount of energy transferred decreases rapidly as the value of the characteristic impedance ratio decreases from 0.7 to 0.0. For the characteristic impedance ratios in tuff, only a 5% change in the values of the percentage of relative strain energy transferred is predicted from acoustic theory.

Characteristic Impedance and Particle Motion

For tuff the plot of peak strain intercept versus detonation pressure for each of the explosives was a curved line, as in granite, indicating that the detonation pressures were not directly proportional to the stress transferred to the medium (figure 67). Thus, elastic theory was inadequate in tuff, as it was in granite, to reconcile the results. The transfer of pressure across a plane boundary due to a plane elastic wave striking at normal incidence is:

TABLE 27. - Energy transfer

Explosive	Total energy H [1]	Relative strain energy transferred to the rock
		$\dfrac{H}{NRT/(\gamma - 1)} \times 100$
	ft-lb/ft^{3}x10^6	percent
AD 10	1.04	1.48
AD 20A	1.20	1.48
AD-P	1.15	1.56
SG 45	2.01	1.62

[1] $H = [E_a/V^{\frac{1}{3}}] \, 4 \, \pi \, (R/V^{\frac{1}{3}})^2$ where $R/V^{\frac{1}{3}} = 1.0$.

$$\frac{P_m}{P} = \frac{2}{1 + Z} \qquad (11)$$

where

P_m = pressure in the medium,

P = detonation pressure,

$Z = (\rho C)_e /(\rho C)_r =$ ratio of characteristic impedances,

ρ = density of explosive or rock,

C = detonation or propagation velocity of explosive or rock,

$(\rho C)_e$ = characterstic impedance of explosive,

and

$(\rho C)_r =$ characteristic impedance of rock.

Assuming that stress in the medium is directly proportional to strain in the medium, equation (11) can be rewritten:
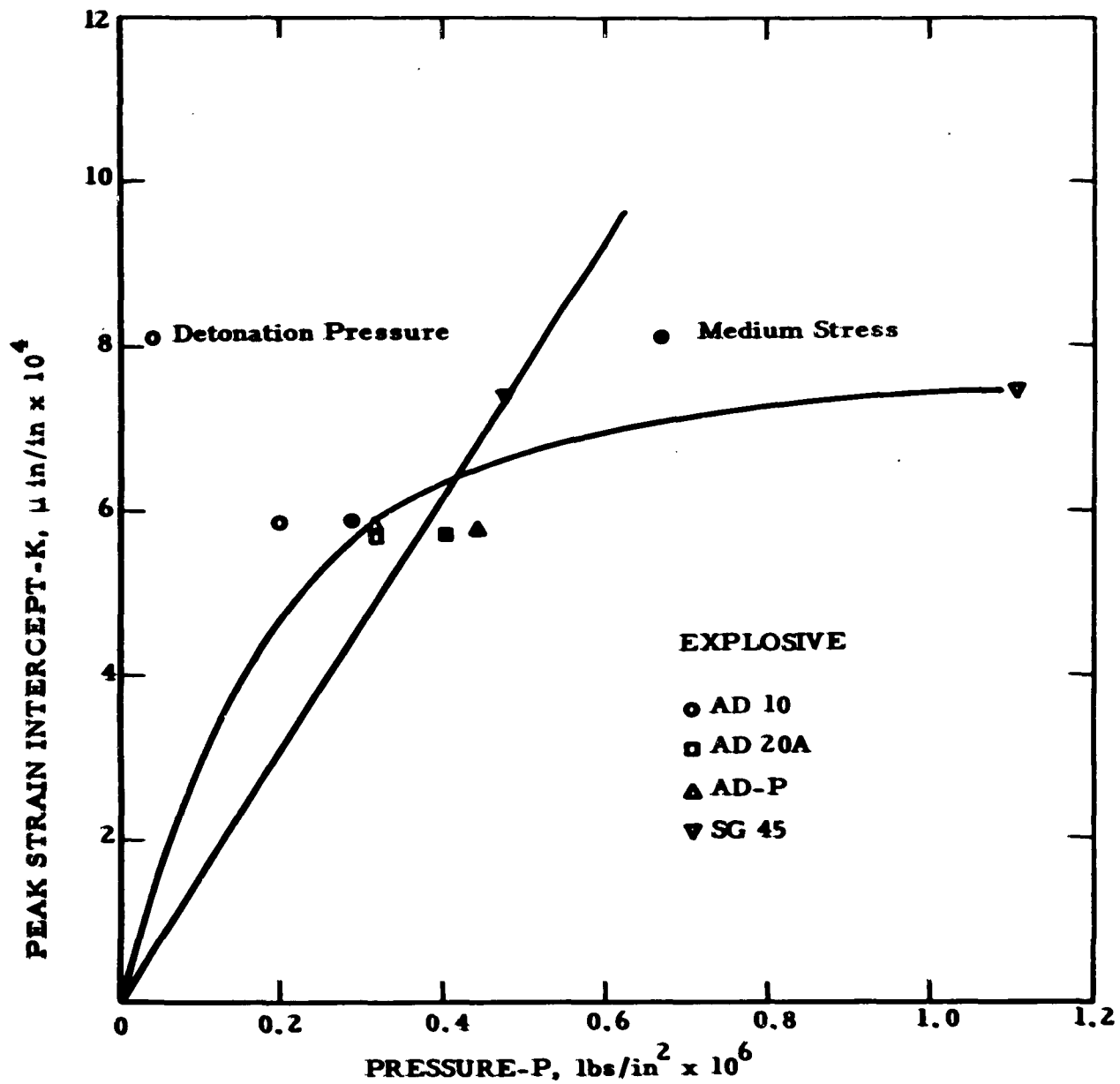
Fig. 67 - Peak Strain vs. Detonation Pressure and Medium Stress.

118.

$$K/P = A \left(\frac{2}{1+Z} \right) \tag{12}$$

where

K = peak strain intercept,

and

A = proportionality constant.

Figure 68 is a log-log plot of the values of K/P versus Z for the data from four explosives in tuff. The dashed line represents equation (12) and obviously does not fit the data. The solid line is the statistically determined straight line fitted to the data:

$$K/P = 15.7 \times 10^{-2} Z^{-1.33} \tag{13}$$

The value of the constant A in equation (12) was chosen to be the same as the statistically determined constant at Z = 1.0. It appears that shock wave transmission across the explosive-tuff boundary has occurred and elastic theory is inadequate to describe the observed data. If the pressure enhancement, P_m/P, is considered, equation (13) conveniently reduces to:

$$P_m/P = Z^{-1.33} \tag{14}$$

The stress in the medium may then be calculated and plotted versus the peak strain intercept for each explosive resulting in a straight line as expected and as shown in figure 67.

The results from four explosives in tuff are not drastically different than those reported from granite and salt (Nicholls and Hooker, 1962). The same analysis was made for values of K/P versus Z for four explosives in salt and six explosives in granite. The calculated values of P_m/P and Z for all three rock types are given in table 28 and plotted in figure 69. These are derived values, obtained from K/P versus Z curves for each rock type. All curves are of the type:

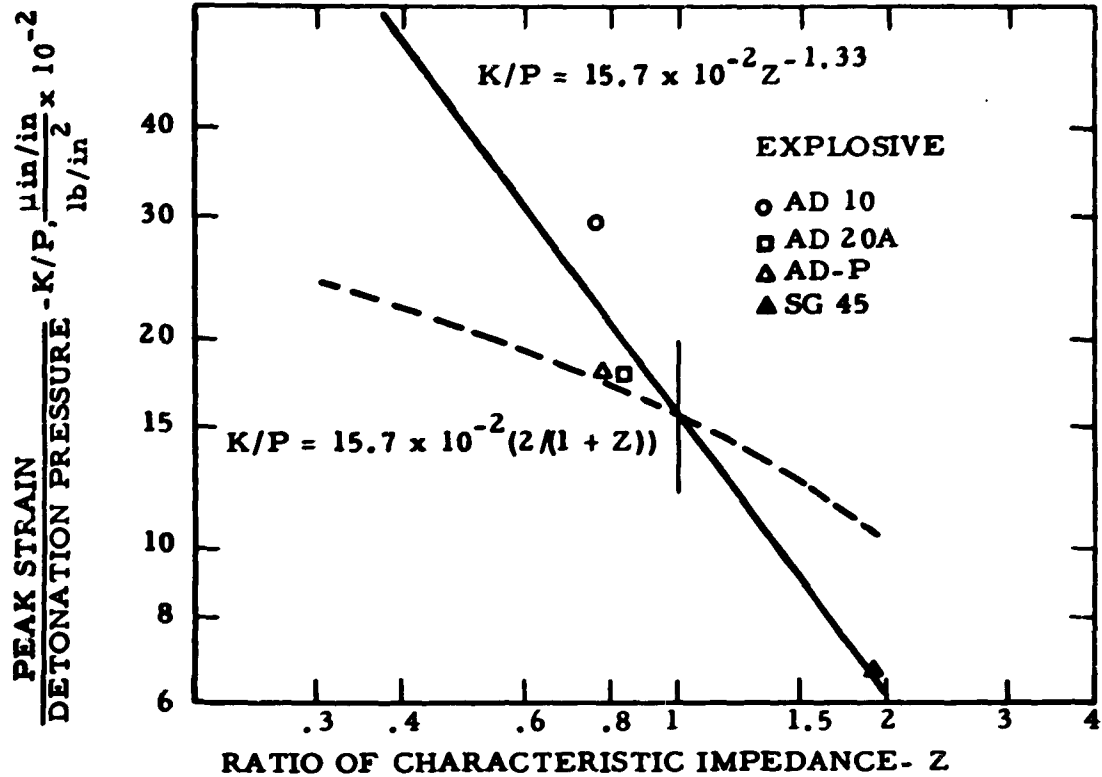$$P_m/P = Z^{-n} \tag{15}$$

and must therefore intersect at Z = 1.0.

Fig. 68 - Peak Strain/Detonation Pressure vs. Ratio of Impedances

In the upper figure:

$$K/P = 15.7 \times 10^{-2} Z^{-1.33}$$

$$K/P = 15.7 \times 10^{-2}(2/(1 + Z))$$

EXPLOSIVE

- o AD 10
- □ AD 20A
- △ AD-P
- ▲ SG 45

Axis labels: PEAK STRAIN / DETONATION PRESSURE $-K/P$, $\dfrac{\mu in/in}{lb/in^2} \times 10^{-2}$

RATIO OF CHARACTERISTIC IMPEDANCE- Z
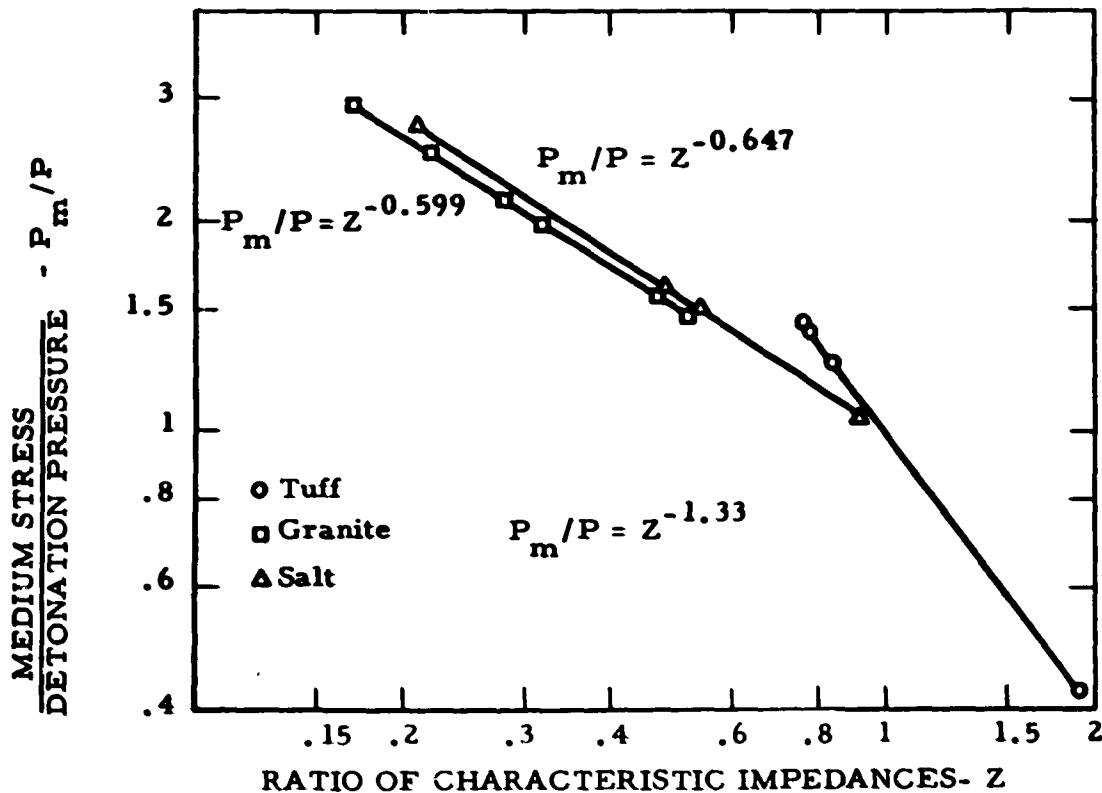
Fig. 69 - Peak Strain/Detonation Pressure vs. Ratio of Characteristic Impedances for Tuff, Granite and Salt.

In the lower figure:

$$P_m/P = Z^{-0.647}$$

$$P_m/P = Z^{-0.599}$$

$$P_m/P = Z^{-1.33}$$

- o Tuff
- □ Granite
- △ Salt

Axis labels: MEDIUM STRESS / DETONATION PRESSURE $- P_m/P$

RATIO OF CHARACTERISTIC IMPEDANCES- Z

120.

TABLE 28.- Pressure enhancement- tuff, granite and salt

Explosive and rock type	Medium stress P_m, lb/in^2 x 10^6	Detonation pressure P, lb/in^2 x 10^6	P_m/P	Z
Tuff				
AD 10	.288	.20	1.44	.76
AD 20A	.403	.32	1.26	.84
AD-P	.445	.32	1.39	.78
SG 45	.473	1.11	.426	1.92
Granite				
AD-P	1.06	.36	2.94	.17
AD 20	1.26	.50	2.52	.22
SG 30	1.48	.69	2.14	.28
Comp. B	1.91	.97	1.97	.32
SG 60	1.95	1.24	1.57	.47
HVG 80	2.43	1.65	1.47	.52
Salt				
AD-P	.663	.23	2.74	.21
TNT	1.21	.75	1.61	.48
SG 45	1.24	.83	1.49	.54
HVG 60	1.73	1.65	1.05	.92

The results from salt and granite are very similar. The results from tuff are different because of the larger value of n. For all three sets of data, the effect of characteristic impedance appears to be greater than the effect predicted by acoustic theory.

The difference between the value of n for tuff and n from salt and granite may have been due to two causes. Shock-wave propagation would be much more prevalent in tuff. Some evidence of a propagation velocity increase was noticed with an increase in stress level although not definite enough for a detailed analysis. The presence of shock waves indicates that the shock wave velocity should be used in the characteristic impedance ratio.

However, the shock wave velocity is not sufficiently well known to justify its use. An additional contributing factor may have been the measured detonation velocities for the explosives used in tuff. The values given in table 8 from which the detonation pressure and characteristic impedance values were calculated, are based upon one detonation rate measurement for each explosive. Electrical "noise" problems prohibited taking additional measurements.

The peak intercepts for particle velocity and acceleration were scaled by the appropriate detonation pressure for each explosive in tuff. These values were then plotted versus the proper characteristic impedance ratio as shown in figures 70 and 71. An equation in the form of a power law function was calculated for each by standard regression analysis methods. The plane wave acoustic law for each is shown as a dashed line intersecting the power law function at $Z = 1.0$. These curves show again a stronger effect than that predicted by simple acoustic theory.

Particle Acceleration

Particle acceleration data from small surface shots (table 2); from calibration shots (table 24); and from the linear array tests (table 21); were scaled and plotted versus scaled distance (figure 72). The data are from SG 45 explosive shots only, in order to eliminate impedance effects. These were all in the Hackberry Mountain tuff. For comparison, data (table 24) from Rainier, a 1.7 Kiloton nuclear shot in the Oak Springs tuff are shown in figure 72. Though the data are at different amplitude levels, they are sufficiently close for prediction purposes. Tests in both rock types were designed so that seismic waves originated in, propagated through, and were recorded in the same tuff medium. The difference in amplitude level may be due to difference in rock type.

Conclusions

Pulse shapes in granite and tuff each have their own characteristics. Absorption and dispersion are much greater in tuff than in granite. The effect of characteristic impedance on explosion-generated strain or particle motion pulses is similar in tuff, granite and salt, although not identical. In all three rock types, the effect is stronger than that predicted by acoustic theory.
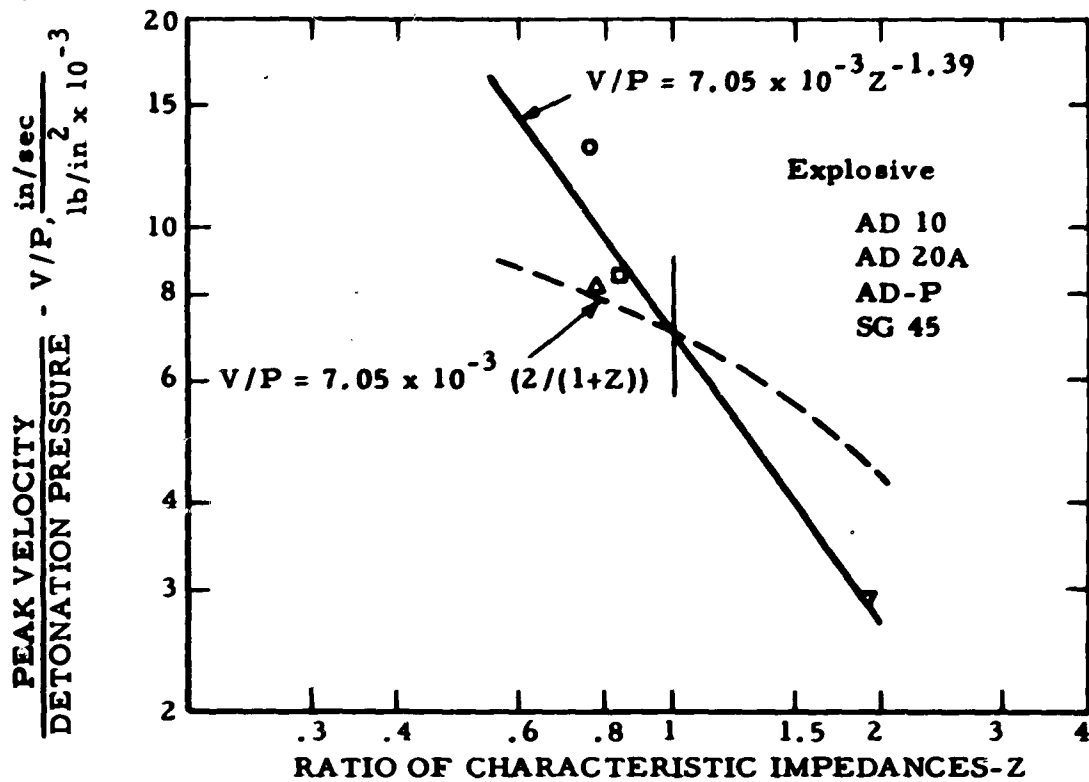
Fig. 70 - Velocity/Detonation Pressure vs. Ratio of Characteristic Impedances

$V/P = 7.05 \times 10^{-3} Z^{-1.39}$

$V/P = 7.05 \times 10^{-3} (2/(1+Z))$

Explosive

AD 10
AD 20A
AD-P
SG 45

$AV^{\frac{1}{3}}/P = 4.99 \times 10^{-2} Z^{-1.44}$

$AV^{\frac{1}{3}}/P = 4.99 \times 10^{-2} (2/(1+Z))$
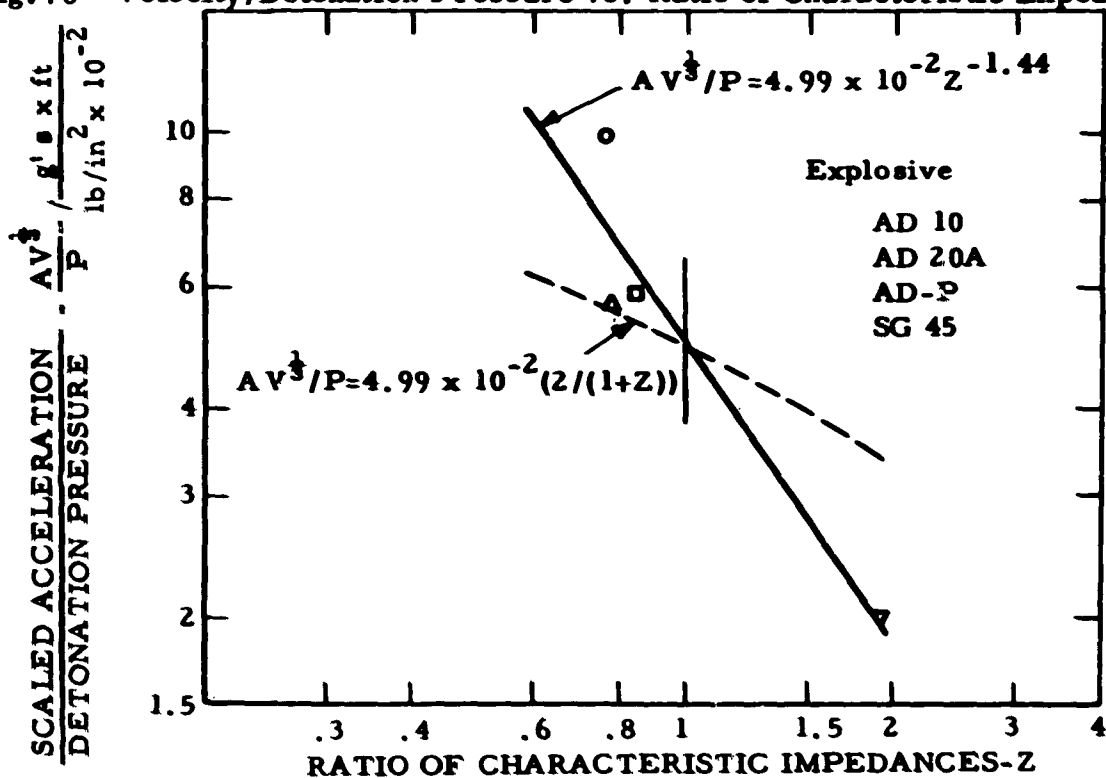
Explosive

AD 10
AD 20A
AD-P
SG 45

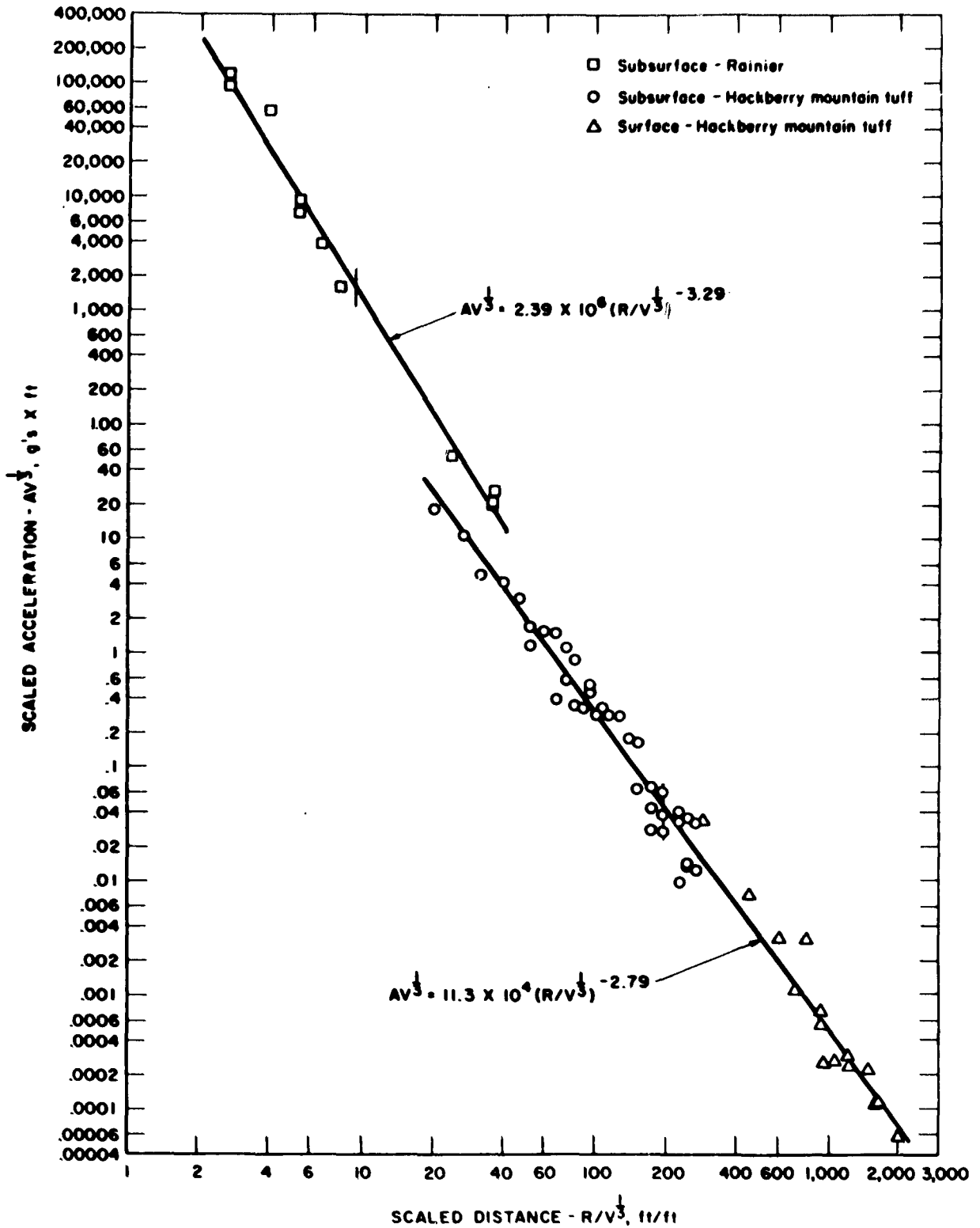Fig. 71 - Scaled Acceleration/Detonation Pressure vs. Ratio of Characteristic Impedances.

Fig. 72 - Particle Acceleration Data Comparison.

124.

Ricker' s relationship between the decay exponents for particle velocity
and acceleration propagation laws are equally valid for tuff and granite.
His theoretical pulse shapes derived in shale are similar to those ob-
served in tuff.

Additional investigations are needed to explain the change in slope of
pressure enhancement versus impedance ratio as observed in tuff and
granite. Tests should be conducted in a soft homogeneous sandstone or
a similar medium.

REFERENCES

Chabai, A. J., R. H. Bishop, et al, 1962, Close-in Phenomena of
    Buried Explosions, Sandia Corporation Report No. SC-4711(RR)
    150 pp.

Courant, R. and K. O. Friedericks, 1948, Supersonic Flow and Shock
    Waves, Interscience Publishers, Inc., New York, New York,
    pp 152-154.

Duvall, Wilbur I., 1953, Strain-Wave Shapes in Rock Near Explosions,
    Geophysics, Vol. 18, No. 2, pp 310-323.

Duvall, Wilbur I. and T. C. Atchison, 1950, Vibrations Associated
    with a Spherical Cavity in an Elastic Medium, Bureau of Mines
    Rept. of Investigation 4692, 9 pp.

Nicholls, Harry R. and W. I. Duvall, 1963, Effect of Characteristic
    Impedance on Explosion-Generated Strain Pulses, Rock
    Mechanics, Proceedings of the Fifth Symposium on Rock
    Mechanics held at the University of Minnesota, May 1962,
    Pergammon Press, pp 331-346.

Nicholls, Harry R. and Verne E. Hooker, 1962a, Comparative Studies
    of Explosives in Salt, Bureau of Mines Rept. of Investigations
    6041, 46 pp.

Nicholls, Harry R. and Verne E. Hooker, 1962,   Shear and Longi-
    tudinal Waves from H E Detonations in Granite- Bureau of
    Mines-Applied Physics Research Laboratory Rept. No.E48.1
    (Semi-final), 115 pp.

Nicholls, Harry R., 1961, In Situ Determination of the Dynamic
    Elastic Constants of Rock, Bureau of Mines Rept. of
    Investigations 5888, 13 pp.

Obert, Leonard and Wilbur I. Duvall, 1949, A Gage and Recording
    Equipment for Measuring Dynamic Strain in Rock, Bureau of
    Mines Rept. of Investigations 4581, 11 pp.

Paine, R. S., D. K. Holmes and H. E. Clark, 1962, Controlling
Overbreak by Pre-splitting, Vol. 1, International Symposium
on Mining Research, Pergammon Press, pp 179-209.

Perret, William R., 1958, Subsurface Motion from a Confined
Underground Detonation, Part I, Sandia Corporation Report
on Operation PLUMBBOB, ITR-1529, 68 pp.

Ricker, Norman, 1942, Further Developments in the Wavelet Theory
of Seismogram Structure, Bulletin of the Seismological Society
of America, Vol. 33, pp 197-228.

Ricker, Norman, 1940, The Form and Nature of Seismic Waves and
the Structure of Seismograms, Geophysics, Vol. 5, No. 4,
pp 348-366.

DISTRIBUTION LIST

Addressee	Copies	
	Technical Summary	Monthly
Chief, Defense Atomic Support Agency, Washington 25, D. C., Attn: Maj. B. M. Carswell	5	3
Director, Advanced Research Projects Agency (ARPA), Washington 25, D.C.	6	3
VELA Seismic Information Analysis Center, Fluid & Solid Mechanics Laboratory, Willow Run Laboratories, Detroit, Michigan	3	1
Director, The Rand Corporation, 1700 Main Street, Santa Monica, California, Attn: Dr. Richard Latter	1	1
California Institute of Technology, Pasadena, California, Attn: Dr. Press and Dr. Benioff	1	1
Air Force Cambridge Research Laboratory (CRZO) Attn: Dr. Norman A. Haskell, Laurence G. Hanscom Field, Bedford, Massachusetts	1	1
Director of Defense Research and Engineering, Department of Defense, Washington 25, D.C.	1	1
AFTAC (TD-1), Washington 25, D.C.	2	1
Director, Military Application, U. S. Atomic Energy Commission, Washington 25, D.C.	2	1
Dr. John Crawford, P.O. Drawer 1267, Ponca City, Oklahoma	1	
Lamont Geophysical Observatory, Palisades, New York, Attn: Dr. Jack Oliver	1	
Defense Documentation Center, Cameron Station, Alexandria, Va., Attn: TISIA-21	20	

Addressee	Technical Summary	Monthly
U. S. Coast & Geodetic Survey, Department of Commerce, Attn: Leonard Murphy, Seismology Branch, Washington 25, D.C.	1	
National Science Foundation, 1951 Constitution Avenue, N.W. Washington 25, D.C. Attn: Earth Sciences Division	1	1
Director, Naval Research Laboratory, Washington 25, D.C., Attn: Library	1	
Chief of Naval Research, Navy Department, Washington 25, D. C., Attn: Code 418	1	
Col. Eric J. Younson, British Defense Staff ACO(W), British Embassy, 3100 Massachusetts Avenue, N.W., Washington 8, D.C.	1	
U. S. Geological Survey, Department of the Interior, Attn: Crustal Studies, Washington 25, D.C.	1	
Director, The Rand Corporation, 1700 Main Street, Santa Monica, California. Attn: Dr. H. L. Brode	2	2
Commander, U. S. Naval Ordnance Laboratory, Attn: Dr. H. G. Snay, White Oak, Silver Spring 19, Maryland	1	1
Lawrence Radiation Laboratory, Box 808, Livermore, California, Attn: Dr. G.T. Pelsor	1	1
Stanford Research Institute, Menlo Park, California, Attn: Mr. Fred Sauer	1	1
Attn: Dr. George DuVall	2	0
Sandia Corporation, Dir. 5112, Albuquerque, New Mexico, Attn: Dr. J. D. Shreve	1	1
Attn: Dr. A. J. Chabai	1	1
Engineering Physics Company, 5515 Randolph Street, Rockville, Maryland, Attn: Dr. V. Cushing	1	1

DISCLAIMER NOTICE

THIS DOCUMENT IS BEST QUALITY
PRACTICABLE. THE COPY FURNISHED
TO DTIC CONTAINED A SIGNIFICANT
NUMBER OF PAGES WHICH DO NOT
REPRODUCE LEGIBLY.